2017-06-01

Characterization of Neuronal Nicotinic Acetylcholine Receptors and their Positive Allosteric Modulators

Doris Clark Jackson
Brigham Young University

Characterization of Neuronal Nicotinic Acetylcholine Receptors and Their Positive Allosteric Modulators

Doris Clark Jackson

A dissertation submitted to the faculty of
Brigham Young University
in partial fulfillment of the requirements for the degree of

Doctor of Philosophy
Neuroscience

Sterling N. Sudweeks, Chair
Arminda Suli
Jonathan J. Wisco
R. Paul Evans
Scott C. Steffensen

Department of Physiology and Developmental Biology

Brigham Young University

ABSTRACT

Characterization of Neuronal Nicotinic Acetylcholine Receptors
and Their Positive Allosteric Modulators

Doris Clark Jackson
Department of Physiology and Developmental Biology, BYU
Doctor of Philosophy
Neuroscience

Neuronal nicotinic acetylcholine receptors (nAChRs) are ligand-gated ion channels that are necessary in memory and cognition. They are pentameric and consist of α and β subunits. They are most commonly heteromeric but, can sometimes be homomeric. nAChRs are activated by many ligands including nicotine (exogenous) and acetylcholine (endogenous).

nAChRs are located on hippocampal interneurons. The interneurons, although sparse, control the synchronous firing of the pyramidal cells. However, the hippocampal interneuron structure and function is quite diverse and not fully characterized. Therefore, we sought to quantify nAChR subunit mRNA levels using real-time PCR of CA1 hippocampal interneurons.

Surprisingly we found that the α3 and β2 mRNA subunits were the highest expressed and highest co-expressed subunits. Additionally, the α4 mRNA subunit was the lowest expressed of the subunits detected. The α4 subunit is one of the most pharmacologically targeted nAChR subunits and is found throughout the rest of the brain at much higher levels than the α3 mRNA subunit. Upon PCR analysis two subpopulations of the α3 and β2 subunits emerged: those that contained 3X more α3 than β2 and those that contained 3X more β2 than α3. Therefore, we hypothesized that two likely α3β2 nAChR stoichiometries are present in hippocampal interneurons. We differentiated their kinetic properties using electrophysiology.

Additionally, like the α4 subunit, the α7 subunit is highly targeted in cognitive therapeutics. Since, the α7 subunit is the most characterized nAChR subunit, there are current efforts to develop allosteric modulators of the α7 subunit. The α7 subunit is found at moderate levels within hippocampal interneurons and remains a valid target. Current treatment options for Alzheimer's disease, and other dementias are limited and only mildly effective. Therefore, we sought to characterize the effect of 3-furan-2-yl-*N*-p-tolyl-acrylamide (PAM-2) on α7.

Furthermore, there are no current methods to distinguish the α7 from the α7β2 nAChRs during whole cell electrophysiological recordings. Therefore, we also characterized the PAM-2 effect on α7β2 nAChRs. Our results highlight at least 2 ways PAM-2 can be used to differentiate α7 from the α7β2 during whole-cell recordings.

Keywords: nicotinic acetylcholine receptors (nAChRs), hippocampus, interneurons, electrophysiology, allosteric modulators, real-time PCR

ACKNOWLEDGMENTS

I am more than grateful for the support of all my committee members. I have received valuable mentoring and research advice from all members. I am grateful for Dr. Hugo Arias and his invitation to research using positive allosteric modulators. It opened a new path of research that I found very rewarding and enjoyable. I am particularly grateful for the years of research and mentoring in Dr. Sudweeks' lab. I am appreciative for all of the funding from the Physiology and Developmental Biology Department and would not have been able to complete my degree without sufficient funding. In addition, Connie Provost was a vital asset to my graduate experience at BYU and in the submission of my dissertation. I am particularly grateful for the support of my husband, daughter, parents, and siblings. All have played a vital role in my success. The opportunity to study at BYU has strengthened my faith and increased my capacities.

TABLE OF CONTENTS

LIST OF TABLES

LIST OF FIGURES

LIST OF SYMBOLS AND ABBREVIATIONS

α: alpha nAChR subunit (subtypes include α1-α10)

β: alpha nAChR subunit (subtypes include β1-β4)

γ: gamma nAChR subunit found at the neuro-muscular junction

δ: delta nAChR subunit found at the neuro-muscular junction

ε: epsilon nAChR subunit found at the neuro-muscular junction

ACh: acetylcholine (solubilized)

AChR/nAChR: nicotinic acetylcholine receptor

AD: Alzheimer's disease

ASD: autism spectrum disorder

ADHD: attention deficit hyperactivity disorder

β-amyloid: a peptide implicated in Alzheimer's disease

CA1, CA3: sub regions of the hippocampus

$CaCl_2$: calcium chloride (dihydrate)

CNS: central nervous system

DG: dentate gyrus; sub region of the hippocampus

EC_{50}, EC_{85}, EC_{max}: concentrations on the dose-response curve representing 50%, 85%, and maximum receptor activation

ECD: extracellular domain

GABA: gamma-aminobutyric acid, a neurotransmitter

GlyR: glycine receptor

KCl: potassium chloride

$MgCl_2$: magnesium chloride

mRNA: messenger ribonucleic acid

NaCl: sodium chloride

Na_2HPO_4: sodium phosphate

n_H: hill slope

Nic: nicotine (solubilized)

OR-2-Ca^{2+}: oocyte storage and perfusion solution; also known as Ringer's solution

PAM-2: 3-furan-2-yl-N-p-tolyl-acrylamide; α7* AChR selective positive allosteric modulator

PNS: peripheral nervous system

PTSD: posttraumatic stress disorder

qPCR: real time-polymerase chain reaction

RMSD: root mean square deviation; relates to the distance between two atoms of interacting proteins

TMD: transmembrane domain

INTRODUCTION

Nicotinic acetylcholine receptors (nAChR) are ligand-gated ion channels that are found in the central nervous system (CNS), peripheral nervous system (PNS), and in skeletal muscle at the neuromuscular junction. nAChRs are integral membrane proteins that create cation permeable pores in the extracellular membrane of cells when the neurotransmitter acetylcholine (ACh) binds. In the PNS and skeletal muscle, they are located post-synaptically, in the classic role of a neurotransmitter receptor that awaits signals from the presynaptic cell. In the CNS however, they can be located pre-terminally, pre-synaptically, and post-synaptically. When located post-synaptically, they function as a normal ligand-gated ion channel, changing the membrane potential of excitable cells like neurons and skeletal muscle when activated. However, when located pre-synaptically, they function in a unique role as modulators for the release of other neurotransmitters like glutamate, GABA, serotonin, dopamine, and acetylcholine.

Each nAChR contains 5 subunits making it a pentameric receptor. Different subunit combinations create different functional receptor subtypes. The skeletal muscle nAChR is formed from combinations of the α1, β1, γ, δ and ε subunits. There are 11 known human genes for neuronal nAChR subunits (α2-7, α9-10, and β2-4) (Rubboli et al., 1994, Sargent, 1993). The most common combinations require two α subunits and three β subunits, or three α subunits and two β subunits. Only the α7 and α9 subunits can form homomers. Given the tremendous possible diversity of neuronal nAChR subtypes, many of the potential pentameric combinations are not fully characterized.

Receptors made from different subunit combinations create receptor subtypes that have different physical properties. These include pharmacological properties like agonist and

antagonist affinity, and kinetic properties like activation, inactivation and desensitization rates. Additionally, nAChR subtypes can have different ion permeabilities. All nAChR subtypes are permeable to Na^+ and K^+, but some subtypes like the α7 homomer are also highly permeable to Ca^{2+}, which allows for activation of a variety of intracellular signaling cascades. The hippocampal interneurons we analyzed are GABAergic neurons and release GABA unto the pyramidal cells resulting in inhibition. Since these interneurons synapse with hundreds of pyramidal cells, the interneurons play a vital role in the synchronous firing of the hippocampus.

The hippocampus has an organized firing pattern. In the major hippocampal pathway called the "trisynaptic circuit," axons enter the hippocampus from the entorhinal cortex and terminate on glutamatergic neurons in the dentate gyrus (DG). The signals then travel from the dentate gyrus to the CA3 region of the hippocampus via the "mossy fibers" (glutamatergic). The third synapse (also glutamatergic) goes from the CA3 region to the CA1 region of the hippocampus (Figure 1) in what are called the "Schaffer collaterals" (Grybko, Sharma, & Vijayaraghavan, 2010). An additional input comes at this stage from the contralateral hippocampus, known as the commissural fibers. This maintains communication between both hemispheres of the hippocampus. Finally, the CA1 region of the hippocampus sends an output signal to the subiculum.

As stated, the pyramidal cells of the hippocampus must fire their output signal synchronously. The nAChRs located in interneurons play a crucial role in the synchronous firing of the hippocampus required for normal cognition. Memory is correlated with theta and gamma frequencies of the pyramidal cells, whereas, attention is correlated with alpha and gamma frequencies (Ward, 2003). It has been shown that desynchronization of this firing can result in a loss of cognition (Hanslmayr, 2012, Mitchell, 2009). Additionally, cognitive diseases like

Alzheimer's disease are characterized by neurodegeneration of the hippocampus. The neurodegeneration disrupts the interneuron-pyramidal cell relationship.

We analyzed the nAChR subunit mRNAs in the CA1 hippocampal interneurons to elucidate the most likely nAChR subtypes expressed on hippocampal interneurons (circled in Figure 1). Our results could lead to improved nAChR targeted therapies in the treatment of cognitive disorders by identifying the most likely targets on hippocampal interneurons. Specifically our work focused on interneurons of the *stratum oriens* and *stratum radiatum* surrounding the CA1 pyramidal neurons (Figure 2) (Graham et al., 2003, Son & Winzer-Serhan, 2006). Using single-cell, real time-PCR (qPCR), we identified the expression of α2, α3, α4, α5, α7, β2, β3, and β4 subunit mRNA in rat hippocampal interneurons. The α6 mRNA subunit was not detected during initial analysis, and therefore, was removed from continued experiments. Statistical analysis of our single-cell qPCR mRNA expression data suggests that the α3 and β2 subunits colocalize more often than any other subunit pair (Sargent, 1993; Wada et al., 1989). However, the characterization of receptors containing the α3β2 subunits is still in its infancy. The current thinking suggests that the most likely stoichiometry is $\alpha3_{(2)}\beta2_{(3)}$, based mainly on evidence from the muscle nAChR and the α4β2 neuronal nAChR – which is thought to contain two α subunits in its pentameric makeup. However, recent experiments involving other α:β combinations that have been better characterized, like the α4β2 and α2β2 subunits, indicate that the most likely functional receptors would be $\alpha3_{(2)}\beta2_{(3)}$ or $\alpha3_{(3)}\beta2_{(2)}$ (Lukas 1988, Moroni et al., 2008, Wu et al., 2006, Zwart et al., 2008). Other stoichiometries are possible, but less likely. In addition, the α3β2 nAChR receptors would likely incorporate additional nAChR subunits such as the α5 subunit – further complicating the native subtypes of the receptor (ChavezNoriega et al., 1997, Wada et al., 1989).

The results of our work quantifying the nAChR subunits mRNAs revealed a highly heterogeneous population of nAChR subunit mRNAs. Furthermore, the α3 subunit is very limited in its expression in other brain regions, possibly making the α3β2 nAChR a valuable therapeutic target for cognitive diseases. Targeting the α3β2 may result in fewer undesired effects while still achieving cognitive improvements. Therefore, we sought to characterize the α3β2 nAChR as a potentially important receptor in hippocampal circuitry.

We characterized this novel receptor—the α3β2—in a simplified cell expression system. We used *Xenopus laevis* oocytes because they are extremely large cells, and when injected with foreign mRNA can produce many channels (i.e., large currents). Additionally, *Xenopus laevis* oocytes do not express native acetylcholine receptors. Also, since these oocytes allow for easier access to the cell surface we can better analyze the ion channel kinetics than neurons in brain slices. The time required for a solution to travel through brain tissue to the channel of interest is not as precise making the interpretation of kinetic data more difficult (Charpantier et al., 2005, ChavezNoriega et al., 1997, Dash, Bhakta, Chang, & Lukas, 2012, Ruud & Henk P. M. Vijverberg Research Institute of Toxicology, 1998).

Previous work has shown that agonists of nAChRs, like nicotine, can improve cognition in low-doses (Houezec, 1993, Levin, 2002, Sacco, 2004). Conversely, nAChR antagonists impair cognition (Levin, 2002). Additionally, both the α7 and β2 knockout mice show impairment in working memory (Fernandes, 2006, Hoyle, 2006, Levin, 2009). Furthermore, a genome-wide association study, also known as GWAS, shows that the β4 subunit is related to attention function in attention deficit hyperactive disorder. Chapter 3 will highlight a new class of drugs targeting nAChR called positive allosteric modulators. They are not agonists but, do

cause an increase in receptor conductance upon activation. This type of modulation may improve cognition like nAChR agonists.

One of the potential therapeutic implications for understanding the role of neuronal nAChRs in hippocampal interneurons is Alzheimer's Disease (AD). The neurons that degenerate first in AD are cholinergic neurons that have synapses with the GABAergic interneurons of the hippocampus (Liu et al., 2009). Since the GABAergic interneurons receive signaling from the cholinergic neurons, the GABAergic neurons contain nAChRs and are the population of neurons analyzed in Chapter 1. The International Alzheimer's Association reports that currently 5 million Americans are living with AD and the number continues to rise. More people die annually of AD than breast cancer and prostate cancer combined, making it the 6th leading cause of death in the United States. The disease impacts the individual as well as the caregivers, the family, and their communities. With years of research dedicated to heart disease and cancer, the disease prevalence of both heart disease and cancer have declined and treatment has improved. The hope is that with continued research in AD we can turn the tide of disease progression and improve treatment options as well.

One of the first signs of AD is memory loss. Unfortunately, when memory loss is first observed, AD has been present for years and has progressed significantly (Mattson, 2004). At this stage of disease, there is little that can be done to halt disease progression or improve quality of life (Corbett, Smith, & Ballard, 2012, Mattson, 2004). Of the treatment options currently available, there is little, if any improvement, for up to six months before improvement becomes negligible.

The most promising method of nAChR targeted therapy in the treatment of cognitive disorders is allosteric modulation. Allosteric modulators bind to a distinct site from the ACh

binding site, and cannot activate the receptor independently. Allosteric modulators require both the binding of the modulator and a ligand to elicit an effect. Allosteric modulation can be positive, negative, or silent. With the binding of a ligand, positive allosteric modulators increase the potentiation, or current, of the electrical signal. Negative allosteric modulators inhibit the electrical signal, but only in the presence of a ligand. Silent allosteric modulators do not potentiate or inhibit the current, but will remove the effect of a positive or negative allosteric modulator.

To further characterize nAChR subtypes, we used positive allosteric modulators to differentiate α7 and α7β2. The most widely characterized nAChR subtype is the homomeric α7. Recent evidence highlights the presence of α7β2 throughout the brain (Moretti, 2014). However, during whole cell, and even single channel recordings, it is extremely difficult to differentiate the subtypes from one another. There is no reliable method in whole cell patch clamp experiments to differentiate using current kinetic analysis or pharmacology. In Chapter 3, we characterize the different effect 3-furan-2-yl-N-p-tolyl-acrylamide (PAM-2) has on α7 and α7β2. Although there are many similar PAM-2 effects on each subtype, we do demonstrate at least 2 ways that PAM-2 can be used to differentiate the α7 from the α7β2.

In conclusion, the following experiments predict possible nAChR subtypes that may be found in hippocampal interneurons and differentiate between subtypes of the α3β2 nAChR. Additionally, PAM-2 may be a promising drug in the treatment of cognitive disorders as it greatly potentiates the conductance of α7* nAChR. Furthermore, we introduce at least 2 ways PAM-2 can be used to differentiate α7 and α7β2 nAChRs.

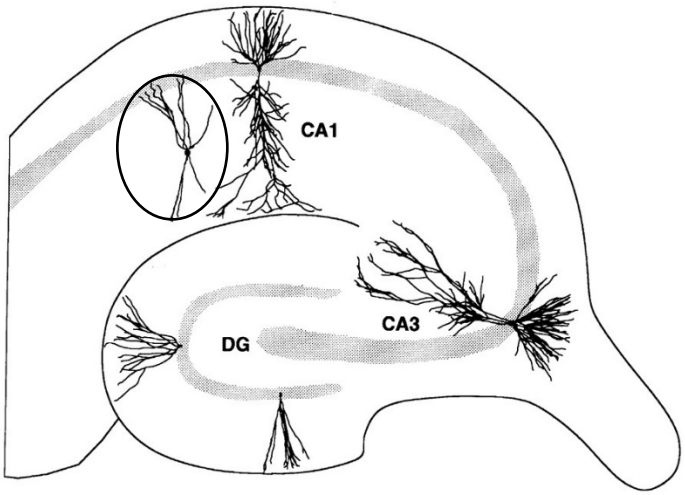

Figure I.1: The Cellular Components of Each Region of the Hippocampus. Specifically, the pyramidal neurons of the CA3 and CA1 regions and the interneurons of the CA1.

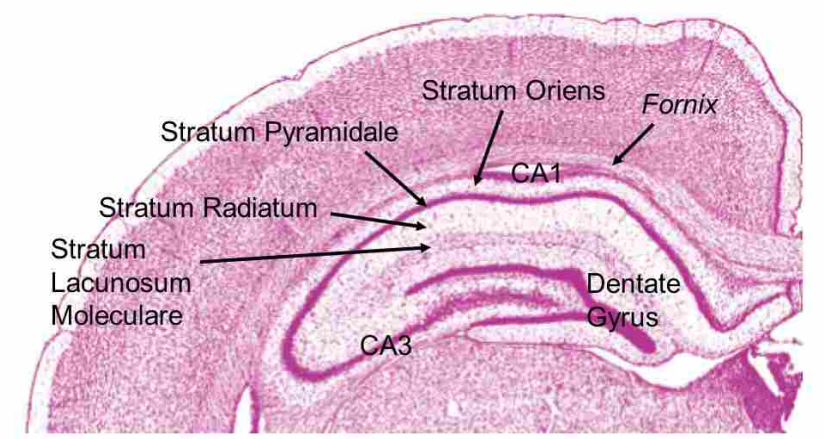

Figure I.2: The Cellular Layers Within the CA1 Region of the Hippocampus.

References

Charpantier, E., Wiesner, A., Huh, K.-H., Ogier, R., Hoda, J.-C., Allaman, G., Fuhrer, C. (2005). a7 Neuronal Nicotinic Acetylcholine Receptors Are Negatively Regulated by Tyrosine Phosphorylation and Src-Family Kinases. *The Journal of Neuroscience, 25*(43), 9836-9849. doi: 10.1523/JNEUROSCI.3497-05.2005

ChavezNoriega, L. E., Crona, J. H., Washburn, M. S., Urrutia, A., Elliott, K. J., & Johnson, E. C. (1997). Pharmacological characterization of recombinant human neuronal nicotinic acetylcholine receptors h alpha 2 beta 2, h alpha 2 beta 4, h alpha 3 beta 2, h alpha 3 beta 4, h alpha 4 beta 2, h alpha 4 beta 4 and h alpha 7 expressed in Xenopus oocytes. *Journal of Pharmacology and Experimental Therapeutics, 280*(1), 346-356.

Corbett, A., Smith, J., & Ballard, C. (2012). New and emerging treatments for Alzheimer's disease. *Expert Review of Neurotherapeutics, 12*(5), 535-543. doi: 10.1586/ERN.12.43

Dash, B., Bhakta, M., Chang, Y., & Lukas, R. J. (2012). Modulation of recombinant, alpha 2(*), alpha 3(*)or alpha 4(*)-nicotinic acetylcholine receptor (nAChR) function by nAChR beta 3 subunits. *J Neurochem, 121*(3), 349-361. doi: 10.1111/j.1471-4159.2012.07685.x

Fernandes, C, Hoyle, E, Dempster, E, Schalkwyk, LC, Collier, DA (2006). Performance deficit of α7 nicotinic receptor knockout mice in a delayed matching-to-place task suggests a mild impairment of working/episodic-like memory. Genes, Brain and Behavior. 5:433-440.

Graham, A. J., Ray, M. A., Perry, E. K., Jaros, E., Perry, R. H., Volsen, S. G., . . . Court, J. A. (2003). Differential nicotinic acetylcholine receptor subunit expression in the human hippocampus. *Journal of chemical neuroanatomy, 25*(2), 97-113. doi: 10.1016/S0891-0618(02)00100-X

Grybko, M., Sharma, G., & Vijayaraghavan, S. (2010). Functional Distribution of Nicotinic Receptors in CA3 Region of the Hippocampus. *Journal of Molecular Neuroscience, 40*(1-2), 114-120. doi: 10.1007/s12031-009-9266-8

Hanslmayr, S (2012). Oscillatory power decreases and long-term memory: the information via desynchronization hypothesis. Front. Hum. Neurosci. 6:74.

Houezec, JL, Halliday, R, Benowitz, N, Callaway, E, Naylor, H, Herzig, K (1993). A low dose of subcutaneous nicotine improves information processing in non-smokers. Psychopharmacology. 114:628-634.

Hoyle, E, Genn, RF, Fernandes, C, Stolerman, IP (2006). Impaired Performance of alpha 7 nicotinic receptor knockout mice in the five-choice serial reaciton time task. Psychopharmacology. 189:211-223.

Levin, E (2002). Nicotinic receptor subtypes and cognitive function. Developmental Neurobiology. 53:633-640.

Levin, E, Petro, A, Rezvani, AH, Pollard, N, Christopher, NC, Strauss, M, Avery, J, Nicholson, J, Rose, JE (2009). Nicotinic α7- or β2 containing receptor knockout: Effects on radial-arm maze learning and long-term nicotine consumption in mice. Behavioral Brain Research. 196:207-213.

Liu, Q., Huang, Y., Xue, F., Simard, A., DeChon, J., Li, G., . . . Wu, J. (2009). A novel nicotinic acetylcholine receptor subtype in basal forebrain cholinergic neurons with high sensitivity to amyloid peptides. *J Neurosci, 29*(4), 918-929. doi: 10.1523/JNEUROSCI.3952-08.2009 [doi]

Lukas, R. (1988). Evidence for Functional and Structural Diversity of Nicotinic Acetylcholine Receptors. In F. Clementi, C. Gotti & E. Sher (Eds.), *Nicotinic Acetylcholine Receptors in the Nervous System* (Vol. 25, pp. 61-75): Springer Berlin Heidelberg.

Mattson, M. P. (2004). Pathways towards and away from Alzheimer's disease. *Nature, 430*(7000), 631-639. doi: 10.1038/nature02621

Moretti, M, Zoli, M, George, AA, Lukas, RJ, Pistillo, F, Maskos, U, Whiteaker, P, Gotti, C (2014). The Novel a7b2-Nicotinic Acetylcholine Receptor Subtype Is Expressed in Mouse and Human Basal Forebrain: Biochemical and Pharmacological Characterization. Molecular Pharmacology. 86:306-317.

Mitchell, JF (2009). Spatial attention decorrelates intrinsic activity fluctuations in macaque area V4. Neuron. 63:879–888.

Moroni, M., Vijayan, R., Carbone, A., Zwart, R., Biggin, P. C., & Bermudez, I. (2008). Non-agonist-binding subunit interfaces confer distinct functional signatures to the alternate stoichiometries of the alpha4beta2 nicotinic receptor: an alpha4-alpha4 interface is required for Zn2+ potentiation. *J Neurosci, 28*(27), 6884-6894. doi: 10.1523/JNEUROSCI.1228-08.2008

Rubboli, F., Court, J. A., Sala, C., Morris, C., Perry, E., & Clementi, F. (1994). Distribution of Neuronal Nicotinic Receptor Subunits in Human Brain. *Neurochemistry international, 25*(1), 69-71. doi: 10.1016/0197-0186(94)90055-8

Ruud, Z., & Henk P. M. Vijverberg Research Institute of Toxicology, U. U. U. T. N. (1998). Four Pharmacologically Distinct Subtypes of α4β2 Nicotinic Acetylcholine Receptor Expressed in Xenopus laevisOocytes. *Molecular Pharmacology, 54*(6).

Sacco, KA, Bannon, KL, George, TP (2004). Nicotinic receptor mechanisms and cognition in normal states and neuropsychiatric disorders. J Psychopharmacol. 18:457-474.

Sargent, P. B. (1993). The Diversity of Neuronal Nicotinic Acetylcholine-Receptors. *Annual Review of Neuroscience, 16*, 403-443. doi: 10.1146/annurev.ne.16.030193.002155

Son, J.-H., & Winzer-Serhan, U. H. (2006). Postnatal expression of alpha 2 nicotinic acetylcholine receptor subunit mRNA in developing cortex and hippocampus. *Journal of chemical neuroanatomy, 32*(2-4), 179-190. doi: 10.1016/j.jchemneu.2006.09.001

Wada, E., Wada, K., Boulter, J., Deneris, E., Heinemann, S., Patrick, J., & Swanson, L. W. (1989). Distribution of Alpha-2, Alpha-3, Alpha-4, and Beta-2 Neuronal Nicotinic Receptor Subunit Messenger-Rnas in the Central Nervous-System - a Hybridization Histochemical-Study in the Rat. *Journal of Comparative Neurology, 284*(2), 314-335. doi: 10.1002/cne.902840212

Ward, Lawrence M (2003). Synchronous neural oscillations and cognitive processes. Trends in Cognitive Sciences. 7:553-559.

Wu, J., Liu, Q., Yu, K., Hu, J., Kuo, Y. P., Segerberg, M., . . . Lukas, R. J. (2006). Roles of nicotinic acetylcholine receptor beta subunits in function of human alpha4-containing nicotinic receptors. *The Journal of physiology, 576*(Pt 1), 103-118. doi: jphysiol.2006.114645 [pii]

Zwart, R., Carbone, A. L., Moroni, M., Bermudez, I., Mogg, A. J., Folly, E. A., . . . Sher, E. (2008). Sazetidine-A is a potent and selective agonist at native and recombinant alpha 4 beta 2 nicotinic acetylcholine receptors. *Mol Pharmacol, 73*(6), 1838-1843. doi: 10.1124/mol.108.045104

CHAPTER 1: Expression of nAChR mRNA in Rat Hippocampal Interneurons

Doris C Jackson, Spencer Thompson, Richard M Burgon, Sterling N Sudweeks.

Department of Physiology and Developmental Biology, College of Life Sciences,

Brigham Young University, Provo, UT, USA

Address correspondence to:

Sterling Sudweeks, PhD, Department of Physiology and Developmental Biology,

Brigham Young University

3045 Life Sciences Building, Provo, UT 84602, Tel: (801)422-8752,

Sterling_Sudweeks@byu.edu

This work was supported by the NIH grant 5K22ES011639 - NIEHS/NIH and internal funding from Brigham Young University.

Key words: neuronal nicotinic acetylcholine receptors, hippocampus, alpha 3, beta 2, stoichiometry, single cell real-time (q-PCR), mRNA

No conflicts of interest to be reported.

TABLES, FIGURES AND LEGENDS: 4 Figures, 7 Tables (2 included in Methods section)

AUTHOR CONTRIBUTIONS: Conceived and designed experiments: RB SS. Performed the experiments: RB SS. Analyzed the data: DJ ST RB SS. Contributed reagents/materials/analysis tools: SS. Composition of the paper: DJ RB SS.

Abstract

Pyramidal cells are the most populous neurons in the hippocampus, yet they are controlled by a sparse population of inhibitory interneurons. However, the hippocampal interneurons are not well understood and are quite diverse on many fronts. Using qPCR of CA1 hippocampal interneurons, we quantified mRNA subunits expression and detailed possible combinations. We also highlighted differences found between the *stratum oriens* and the *stratum radiatum*.

We show that almost all interneurons in the CA1 of the rat hippocampus contain detectable levels of nicotinic acetylcholine receptor (nAChR) mRNA. Our research highlights the complexity of the CA1 nAChR population. Interestingly, the α3 nAChR subunit is one of the highest expressed subunit mRNAs while the α4 is one of the least likely subunits to be detected in the CA1 interneurons. Not as surprisingly, the β2 nAChR subunit is the other highest expressed mRNA. In addition, the subunit co-expression Pearson correlation values highlight key differences between the *stratum oriens* and the *stratum radiatum.* Our estimation is that there are approximately 119 different mRNA combinations that are likely in rat CA1 interneurons.

These results provide a new and valid avenue in cognitive therapies by targeting α3 containing nAChRs. Currently, the nAChR targeted cognitive therapies focus on the α4β2 nAChR and the α7 nAChR. This new insight may improve therapies for Alzheimer's Disease, Autism Spectrum Disorder, Dementia, and Attention-Deficit Hyperactivity Disorder.

Introduction

Understanding the scope of expression of nicotinic acetylcholine receptors (nAChRs) within the interneurons of the hippocampus would lend great insight for cognitive therapies used in Alzheimer's Disease (AD), Attention-Deficit Hyperactivity Disorder (ADHD), Autism Spectrum Disorder (ASD), and Post-Traumatic Stress Disorder (PTSD). The GABAergic interneurons are controlled by nAChRs found on their dendrites, soma, and on the axon terminal (Jones, 1997). These GABAergic neurons control the synchronous firing of the highly populated pyramidal neurons (Cobb, 2005). Therefore, modulation of the nAChRs contributes to the regulation of glutamatergic pyramidal neurons (Ji, 2000).

When considering our electrophysiological results, we suspect that the nAChR assembly is made of various combinations of eight subunits: α2-α5, α7, and β2-β4. The nAChRs in hippocampal interneurons are in a key position to modulate cognitive functions because interneurons play a major role in coordinating hippocampal activity, reviewed in Freund (1996). Accordingly, nAChRs have been implicated in diseases affecting cognition, of which Alzheimer's disease is the most principal (Gray, 1996).

Compositional variations of nAChR subunits within the hippocampus have been shown to mediate nicotinic receptor kinetics (Sudweeks, 2000) and enable plasticity in interneuron function (Alkondon, 2001). Of the neuronal nAChR subunits, α7 has been studied most extensively. Use of subunit-specific antagonists to α7 homomeric receptors (either α-bungarotoxin or methyllycaconitine) has provided an important tool in isolating contributions of this subunit in receptor kinetics, physiology, and disease. High-affinity binding, for example, has been shown for α7 to β-amyloid, a peptide implicated in Alzheimer's disease (Wang, 2000), which binding results in the blockage of current flow through the nAChR (Pettit, 2001). There

are many functional roles (and resultant diseases or disorders) attributed to the α7 nAChR (within and outside of the hippocampus) including depression, cognition, gastric cancer, and memory (Zhang, 2016, Chen, 2015).

The paucity of other highly subunit-specific antagonists of the nAChR has impeded progress in characterizing the roles of other subunit combinations to the extent of α7. Until more subunit-specific agents are discovered, other means for characterizing the individual nAChR subunits must be utilized. On-going studies to characterize the extent of nAChR subunit co-expression within individual neurons may identify trends shared by functionally distinct networks or subpopulations of neurons (Jones, 1999). In addition, the identification of co-expression trends between nAChR subunits and other neurochemical markers may facilitate more comprehensive characterization of the nAChR and of neuronal subpopulations. Therefore, we sought to differentiate and classify hippocampal interneuron expression of neuronal nAChR subunit mRNA through single-cell qPCR.

Methods

Slice Preparation

All CA1 hippocampal slice and interneuron aspiration experiments were prepared and carried out as described previously (Sudweeks, 2000). In brief, to obtain the interneurons, coronal brain slices (either 300 or 350 μm thick) were made from 8 to 23 day old Wistar rats using a Vibratome 1000-Plus. The slices were cut in ice-cold oxygenated (95% O_2, 5% CO_2) artificial cerebrospinal fluid and placed in room-temperature oxygenated ACSF for at least 30 minutes prior to placing in microscope recording chamber. IUCAC approval was obtained for all animal experiments.

Cytoplasm Aspiration

An upright microscope with infrared light was used to individual hippocampal interneurons from the Amun's horn (CA1) *stratum oriens* and *stratum radiatum* were visually identified as neurons outside the pyramidal cell layer. Interneurons were then aspirated into a standard whole-cell patch-clamp pipette containing 5 µL Intracellular Fluid as described previously (Sudweeks, 2000).

Electrophysiology

A whole-cell recording configuration of the interneuron was obtained in voltage-clamp mode prior to cytoplasm aspiration. Interneuron membrane potentials were held at -70mV. Where recordings were performed, responses were induced by the gravity flow application of 1 mM ACh for 1 second, using an Axon 200. Whole-cell recordings were filtered at 1 kHz, and sampled at 100 Hz, using the pCLAMP Clampex software (version 7.01.31, Axon Instruments). Acetylcholine (ACh) was applied using an electronically triggered valve (General Valve Co., Fairfield, NJ, USA) connected to a synthetic quartz tube (inner diameter of 320 µm, Polymicro Technologies Inc., Phoenix, AZ, USA) placed approximately 90—120 µm from the cell body. The flow rate for the ACh application from the gravity flow perfusion system was 250 µl min. A washout period of at least 3 min was included between subsequent recordings.

Primers and Probes

The primers and probes were designed using either Vector NTI version 7.0 (Invitrogen) or Primer Express version 2.0 (ABI Prism) software.

RT Reaction

A cDNA library representing each CA1 hippocampal interneuron was made by running a reverse transcription reaction using BIORAD iScript cDNA Synthesis Kit with a final volume of 10 µl.

Multiplex Reaction and Real-time Quantitative PCR

A multiplex PCR reaction was run (15 cycles) for each aspirated interneuron using all neuronal nAChR primers and the primer for 18s rRNA (see Table 1 and Table 2) with a final volume of 75 µl. The α6 subunit was not examined because initial experiments showed no detection of this subunit in any hippocampal interneurons examined. The multiplex reaction was run using Platinum® *Taq* DNA Polymerase and PCR nucleotides (10mM). A second round of PCR was run (60 cycles) for each specific target (18s, α2–α5, α7, β2, β3, β4) using an ABI 7000 Sequence Detection System utilizing BIORAD iTaq Supermix with ROX. Cycle threshold values for each target were compared to the reference gene 18s for analysis (more in Real-Time Analysis).

Standard curves (efficiency tests) for each cDNA target were developed by running 60-cycle real-time quantitative PCR assays on positive controls (rat whole-brain homogenate) for six known concentrations (100, 33.3, 10, 3.33, 1, 0.333 ng cDNA/µL). Two types of negative controls were run as well. First, we aspirated extracellular fluid and tested for the presence of nAChR mRNA. Any subunit that had a cycle threshold greater than the mRNA detected in the extracellular fluid was omitted from that interneuron's profile. The second negative control was to simply run the quantitative PCR assay with no cellular components. This was used to detect any mRNA contaminants.

To correct the standard curves for efficiency so all mRNAs were equally efficient, upstream (primer +) and downstream (primer –) primer concentrations were adjusted to optimize amplification. The efficiency of the amplification reaction is calculated using the slope of the log(concentration) vs. CT plot. The formula for PCR efficiency $= 10^{(-1/slope)} - 1$ (Bustin, 2004). Reaction efficiencies were run in triplicate and the amplification efficiencies were compared using an ANOVA to determine if there were significant differences between any of the primer/probe sets (18s, α2–α5, α7, β2, β3, β4).

To calculate primer efficiencies, triplicate reactions of each cDNA target were averaged and a linear regression equation was calculated (SLOPE function, Microsoft Excel) of the CT values corresponding to the six known concentrations (100, 33.3, 10, 3.33, 1, 0.333 ng cDNA/μL) in the standard curve primer efficiency tests. The PCR efficiency was then determined by incorporating the slope of the linear equation using the formula described above (see Multiplex Reaction and Real-time Quantitative PCR) (Burgon 2005).

Data and Statistical Analysis

Following the real-time quantitative PCR on hippocampal interneurons, raw fluorescence (ΔRn) values across 60 cycles were curve-fit using a Boltzmann Sigmoidal function with an output of either 2000 or 4000 data points in the new curve using GraphPad v. 4.0 software. The second derivative graph for the curve-fit data was then determined, also using Graphpad. The cycle threshold (CT) value used was the cycle number of the maximum second derivative value of the fluorescence.

For comparison of expression levels between cDNA targets, fold expression values from the triplicate CT averages were calculated as compared to the lowest level of cDNA detection using the $2^{-\Delta\Delta Ct}$ method described by Livak (2001). Significance between relative levels of

mRNA expression was calculated by comparing mean fold expression values using a Mann-Whitney test (calculated using InStat ver. 3.05). Blinding was not used because it is not an appropriate approach to mRNA expression analysis or qPCR.

For the qPCR analysis, the proportion of neurons expressing a particular mRNA is equal to the number of observed positive neurons divided by the total number of neurons analyzed for that mRNA transcript. The standard error of the proportion (S.E.P.) was calculated for each mRNA transcript examined using the following formula (Moore, 1995):

Equation 1:

$$S.E.P. = \sqrt{\frac{p(1-p)}{n}}$$

where p = the proportion of neurons in the population with detectable expression, and n = the number of neurons in that population.

To test for significant expression of each mRNA when compared to the background qPCR calculated false positive proportion, and to compare the mRNA expression of the two populations with functional nAChR responses, we used a *z*-test for comparing two sample proportions. The formula is (Moore and McCabe, 1995):

Equation 2:

$$z = \frac{\hat{p}_1 - \hat{p}_2}{\sqrt{\hat{p}(1-\hat{p})\left(\frac{1}{n_1} + \frac{1}{n_2}\right)}}$$

where $\hat{p}_x$ is the proportion of cells with detected expression in each population, n_x is the number of neurones examined in that population, and $\hat{p}$ (no subscript) is the pooled estimate of $\hat{p}_1$ and $\hat{p}_2$. The calculation for $\hat{p}$ is (Moore and McCabe, 1995):

Equation 3:

$$\hat{p} = \frac{\text{Total count of successes in both samples}}{\text{Total count of observations in both samples combined}}$$

Each *z*-value was compared to a normal curve using the Excel NORMSDIST(absolute value of *z*) function, which gives the probability (*p*) that the two proportions are equal. The proportions were considered significantly different when $p \leq 0.01$.

Materials

Artificial cerebrospinal fluid: 124 NaCl, 2 KCl, 1 NaH_2PO_4, 26 $NaHCO_3$, 11 Glucose, 2 $CaCl_2$, 1 $MgSO_4$ (in mM): Sigma-Aldrich, 3050 Spruce Street, St. Louis, MO 63103 USA.

All primers, all probes, Vector NTI version 7.0, Platinum® *Taq* DNA Polymerase, PCR nucleotides: Invitrogen/Thermo Fisher Scientific, 168 Third Avenue, Waltham, MA USA 02451 USA.

Vibratome 1000-Plus: Pelco, Ted Pella, Inc., P.O. Box 492477, Redding, CA 96049-2477 USA.

Nikon E600-FN Microscope: A.G. Heinz, 20291 Valencia Circle, Lake Forest, CA 92630-8155 USA.

Borosilicate capillaries: Harvard Apparatus, 84 October Hill Road, Holliston, Massachusetts 01746 USA.

Intracellular Fluid: 10 $MgCl_2$, 0.1 $CaCl_2$, 1 EGTA, 10 HEPES, 135 K-Gluconate, and 2 Na-ATP (in mM): Sigma-Aldrich, 3050 Spruce Street, St. Louis, MO 63103 USA.

Multiclamp 700A: Axon Instruments/Molecular Devices, 1311 Orleans Drive, Sunnyvale, CA 94089 USA.

ABI 7000 Sequence Detection System and Primer Express version 2.0, ABI Prism: Applied Biosystems, 850 Lincoln Centre Drive, Foster City, CA 94404 USA.

iScript cDNA Synthesis Kit and iTaq Supermix with ROX: BIORAD, 2000 Alfred Nobel Drive, Hercules, California 94547 USA.

GraphPad v. 4.0 and GraphPad Instat v. 3.05: GraphPad Software, Inc., 7825 Fay Avenue, Suite 230, La Jolla, CA 92037 USA.

Microsoft Excel: Microsoft Building 92, 15010 NE 36th St, WA 98052-6399 USA.

Results

Our results highlight the heterogeneity of nAChR mRNAs in the hippocampal interneurons as demonstrated by the variety of kinetic responses during whole-cell electrophysiology and ACh applications (Figure 1). We sought to dissect the population of nAChR subtypes by through single cell real-time-PCR (qPCR) of the *stratum oriens* and *stratum radiatum.* Of the 93 cells analyzed, 83, or 89.2%, expressed detectable nAChR mRNA. Figure 2 quantifies the number of mRNA subunits found in each cell. We found that each cell had an

average of 3.8 (± 0.22 S.E.M.) mRNA subunits detected with a slight kurtosis and skewness to the left.

The simplified summary of expression is given in Table 3 which reports the proportion of expression of the number of cells in which at least one subunit was expressed divided by the total number of cells expressing at least one nAChR mRNA subunit (n=83). Somewhat surprisingly, the α3 subunit was one of the most common subunits expressed, found in 54% of the interneurons examined. In addition, the α4 subunit had the lowest expression of the subunits analyzed (27%). Figure 3 shows the relative expression of each subunit as histograms normalized to the median expression level for all nAChR subunits detected. This result highlights the high level of expression and the larger number of cells that express the α3, β2, and α5 mRNA subunits. The α4 histogram reiterates the small number of cells expressing α4, but adds that the relative expression levels are low as well when compared to the average fold expression (Figure 3).

To extend the proportion analysis further, we calculated the most commonly co-expressed pairs of subunits. The two subunits that co-express at the highest rate are the α3 and β2 (n=69, cells expressing at least 2 subunits) (Table 4).

A Mann-Whitney test of all subunits examined showed that only the α3 had a significantly different relative expression in the *stratum oriens* compared to the *stratum radiatum*, with the *stratum oriens* having overall larger values of expression ($p = 0.0165$, α3 *stratum oriens*, mean±SEM = 3.47±1.11, α3 *stratum radiatum*, mean±SEM = 1.24±0.21). The α2 subunit and α4 subunit had p-values that were not quite significant, but a larger sample size may reveal the true trend (α2 $p=0.0603$, *stratum oriens* larger; α4 $p=0.0945$, *stratum radiatum* larger).

In addition, we calculated the Pearson r values for subunit co-expression regardless of location in the *stratum oriens* or *stratum radiatum* (Figure 4.A). Our results show that all of the β mRNA subunits are highly correlated with each other. Also, the α5 and α3 fold expression levels are moderately correlated with the β2 mRNA subunit (Figure 4.A). The α5 mRNA subunit is also moderately correlated with the β4 subunit (Figure 4.A). Lastly, no other subunits appear to be correlated regarding mRNA expression levels.

We then assessed all the Pearson r values dependent on area. The *stratum radiatum* results show a wide range in correlation values (Figure 4.B). The range is similar to the *stratum oriens*; however, the *stratum oriens* appears to have two groupings (those not correlated and those with very strong correlations, Figure 4.B). Therefore, we tested the Pearson r correlation values for significance across the *stratum oriens* and *stratum radiatum*. Table 5 summarizes our results. We only tested values greater than 0.9 in either the *stratum oriens* or *stratum radiatum*. Surprisingly, all our tests show significance p-values ($p<0.05$, two-tailed).

In addition to 2-way subunit combinations, we also analyzed all 3-way, 4-way, 5-way, 6-way, 7-way, and 8-way combinations that were observed. The expected values were calculated by simply multiplying the portion of expression for each subunit in the combination (values from Table 3). As an example, the expected proportion co-expressing α2 + α3 would be 0.37 X 0.54 = 0.2, or 20%. The actual proportion of cells observed with both α2 + α3 was 0.23. Therefore, the Observed/Expected value is 1.1, very close to what would be expected. A *z*-test of two proportions indicated that 63 different combinations appeared more often than expected (significant if $p<0.01$) (Table 6).

Table 7 lists all the mRNA subunit combinations we observed, as well as their location in either the *stratum oriens* or *stratum radiatum*. The two most common combinations were

α3α4α5α7β2and α3α5β2β3β4. The former occurred 4 times solely in the *stratum radiatum* while the later appear 2 times in the *stratum radiatum* and 2 times in the *stratum oriens*.

Our analysis revealed 59 combinations of mRNA subunit expression in the 93 cells tested. Of the 93 cells, 10 cells did not have detectable levels of expression and 42 cells had a unique combination of mRNA subunits. Using the coverage estimation calculation provided by Chao and Lee (1992), we estimated that we had 49.4% coverage.

Estimated sample coverage = 1 - (# single observations / # of total observations)

= 1 – (42/83)

= 0.494

This implies that our data collection only accounted for about one-half of all the possible mRNA subunit combinations expressed in CA1 interneurons. Chao and Lee also provide a way to calculate the estimated number of possible combinations.

= (# of combinations observed) / coverage

= 59 / 0.494

=119.4

Therefore, there are likely at least 119 different mRNA subunit combinations that could be found in the CA1 of the rat hippocampus.

Discussion

Our results are not able to completely differentiate nAChR mRNA subunit expression between the *stratum oriens* and the *stratum radiatum.* However, they do bring to light some interesting conclusions. Namely, the high rate of expression of the α3 mRNA subunit and the overall diversity with an estimated 119 different combinations of mRNA subunit expression.

We would like to add to these results and explore changes in subunit concentrations during development (Alkondon, 2007, Gahring, 2005, Rogers, 1998, Winzer-Serhan, 2005). The role of nAChRs in development may be quite diverse considering that nAChRs are found on glial cells, pyramidal cells, and neurons (Didier, 1995). Therefore, we feel it imperative that future studies should focus on understanding early development of the hippocampus. This could improve treatment of ADHD or early interventional therapies for ASD. Likewise, understanding normal aging as opposed to dementia or AD may improve targeted therapies since some nAChR subtypes have been shown to be sensitive to β-amyloid (Pettit, 2001, Wang, 2000).

Previous studies reporting quantitative mRNA expression between *strata radiatum* and *oriens* found higher proportion of interneurons expressing α2 in the *stratum oriens* and a higher proportion of interneurons expressing α5, β2, and β4 in the *stratum radiatum* (Sudweeks 2000, Khiroug, 2004). This study, however, indicated no significant difference in the detection of these subunits between the two strata (*stratum radiatum*: n=45 samples each ran in triplicate, *stratum oriens*: n=38 samples each ran in triplicate). Yet, we did find a significant difference in α3 expression between the two strata. These discrepancies may have resulted in differences in the number of PCR cycles performed. In the study mentioned above, sixty-five cycles were run on their target transcripts, while we measured amplification across seventy-five cycles of PCR. Running a higher number of amplification cycles may have afforded us a more sensitive analysis of the target mRNAs. Additionally, with the high level of diversity demonstrated in the hippocampal interneurons, it should not be surprising that different samples would highlight different results.

Considering that only the α3 mRNA subunit had statistically different expression levels in the *stratum oriens* and *stratum radiatum* we found the results in Figure 4 and Table 5 quite

surprising. We expected the correlations between regions to not be statistically different considering the expression levels were not different (except α3). This may suggest different functional roles of the *stratum oriens* and *stratum radiatum.* Figure 4.B showing more polarized groupings of the Pearson r values in the *stratum oriens* could suggest a more selective expression of subtypes than the *stratum radiatum* which shows a broader range its Pearson r values. This could indicate a difference in the functional properties of nAChRs in each strata.

One interesting result is that of those interneurons that expressed only 1 subunit the majority of those interneurons expressed the α7 mRNA. Since the α7 subunit can form a homomer those results are expected. However, there were a few interneurons with sole detection of β2, β4, or the α5 mRNA subunit. However, none of the other subunits investigated here form homomeric channels. The results are likely the result of the snapshot view of mRNA levels at any one time in the interneuron. mRNA levels likely rise and fall in response to cellular communication.

The high levels of co-expression of α3 and β2 were somewhat surprising because the α3 has only been shown to be in the medial habenula and the sympathetic ganglion (Yeh, 2001). However, our results suggest that that the α3 subunit has a significant role in hippocampal interneurons. Since the α3 and β2 subunits had the highest overall expression and the highest co-expression rate, it highlights the importance of further characterizing the α3β2 nAChR (Jackson, 2017).

We suggest that the α3β2, and even the α3β4 nAChRs, may play a more important role in the hippocampus than the α4β2 nAChRs. Our results also suggest that α3 containing cells frequently expressed α5 mRNA as well. This may suggest a likely incorporation of α5 subunits into α3 containing nAChRs. Not as surprising were the relatively abundant α7 mRNA

expression results. They appear to be fairly average in the relative expression levels and the proportion of expression. This validates the use of α7 targeted therapies. Considering that α3 is found in very few regions of the brain and α7 has a more ubiquitous expression, α3 targeted therapies may prove effective (Vernallis, 1993, Ullian, 1997, Lindstrom, 1996, Yeh, 2001).

Future studies may include reconstituting the significant combinations of nAChR subunit co-expression (Table 4) into cellular expression systems such as *Xenopus laevis* oocytes. Studies using expression systems benefit from the finer controllability of diffusion rates and drug application concentrations versus interneurons within the brain slice. Findings from electrophysiological recordings in response to pharmacological application can then be used to elucidate the characteristics and contributions of the significant nAChR subunit co-expression combinations identified in this study (Table 4). These studies would then help us understand the role of nAChRs in modulating hippocampal function. Further pursing these results may identify networks or subpopulations in the hippocampus and throughout the CNS affected in the pathogenesis of neurodegenerative diseases and ultimately give rise to the discovery of treatments that prevent or abate these disorders. The results in this study are a gateway to the characterization of the diverse range of hippocampal nicotinic receptor subtypes.

Table 1.1: Summary of Amplicon Lengths (base pairs) and Oligo Sequences of the nAChR Subunit Probes Used in qPCR.

Real-time PCR probes	Length	Probe
nAChR β2 rat	77 bp	CCCAGCCAAGCCCTGCACTGAT
nAChR β3 rat	145 bp	AAGGACCCCATGGACCGCTTCT
nAChR β4 rat	72 bp	CTGGTCAGGGTCCCTCATCCCAG
nAChR α2 rat	103 bp	CTCCATGGCTCCCCGGATCTGAA
nAChR α3 rat	68 bp	TTGAACCTGCTCCCCAGGGTCATG
nAChR α4 rat	356 bp	TGGGTGAAGCAGGAGTGGCACGA
nAChR α5 rat	77 bp	TGTCTTTGCCATCAACATCCACCACC
nAChR α7 rat	214 bp	CAAGAGCTCCTGCTACATTGACGTTCGC
18s rRNA rat	133 bp	TGGAGCGATTTGTCTGGTTAATTCCGATAAC

Table 1.2: Summary of Oligo Sequences of the nAChR Subunit Primers (+ and -) Used in qPCR.

Real-time PCR primers	+ Primer	- Primer
nAChR β2 rat	CTGCGGCTGACCCATGTAC	TGGGCTCAGCTCGGAAAG
nAChR β3 rat	CCCGAGATGGCTTTGCAT	GGAAAGCGACCAGAACTCTTTC
nAChR β4 rat	CGTCCCGGTCTTGAAGTCA	CAGTATCAGCTGTGGCCAAGTG
nAChR α2 rat	TGCCCAGGTGGCTGATG	CATGTTAGTCTCTAGCCAATGG TATGA
nAChR α3 rat	TTGGGTCAAGGCCGTGTT	TCACCACTGGTCGGCCTAGT
nAChR α4 rat	CCAGATGATGACAACCAACG	CCACACGGCTATGAATGCTC
nAChR α5 rat	GATTTTCGTGACCCTATCCAT TATG	GCGTTGTGTGTGGAGGAAGA
nAChR α7 rat	TTGCCAGTATCTCCCTCCAG	CTTCTCATTCCTTTTGCCAG
18s rRNA rat	GTGCATGGCCGTTCTTAGTT G	GCCACTTGTCCCTCTAAGAAGT TG

Table 1.3: The Proportion of Cells Containing Each nAChR mRNA Subunit (n=93). Ten of the 93 interneurons tested did not contain detectable levels of any nAChR mRNA subunit analyzed.

Proportion of Cells containing each subunit	
Subunit	Proportion
α3	0.54
β2	0.54
α5	0.43
α7	0.42
β4	0.42
β3	0.40
α2	0.37
α4	0.27

Table 1.4: The Proportion of Subunit Co-expression for the Highest 8 Subunit Pairs (n=69, the number of cells that contained at least 2 mRNA subunits).

Subunit Co-expression of nAChR mRNA	
Percentage	Subunit Co-expression
52%	α3 and β2
49%	α3 and α5
44%	α7 and β2
42%	α5 and β2
41%	α3 and β4
41%	β2 and β4
39%	α3 and β3
38%	β2 and β3

Table 1.5: T-test for Pearson Correlation Coefficients for Subunit Co-expression in the *stratum oriens* and the *stratum radiatum*. The selected comparisons were done because at least one location (*oriens* or *radiatum*) had a Pearson correlation coefficient >0.90. All regions analyzed showed significance in at the 0.05 level using a two-tailed t-test.

Comparison of Pearson Correlation Coefficients				
subunit	subunit	*Stratum oriens*	*Stratum radiatum*	p-value
α3	α5	0.961	0.361	<0.0001
α3	β4	0.987	0.937	0.00527
α5	β2	0.996	0.053	<0.0001
α5	β3	0.986	0.858	<0.0001
α5	β4	0.926	0.118	<0.0001
β2	β3	0.989	0.428	<0.0001
β2	β4	0.944	0.759	0.00829
β3	β4	0.938	0.565	0.00022

Table 1.6: A Summary of all mRNA Subunit Combinations Observed More Often than Would be Expected (observed/expected>1). Expected values were calculated by multiplying the proportion values from Table 3.

Combination	Observed/Expected	Combination	Observed/Expected
α3+α5	1.6	α4+α5+α7+β2	4.1
α3+α4+α7	2.7	α4+α7+β2+β3	4.5
α3+α5+β2	2.2	α4+α7+β2+β4	3.4
α3+α5+β3	2.3	α4+α7+β3+β4	4.0
α3+α5+β4	2.3	α4+β2+β3+β4	3.1
α3+β2+β3	2.1	α5+α7+β2+β3	3.3
α3+β2+β4	2.0	α5+α7+β2+β4	2.6
α3+β3+β4	2.4	α5+α7+β3+β4	3.2
α4+α7+β2	3.0	α5+β2+β3+β4	3.9
β2+β3+β4	2.3	α7+β2+β3+β4	3.4
α2+α3+α5+β3	2.9	α2+α3+α7+β2+β3	4.9
α2+α3+α7+β2	2.4	α3+α4+α5+α7+β2	7.7
α2+α3+β2+β3	2.6	α3+α4+α7+β2+β3	6.6
α2+α4+α7+β2	3.9	α3+α4+α7+β2+β4	6.3
α2+α7+β2+β3	3.0	α3+α4+α7+β3+β4	7.4
α3+α4+α5+α7	4.1	α3+α4+β2+β3+β4	5.8
α3+α4+α5+β2	3.9	α3+α5+α7+β2+β3	5.7
α3+α4+α7+β2	4.6	α3+α5+α7+β2+β4	4.4
α3+α4+α7+β3	3.6	α3+α5+α7+β3+β4	6.0
α3+α4+α7+β4	3.4	α3+α5+β2+β3+β4	7.3
α3+α4+β2+β3	2.8	α3+α7+β2+β3+β4	6.4
α3+α4+β2+β4	3.3	α4+α7+β2+β3+β4	7.4
α3+α4+β3+β4	3.6	α5+α7+β2+β3+β4	6.0
α3+α5+α7+β2	3.3	α2+α3+α5+α7+β2+β3	8.5
α3+α5+α7+β3	3.1	α2+α3+α7+β2+β3+β4	8.7
α3+α5+β2+β3	3.5	α3+α4+α5+α7+β2+β3	11.6
α3+α5+β2+β4	3.5	α3+α4+α5+α7+β3+β4	12.4
α3+α5+β3+β4	4.5	α3+α4+α7+β2+β3+β4	13.8
α3+α7+β2+β3	3.3	α3+α5+α7+β2+β3+β4	11.1
α3+α7+β2+β4	2.7	α4+α5+α7+β2+β3+β4	12.4
α3+α7+β3+β4	3.4	α3+α4+α5+α7+β2+β3+β4	23.0
α3+β2+β3+β4	4.0		

Table 1.7: A List of All Observed Subunit mRNA Combinations by Location.

Combination	Number of Occurrences (Radiatum)	Number of Occurrences (Oriens)	Combination	Number of Occurrences (Radiatum)	Number of Occurrences (Oriens)
No nAChR mRNA	4	6	α2α4α7β2	-	1
α2	2	-	α2β2β3β4	1	-
α3	-	1	α3α4β2β4	1	-
α4	1	-	α3α5β2β4	-	2
α5	1	1	α3α7β2β3	-	1
α7	1	1	α3β2β3β4	-	1
β2	2	1	α4α5β2β4	-	1
β3	2	1	α4α7β2β3	1	-
α2α3	2	-	α5α7β2β3	1	-
α2α7	-	1	α5α7β2β4	1	-
α2β2	1	-	α2α3α4α5β 2	1	-
α2β4	2	-	α2α3α4α7β2	1	-
α3β4	-	1	α2α3α5β3β4	-	1
α4α7	1	-	α2α4α7β2β3	1	-
α5β4	1	-	α3α4α5α7β2	4	-
α7β3	1	-	α3α4α5β2β4	-	1
α7β4	1	-	α3α4α5β3β4	1	-
α2α3α5	1	-	α3α5β2β3β4	2	2
α2α3β2	-	1	α2α3α4α7β2β4	-	1
α2α7β2	-	1	α2α3α5α7β2β3	1	-
α2β3β4	1	1	α2α3α5β2β3β4	1	-
α3α4α7	-	1	α2α3α7β2β3β4	-	1
α3α5α7	2	-	α3α4α7β2β3β4	-	1
α3α5β2	1	-	α3α5α7β2β3β4	2	-
α3α5β3	1	-	α2α3α4α5α7β2β3	1	-
α3α7β3	-	1	α2α3α4α7β2β3β4	-	1
α7β2β4	1	1	α2α3α5α7β2β3β4	-	2
α2α3α5β3	1	-	α3α4α5α7β2β3β4	-	3
α2α3α5β4	-	2	α2α3α4α5α7β2β3β4	1	1
α2α3β2β3	1	-			

Figure 1.1: Kinetically Diverse Population of nAChRs. This figure is a representation of the diversity of responses while patching onto rat hippocampal interneurons. The arrow indicates a 1 second, 1 mM ACh application. Patches were made on the neuron cell bodies.

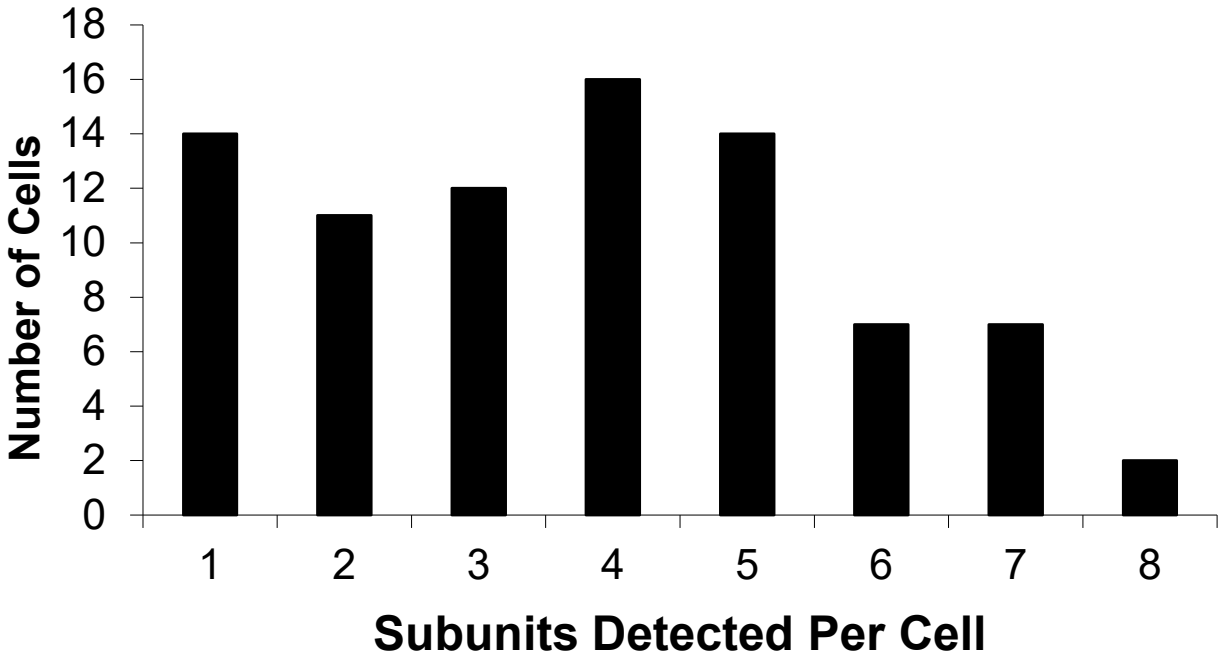

Figure 1.2: Count of nAChR Subunit Expression. A histogram reporting the number of nAChR mRNA subunits detected using qPCR (n=83). The average number of subunits per cell was 3.8 ± 0.22 (mean±SEM) with slight kurtosis and skewness to the left.

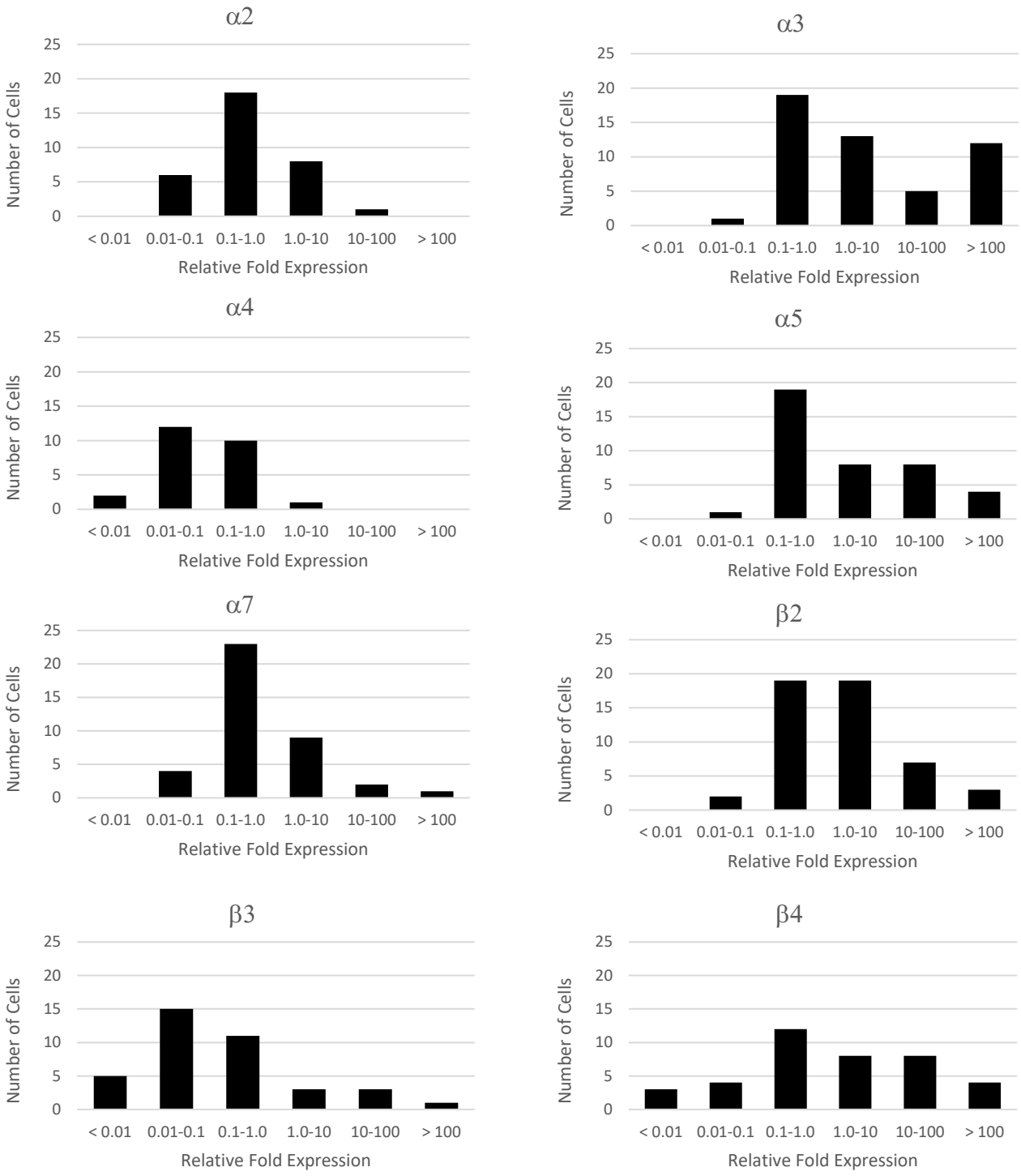

Figure 1.3: nAChR Subunit Relative Expression by Subunit. All nAChR mRNA subunits have variable expression levels as indicated by the histograms. Relative expression levels were binned with 1 being the mean fold expression of the cells.

A.

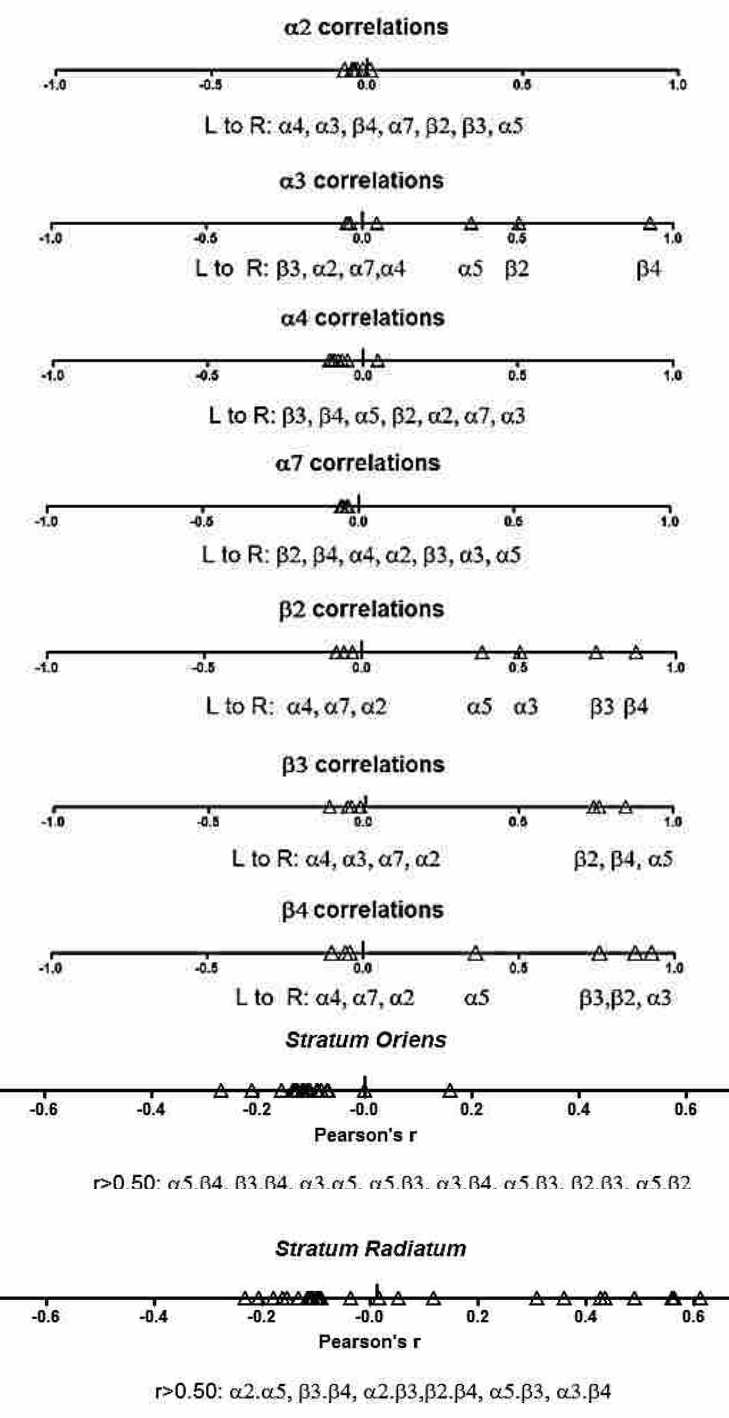

B.

Figure 1.4: Pearson r Correlations of the Average Fold Expression for 2-way Comparisons. A. Correlations of combined data from both the *stratum oriens* and *stratum radiatum.* B. Correlations of both the stratum oriens and *stratum radiatum.* The *stratum radiatum* has a greater variability in Pearson r values while the *stratum oriens* has Pearson r values centered near zero and a separate group with values greater than 0.90. Noted correlations listed from smallest to largest.

References

Alkondon M, Albuquerque EX (2001). Nicotinic acetylcholine receptor alpha7 and alpha4beta2 subtypes differentially control GABAergic input to CA1 neurons in rat hippocampus. J Neurophysiol 86:3043-55.

Alkondon M, Pereira ERF, Albuquerque EX (2007). Age-dependent changes in the functional expression of two nicotinic receptor subtypes in CA1 stratum radiatum interneurons in the rat hippocampus. Biochem Pharmacol 74:1134–1144.

Bustin, S. (2004). AZ of Quantitative PCR. Bustin SA: IUL Biotechnology, No. 5.

Chen WY, Huang CY, Cheng WL, Hung CS, Huang MT, Tai CJ, et al. (2015). Alpha 7-nicotinic acetylcholine receptor mediates the sensitivity of gastric cancer cells to 5-fluorouracil. Tumour Biol. 36:9537-44.

Cobb SR, Buhl EH, Halasy K, Paulsen O, Somogyi P (2005). Synchronization of neuronal activity in hippocampus by individual GABAergic interneurons. Nature 378:75–78.

Didier M, Bix G, Berman SA, Bursztajn S (1995). Expression of the alpha 4 neuronal nicotinic acetylcholine receptor subunit in the developing mouse hippocampus. Int J Dev Neurosci 12:703-13.

Freund, TF, Buzsaki, G (1996). Interneurons of the hippocampus. Hippocampus 6: 347-470.

Gahring LC, Persiyanov K, Rogers SW (2005). Mouse strain-specific changes in nicotinic receptor expression with age. Neurobiol Aging 26:973–980.

Gray, FH, Adle-Biassette, H, Levy Y, Wingertsmann L, Hery C, Tardieu M (1996). [Neuronal apoptosis in the course of human immunodeficiency virus infection]. Bull Acad Natl Med 180:1855-67; discussion 1867-8.

Jackson DC, Hall MK, Sudweeks SN (2017). The Human α3β2 Neuronal Nicotinic Acetylcholine Receptor Forms Two Distinguishable Subtypes. (In-preparation).

Ji D, Dani JA (2000). Inhibition and disinhibition of pyramidal neurons by activation of nicotinic receptors on hippocampal interneurons. J Neurophysiol 83:2682–2690.

Jones S, Sudweeks S, Yakel JL (1999). Nicotinic receptors in the brain: correlating physiology with function. Trends Neurosci 22:555-61.

Jones S, Yakel JL (1997). Functional nicotinic ACh receptors on interneurones in the rat hippocampus. J Physiol 504:603–610.

Khiroug SS, Khiroug L, Yakel JL (2004). Rat nicotinic acetylcholine receptor α2β2 channels: comparison of functional properties with α4β2 channels in *Xenopus* oocytes. Neuroscience 124:817-822.

Lindstrom J. (1996) in Ion Channels, ed Narahashi T. (Plenum Publishing Corp. New York), 4:377–450.

Livak K, Schmittgen T (2001). Analysis of relative gene expression data using real-time quantitative PCR and the 2 ddCT method. Methods 25: 402–408.

Moore DS (1995) The Basic Practice of Statistics. pp 487-509. WH Freeman press. New York, New York USA.

Moore DS & McCabe GP (1993) Introduction to the Practice of Statistics (2nd edition). pp 590-596. WH Freeman press. New York, New York USA.

Pettit DL, Shao Z, Yakel JL (2001). beta-Amyloid(1-42) peptide directly modulates nicotinic receptors in the rat hippocampal slice. J Neurosci 21:RC120.

Rogers SW, Gahring LC, Collins AC, Marks M (1998). Age-related changes in neuronal nicotinic acetylcholine receptor subunit α4 expression are modified by long-term nicotine administration. J Neurosci 18:4825–4832.

Sudweeks SN, Yakel JL (2000). Functional and molecular characterization of neuronal nicotinic ACh receptors in rat CA1 hippocampal neurons. J Physiol 527 Pt 3:515-28.

Ullian E, McIntosh J, Sargent P (1997). Rapid Synaptic Transmission in the Avian Ciliary Ganglion Is Mediated by Two Distinct Classes of Nicotinic Receptors. J. Neurosci. 17:7210–7219.

Vernallis A, Conroy W, Berg D (1993). Neurons assemble acetylcholine receptors with as many as three kinds of subunits while maintaining subunit segregation among other receptor subtypes. Neuron. 10:451-464.

Wang HY, Lee DH, Davis CB, Shank RP (2000). Amyloid peptide Abeta(1-42) binds selectively and with picomolar affinity to alpha7 nicotinic acetylcholine receptors. J Neurochem 75:1155-61.

Winzer-Serhan UH, Leslie FM (2005). Expression of α5 nicotinic acetylcholine receptor subunit mRNA during hippocampal and cortical development. J. Comp. Neurol 481:19–30.

Yeh JJ, Yasuda RP, Dávila-García MI, Xiao Y, Ebert S, Gupta T, *et al.* (2001), Neuronal nicotinic acetylcholine receptor α3 subunit protein in rat brain and sympathetic ganglion measured using a subunit-specific antibody: regional and ontogenic expression. Journal of Neurochemistry 77: 336–346.

Zhang JC, Yao W, Ren Q, Yang C, Dong C, Ma M, Wu J, Hashimoto K (2016). Depression-like phenotype by deletion of α7 nicotinic acetylcholine receptor: Role of BDNF-TrkB in nucleus accumbens. Sci Rep. 6:36705.

CHAPTER 2: The Human alpha 3 beta 2 Neuronal Nicotinic Acetylcholine Receptor Forms Two Distinguishable Subtypes

Doris C Jackson, Marcel K Hall, Sterling N Sudweeks

Brigham Young University, Provo, UT, 84602

Address correspondence to:

Sterling Sudweeks, PhD, Department of Physiology and Developmental Biology,

Brigham Young University

3045 Life Sciences Building, Provo, UT 84602, Tel: (801)422-8752,

Sterling_Sudweeks@byu.edu

This work was supported by internal funding from Brigham Young University.

Key words: neuronal nicotinic acetylcholine receptor (nAChR), alpha 3, beta 2, stoichiometry, ligand-gated ion channel, cognition, electrophysiology, desensitization, nicotine, acetylcholine (ACh), *Xenopus laevis* oocyte, dose-response curve

No conflicts of interest to be reported.

TABLES, FIGURES AND LEGENDS: 6 Figures, 1 Table

AUTHOR CONTRIBUTIONS: Conceived and design experiments: DJ SS. Performed experiments: DJ MH. Analyzed the data: DJ SS. Contributed reagents/materials/analysis tools: SS. Wrote the paper: DJ MH SS.

Abstract

The hippocampal interneuron population is diverse yet almost always contains nicotinic acetylcholine receptors (nAChRs). The nAChRs regulate the release of GABA on to glutamatergic pyramidal cells. The highest co-expressed nAChR subunits in the Amun's horn (CA1) of the rat hippocampal interneurons are the α3 and β2 subunits yet the α3β2 subtype(s) has not been extensively characterized.

We expressed the human α3β2 nAChRs in *Xenopus laevis* oocytes to differentiate possible subtypes using two-electrode whole cell voltage clamp. We can distinguish at least two subtypes based on their acetylcholine (ACh) and nicotine affinities. Regarding acetylcholine, injecting 5X more β2 mRNA gives an EC_{50}=12 μM±1.7, while injecting 5X more α3 mRNA gives an EC_{50}=264±1.6 μM. Additionally, these mRNA ratios yields significant differences in rise time, half width, and ACh desensitization ($p<0.05$). The desensitization after 30 seconds of ACh exposure revealed the clearest kinetic differences between subtypes.

In summary, the human α3β2 neuronal nAChR subunits can form at least two different and functional subtypes that can easily be distinguished with long term ACh applications. These hippocampal subtypes could provide new drug targets for cognitive therapies for diseases such as Alzheimer's Disease (AD), Autism Spectrum Disorder (ASD), and Attention Deficit Hyperactivity Disorder (ADHD).

Introduction

Neuronal nicotinic acetylcholine receptors (nAChRs) are important in the synchronous firing of the hippocampus (Grybko, 2010, Ji, 2000). These receptors are found in the interneurons of the hippocampus (Cobb, 2005, Winzer-Serhan, 2005, Jones, 1997). Hippocampal interneurons are relatively sparse compared to pyramidal cells and glial cells, but are necessary in cognition as evidenced by the cognitive drugs that target nAChRs (Dannenberg, 2015, Bezaire, 2016). Overall, the nAChR population in the interneurons is extremely heterogeneous and not fully characterized (Sudweeks, 2000, Szabó, 2014, Jackson, 2017). Patch clamp recordings of the rat hippocampus reveal a large diversity of electrophysiological properties indicating a large diversity of receptors subtypes (Figure 1). Rates of subunit co-expression in the rat hippocampus indicate that the α3 and β2 subunits are the highest co-expressed subunits within the *stratum oriens* and *stratum radiatum* of the CA1 (Amun's horn) (Jackson, 2017). Yet, the α3β2 nAChR subtypes have not been differentiated.

Cognitive therapeutics targeting nAChRs in the hippocampus are only mildly effective and often target the α7 containing nAChRs (Wallace, 2011, Aracava, 2005, Martin, 2004, Leiser, 2009, Soderman, 2011, Thomsen, 2010). Other nAChR-targeted therapies often target the α4β2 nAChR (Rode, 2012, Timmerman, 2012, Sater, 2009). Both the α7 homomer and α4β2 heteromer are found throughout the brain. However, the α4 subunit is expressed at relatively low levels among the CA1 hippocampal interneurons and may be one reason why cognitive therapies targeting the α4β2 are only mildly effective (Jackson, 2017). The α7 is often found pre-synaptically and helps regulate neurotransmitter release (Liu, 2003). Due to the high co-expression level of α3β2 and possible different location within the neuron we feel that α3β2 subtypes should be fully investigated as possible drug targets. The α3β2 nAChR has been

somewhat characterized (Chavez-Noriega, 1997, Wang, 1998, Chavez-Noriega, 2000, Wu, 2008, Wang, 2015), but the distinction between two different α3β2 subtypes has not been explored. Like the α4β2 and the α2β2 nAChRs, we believe that there are at least 2 stoichiometries of the α3β2 nAChR (Papke, 1989, Ussing, 2013, Zwart, 1998, Khiroug, 2004, Dash, 2014). We are excited about the possible therapeutic targets that α3β2 nAChRs could serve as for various diseases affecting the hippocampus such as Alzheimer's disease (AD), autism spectrum disorder (ASD), ethanol and/or nicotine addiction, and attention deficit hyperactivity disorder (ADHD) (Kamens, 2009). Therefore, we sought to characterize the kinetic properties of the α3β2 nAChRs, and differentiate possible subtypes.

Methods

Plasmids containing human α3 (hα3) and human β2 (hβ2) genes were transformed into One Shot® *E. coli* chemically competent cells, and plasmid DNA was then isolated and purified using the HiSpeed® plasmid purification kit. Plasmids containing the hα3 and hβ2 genes were linearized by restriction digest with SacI. The mRNA was then transcribed, capped on the 5' end, a poly(A) tail was added (optional), and LiCL purification was performed using the mMessage mMachine® T7 Ultra Kit according to the protocol provided. RNA was re-suspended in Tris-EDTA Buffer, mixed in various ratios, aliquoted, and stored at -20˚C. For some nAChR subtypes, the poly(A) tail appears to increase expression yield. However, we had similar results with or without the poly(A) tail addition.

Ratios of hα3 (1.0 μg/μL) and β2 (1.0 μg/μL) AChR subunit mRNAs were injected into *Xenopus laevis* oocytes. Naive *Xenopus laevis* oocytes are not responsive to ACh, but when injected with the appropriate mRNA they are also able to express a high yield of nAChR protein. The ratios of α3:β2 1:5 and α3:β2 5:1 were used to increase the likelihood of expression of each

probable stoichiometry ($\alpha3_{(2)}\beta2_{(3)}$ and $\alpha3_{(3)}\beta2_{(2)}$ respectively) (Nelson, 2003, Moroni, 2006). Each oocyte was injected with 50.6 nL of mRNA for a total of 50.6 ng of mRNA per oocyte. The injection needles and recording needles were made of borosilicate glass. Following injection, the oocytes were stored in Ringer's solution (OR-2-Ca^2-pen-strep) at 17-19˚C for 6-9 days on a rocker (pH~7.5). This solution consists of (in mM unless noted): 82 NaCl, 2.5 KCl, 1 Na_2HPO_4, 5 HEPES, 1 $CaCl_2$, 1 $MgCl_2$, 0.5 theophylline, 100,000 units penicillin, and 10 mg streptomycin. After 9 days any oocytes not recorded on were stored at 4˚C to stop further maturation of the cell until the oocyte was used for recordings.

Recordings of the cell's electrical activity were obtained through two-electrode voltage clamp. Traces were recorded using Clampex 9.2 software and analyzed on ClampFit 9.2. Various concentrations of Acetylcholine (ACh) and Nicotine (Nic) were suspended in OR-2 solution and were perfused (1 psi) over the oocyte every 90 seconds and the cell's responses were recorded (ACh concentrations between 100 nM and 100 mM; Nic concentrations between 1 mM and 1.5 M). Except for the desensitization tests, ACh was perfused for 3 seconds every 90 seconds and nicotine was perfused for 1 sec every 90 seconds. To measure the degree of desensitization, the EC_{85} (effective concentration 85% of maximum response) for each subtype was applied for 60 seconds with a 2 minute wash between applications (replicates of 3). We did not blind our experiments since the protocols for ACh and nicotine were different. In order to analyze the response, it was necessary to know the ligand and the exact concentrations applied.

For voltage clamp recordings, the oocytes were clamped at -60 mV while solutions were perfused at 17 $ml \cdot min^{-1}$. The IV plot was generated by clamping the oocyte at -90, -75, -60, -45, -30, -15, 0 (all in mV), and then we performed the same procedures as the voltage clamp recordings. All ligands were dissolved in OR-2-Ca^{2+} without theophylline, streptomycin, and

penicillin. Solutions were perfused using an 8-valve (pinch), computer controlled, pressurized perfusion system. Oocytes were impaled with microelectrodes filled with 3 M KCl and a resistance between 0.1-2 MΩ. Clampex 9.2 was used to run the electrophysiology protocols through a GeneClamp 500B amplifier and Digidata 1322A digitizer. Data was sampled at 5 kHz and filtered at 2 kHz. Peak amplitudes ranged from 3 nA to 200 nA. The range in peaks was dependent on each oocytes protein expression level as well as the concentration of acetylcholine used to generate the response.

All recordings were normalized to the maximums (E_{MAX}) for each subtype. This was necessary since each oocyte expressed a different number of channels based on health, efficiency, and incubation time. Upon collection of the recordings, we used Clampfit to analyze multiple parameters for each recording including rise time, half-width (width of the peak at 50% of the peak amplitude), and desensitization. For our analysis, we compared the 1:5 and 5:1 results at the EC_{50} (10 μM, 333 μM respectively) and the EC_{85} (333 μM, 10 mM respectively). However, for desensitization we only compared the EC_{85}. Analysis of the steady state currents were compared at 30 seconds during the 60 second ACh application.

Data and Statistical Analysis

Analysis of previously collected qPCR data (Jackson, 2017) was extended to determine if there was more than one stoichiometry of the hα3 and the hβ2 nAChR. Microsoft Excel (2013) was used to analyze the data for all figures except Figure 2 and Figure 4. Specifically, the "=AVERAGE()" and "=STDEV()/(SQRT(COUNT()))" were used to calculate the mean and standard error of the mean. These values were then used to generate Figure 1 using "Insert Bar Graph" (Excel, 2013). Likewise, Figure 5A-B and Figure 6 were generated using the same calculations and tools. Also, the approximate EC_{50} and approximate EC_{85} (effective

concentration 85% of maximum response) were used as the points of comparison for the kinetic parameters (rise time and half-width). The data points for Figure 3 were also generated using the formula for mean and standard error of the mean. However, a scatterplot fitted with a linear trendline is more appropriate to present this data than a bar graph. Only the first 5 points of Figure 3 were fitted for the trendline because the data shows a strong inwardly rectifying channel. Fitting the line linearly better estimates the reversal potential of an inwardly rectifying channel. Figure 4 was generated using GraphPad Prism v. 4. The data was fit using the "sigmoidal dose-response (variable slope)" tool. The hill slopes, EC_{50} values, and R^2 values, as well as their respective standard errors, were provided in the curve fit analysis. Grubb's outlier tests were used to for all data sets (alpha=0.05). For statistical tests, $p<0.05$ is used as the level to determine significance (*). We report all means and standard errors of the mean as $\bar{x}$±SEM. GraphPad InStat v. 3 was used to calculate all ANOVAs. ANOVAs were calculated as "ordinary" and assumed to be Gaussian distributions. Tukey post-hoc tests were performed only if the $p<0.05$. Figure 2.A and 2.B are example traces that were collected using Clampex 9.2 and analyzed with Clampfit 9.2 (Axon Instruments). Screen shots were taken and then cropped in Paint (Windows 7). Figure 2.C and 2.D were generated using Adobe Illustrator CC (2017). Also, since each oocyte varies in the number of nAChR proteins it expresses it is necessary to normalize the data for comparison.

Materials

Plasmids: hα3 (Origene# SC126406), hβ2 (Origene# SC309051), pCMV6-XL4 plasmid: OriGene Technologies Inc., 9620 Medical Center Drive, Suite 200, Rockville, MD, USA, 20850.
One Shot® *E. coli* chemically competent cells (Invitrogen), mMessage mMachine® T7 Ultra Kit: Thermo-Fischer Scientific 168 Third Avenue, Waltham, MA, USA, 02451.
HiSpeed® plasmid purification kit: Qiagen, 19300 Germantown Road, Germantown, MD, USA, 20874.

SacI restriction enzyme: New England Biolabs, 240 Country Road, Ipswich, MD, USA, 01938-2723.

Tris-EDTA Buffer: BioExpress Corporation, 420 N Kays Dr, Kaysville, UT, USA 84037. Defolliculated *Xenopus laevis* oocytes. Animal husbandry and surgery using anesthesia and analgesia were performed by Ecocyte BioScience. 111 Ramble Ln #109, Austin, TX, USA, 78745.

Oocyte injection, Nanoject II microinjector: Drummond Scientific Company, 500 East Park Way, Broomall, PA, USA 19008.

Injection (1.12 mm OD x 0.51 mm ID) and recording (1.5 mm OD x 1.17 mm ID) capillary tubes: Harvard Apparatus, 84 October Hill Road, Holliston, MA, USA, 01746.

Needles were pulled using Model P-97 puller: Sutter Instrument Company, 1 Digital Drive, Novato, CA, USA, 94949.

Data acquisition software for electrophysiological recordings (Clampex 9.2) and recording analysis (Clampfit 9.2). GeneClamp 500B amplifier. Digidata 1322A digitizer. Axon Instruments, Molecular Devices, 1311 Orleans Drive, Sunnyvale, CA, USA, 94089.

Reagents for OR-2 Ca^{2+} solution: NaCl, KCl, Na_2HPO_4, HEPES, $CaCl_2$, $MgCl_2$, theophylline, penicillin, streptomycin; Acetylcholine chloride, Nicotine tartrate: Sigma-Aldrich, 3050 Spruce Street, St. Louis, MO, USA, 63103.

Pinch valve perfusion system (product #s 13-pp-54, and 09-08). Automate Scientific Inc., 3271 Adeline Street, Unit B, Berkeley, CA, USA, 94703.

GraphPad Prism v. 4 and GraphPad Instat v. 3.05: GraphPad Software Inc., 7825 Fay Ave #230, La Jolla, CA 92037 USA.

Microsoft Excel: Microsoft Building 92, 15010 NE 36th St, WA 98052-6399 USA.

Results

The qPCR data previously collected indicated that the α3 and β2 nAChR subunits are the highest co-expressed subunits in the rat CA1 hippocampal interneurons (specifically, the *stratum oriens* and *stratum radiatum*) (Jackson, 2017). Further analysis revealed that the mRNA is expressed in a 1:1 (α3:β2) ratio. However, no individual interneuron expressed a 1:1 ratio. Instead, we found that about half had greater α3 expression, while the other half had greater β2 expression. The two populations showed either a 3:1 ratio or a 1:3 of α3:β2 mRNA on average (Figure 1).

Injection of hα3 and hβ2 mRNA into *Xenopus laevis* oocytes at a 1:5 and 5:1 revealed two functional receptor subtypes. Both subtypes responded to ACh application; however,

extended ACh applications at their respective EC_{85} revealed distinct kinetic differences (Figure 2).

The IV plot shows a similar reversal potential between the subtypes suggesting that there is no difference in ion selectivity. Also, the reversal potential suggests that, like other nAChR subtypes, the channels are permeable to both Na^+ and K^+ (Figure 3). The IV plot also shows that both subtypes are strong inwardly rectifying channels.

The dose-response curves (Figure 4) reveal a statistical difference in the ACh and nicotine affinities when comparing subtypes (ANOVA $p<0.0001$, $p<0.0001$ respectively, Table 1). The 1:5 injected ratio has greater affinity for ACh and nicotine than the 5:1 injected group. We also show that both subtypes have a lesser affinity for nicotine (Figure 4.B). The 1:5 injected ratio, like ACh, has a greater affinity for the ligand (Table 1). However, Figure 4.B reveals a bi-phasic curve for the 5:1 injected oocytes. Since, the dose-response curves for nicotine are more separated than the dose-response curves for ACh it is easier to fit the biphasic model.

In addition, we used t-tests to compare the peak amplitude for each injection ratio. When comparing the EC_{85} and the EC_{50} values on the ACh dose-response curve, the peak amplitudes for the 5:1 are statistically different at each ($p<0.0001$, $p<0.001$) with the 5:1 injections resulting in larger currents. Likewise, we compared the E_{MAX} of nicotine (333 M for 1:5, 1 M for 5:1) and found a significant difference in the relative peak sizes as well. Like ACh, the 5:1 injection ratio resulted in larger peak amplitudes.

Our results of the kinetic properties show that when applying ACh for only 3 seconds, the two subtypes are more similar than different. However, there are two parameters that are statistically significant: the half-widths and rise-times (Figure 5). Yet, the results differ

depending on concentration. Figure 6 reveals the most distinguishable characteristic: with extended 60 second ACh applications, the two subtypes show marked differences in desensitization. The 1:5 injected oocytes are significantly more desensitized at their steady state than the 5:1 injected oocytes. After 30 seconds only 12.6±1.4% remained for the 1:5 oocytes while 81.6±2.1% ($\bar{x}$±SEM) of the original peak amplitude remained for the 5:1 oocytes (Figure 6).

Discussion

The data suggests that there are at least two likely stoichiometries for the α3β2 nAChR. The nicotine dose-response curves appear to be a mixture of α3β2 subtypes. The 1:5 nicotine dose-response curve does not show a biphasic curve because it only represents the lower nicotine concentrations where certain subtypes may not be activated. The biphasic may not represent all of the possible stoichiometries, but the two most likely based on α4β2 and α2β2 stoichiometries (Covernton, 2000, Houlihan, 2001, Bussion, 2001, Exley, 2006). The ACh dose-response curve for the 1:5 injected oocytes, like the nicotine curve, appears best fit with a monophasic sigmoidal dose-response curve. However, even though the 5:1 injected oocytes also fit best with a monophasic sigmoidal dose-response curve, there are a few points on the curve that would suggest multiple contributing subtypes. However, the ACh dose-response curve are two close to distinguish considering. The 5:1 injection would increase the likelihood of $\alpha3_{(3)}\beta2_{(2)}$ subtypes expression over the $\alpha3_{(2)}\beta2_{(3)}$ subtype expression. In addition, our results indicate that the $\alpha3_{(2)}\beta2_{(3)}$ is either less efficient in formation resulting in overall smaller peak amplitudes, or has lower efficacy. To determine if efficiency or efficacy or both are contributing to peak amplitude size, single channel recordings would be necessary.

One explanation for the increase in peak amplitude with the 5:1 injected oocytes is that there is another possible binding site at the α3/α3 junction. Like the α4β2 nAChR, when more α4 is present it has been suggested than an additional binding site is found at the additional α4/α4 junction (Moroni, 2006). This may also be true of the α3β2 nAChR. However, this is simply one explanation. The $\alpha3_{(3)}\beta2_{(2)}$ may simply be a more favored protein expression. Since, the n_H are similar, the different stoichiometries may have the same likelihood for channels opening. A larger n_H could indicate greater cooperativity of the binding sites. Yet, by simply having more binding sites, this may increase the likelihood of binding without a change in the cooperativity of binding.

Regarding nicotine, our EC_{50} values are larger than those previously reported (Wang, 1998), but previous studies do not distinguish between α3β2 subtypes. However, Wang et al. used nAChRs transfected in HEK cells whereas we used *Xenopus laevis* oocytes. We hope to follow up our research using HEK cells as well to confirm our findings regarding both injection ratios.

When considering how other nAChR subtypes assemble and the qPCR data from Jackson (2017), the data suggests that there are two likely stoichiometries: the $\alpha3_{(2)}\beta2_{(3)}$ (from a 1:5 mRNA ratio) and the $\alpha3_{(3)}\beta2_{(2)}$ (from a 5:1 mRNA ratio) (Papke, 1989, Zwart, 1998, Nelson, 2003, Khiroug, 2004). The injection ratios will likely not produce a homogenous population of one stoichiometry, but our results indicate that there are enough of each stoichiometry to distinguish their kinetic properties even though the nicotinic curve is biphasic (Figure 4.B). It has been shown previously that sometimes a low, or broad, n_H (hill slope) may indicate multiple contributing stoichiometries, but considering the error bars and the fit of our curves, we are

likely getting very little contribution from the less likely stoichiometries of $(\alpha 3)_1(\beta 2)_4$ and $(\alpha 3)_4(\beta 2)_1$.

The most noteworthy difference between the two injected subgroups is desensitization with prolonged ACh application. The 1:5 injected oocytes are much more easily desensitized than the 5:1 injected oocytes. However, contrary to the α4β2 nAChR published results, the desensitization of ACh on the α4β2 nAChR also increases with more β2 subunit expression (Zwart 1998, Nelson, 2003, Carbone, 2009). Like the α4β2 and α2β2 ACh dose response curve increasing the number of β2 subunits in the subtype also increases the ACh affinity and shifts the dose-response curve left (Papke, 1989, Zwart, 1998, Nelson, 2003, Khiroug, 2004).

The β2 nAChR subunit has been shown to be widely expressed throughout much of the rat brain (Hill, 1993). However, expression of the α3 subunit is much more restricted, being previously identified in the sympathetic ganglion, medial habenula, and the autonomic ganglion (Vernallis, 1993, Ullian, 1997, Lindstrom, 1996, Yeh, 2001). They have also been identified outside of the nervous system in the adrenal gland (Campos-Caro, 1997), thymus (Mihovilovic, 1993), respiratory epithelial cells (Zia, 1997), and keratinocytes (Grando, 1995, 1996). With the identification of the α3 subunit being highly expressed in hippocampal interneurons (Jackson 2017), the characterization of the α3β2 nAChRs is beneficial. We can now add it to the list of nAChR subtypes that should be screened for cognitive drug development.

Current nAChR therapies target either the α7 or the α4β2 subtypes (Sarter, 2009). Also since the α3β2 appears to be more restricted to hippocampal interneurons, drugs targeting the α3β2 may be more selective than current therapies. Likewise, drugs targeting the α3β2 subtype may alter the hippocampal firing to a different degree, or in a different manner current therapies. There is even the possibility of combining α3β2 targeted therapies with current therapies in cases

where such would be beneficial. Many cognitive diseases like AD and ASD currently have few effective treatment options. Therefore, characterization of a new protein target in the hippocampus may widen the possible therapeutics and give further insight into disease development.

In conclusion, multiple α3β2 nAChR subtypes have been identified. Although similar in many respects they do have distinguishable properties. Both subtypes are valid novel targets for cognitive therapies and further research may yield great implications.

Supporting Information

Controls were done to ensure that the hα3 nor the hβ2 mRNA are not able to form a functional nAChR by themselves. Following the methods previously outlined, we injected solely hα3 mRNA or hβ2 mRNA, waited 7 days and then performed electrophysiological recordings with ACh. The recordings were under the same conditions and restraints as all other recordings. We found no evidence that the hα3 or the hβ2 forms a functional homomeric receptor.

Table 2.1: Summary of ACh and Nic Dose-Response Curves.

Table 2.1	1:5 ACh	5:1 ACh
EC-50 (μM)	12±1.7	264±1.6
Hill Slope	0.48±0.13	0.55±0.15
R^2	0.74	0.77
ANOVA		$p<0.0001$
	1:5 Nic	5:1 Nic
EC-50 (mM)	25±1.5	21±1.6
Hill Slope	1.0±0.46	1.4±0.90
$EC\text{-}50_2$ (mM)	N/A	415±7E18
$Hill\ Slope_2$	N/A	15±1680
R^2	0.67	0.57
ANOVA		$p<0.0001$

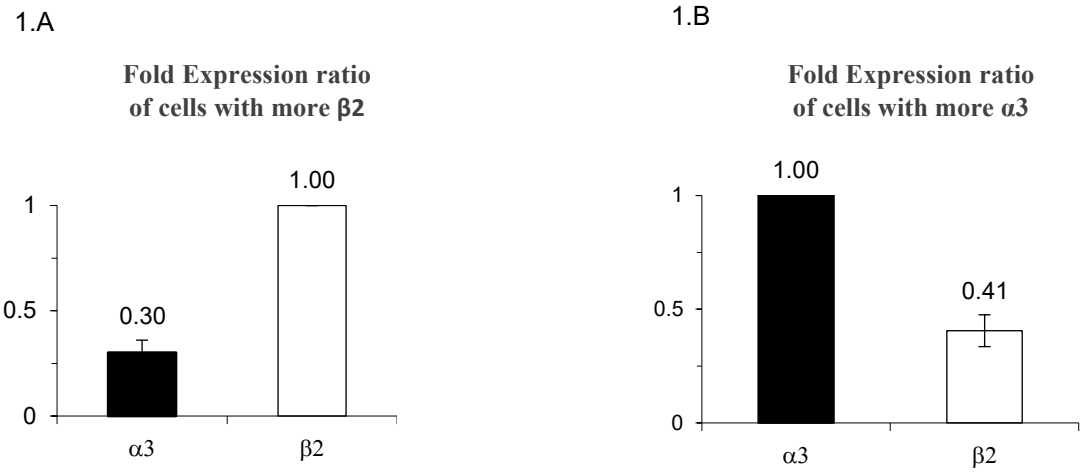

Figure 2.1: Ratio of α3 and β2 Expression in Hippocampal Interneurons. The most commonly co-expressed subunits, the α3 and β2, were analyzed further to identify two populations. (A) 56% of the interneurons tested in Jackson (2017) expressed in a 1:3 α3:β2 ratio. (b) 44% of the interneurons tested in Jackson (2017) expressed in a 3:1 α3:β2 ratio. Of the 93 cells analyzed, 34 co-expressed α3 and β2. Therefore, n=19 for 1.A and n=15 for 1.B (total n=34).

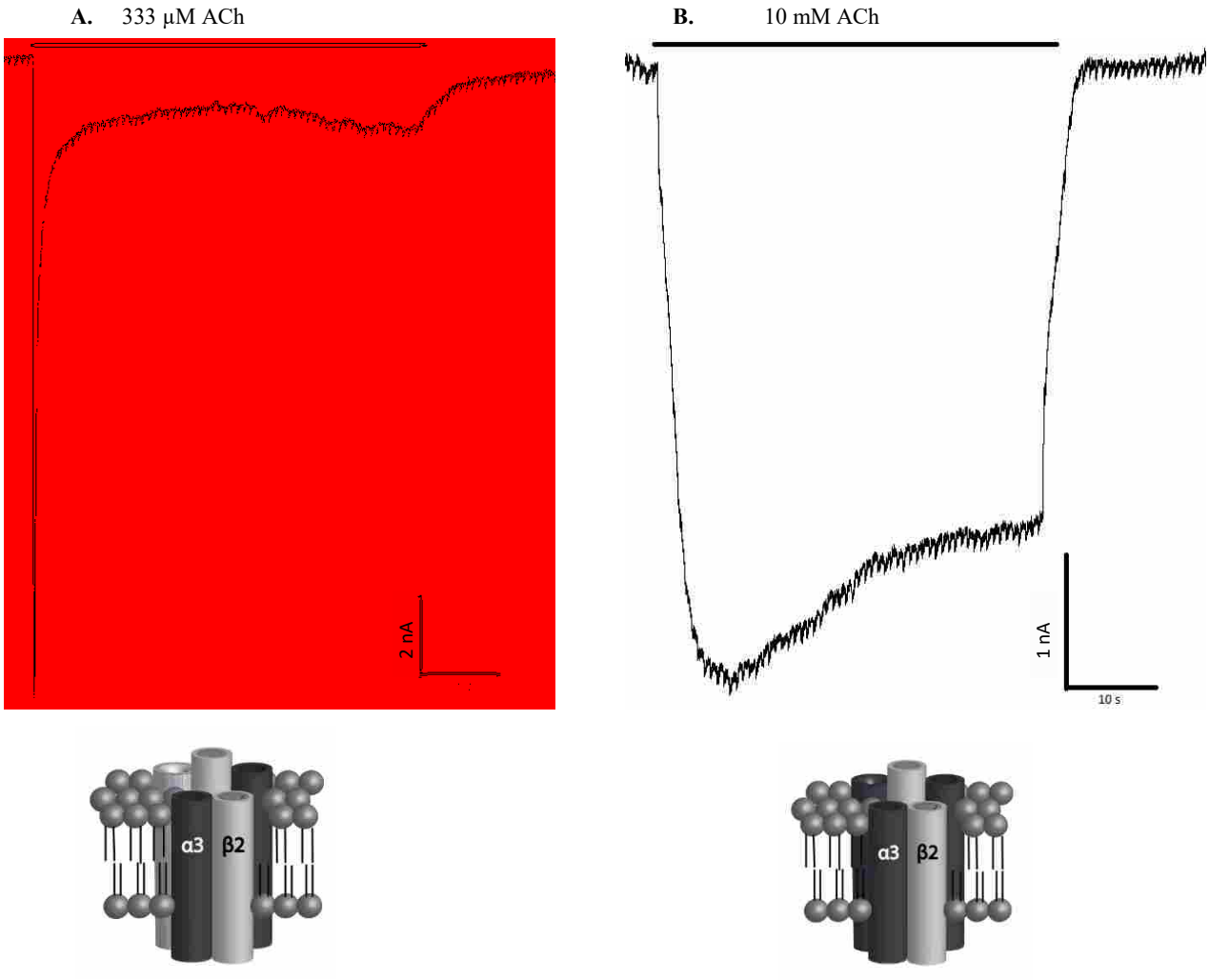

Figure 2.2: Sample Traces and Likely Stoichiometries. Injection of hα3 and hβ2 mRNA into *Xenopus laevis* oocytes at a (A) 1:5 and (B) 5:1 ratio formed functional and distinguishable receptors. The respective oocytes were perfused with 333 µM and 10 mM ACh for 60 seconds to characterize desensitization. The likely stoichiometries are shown respectively.

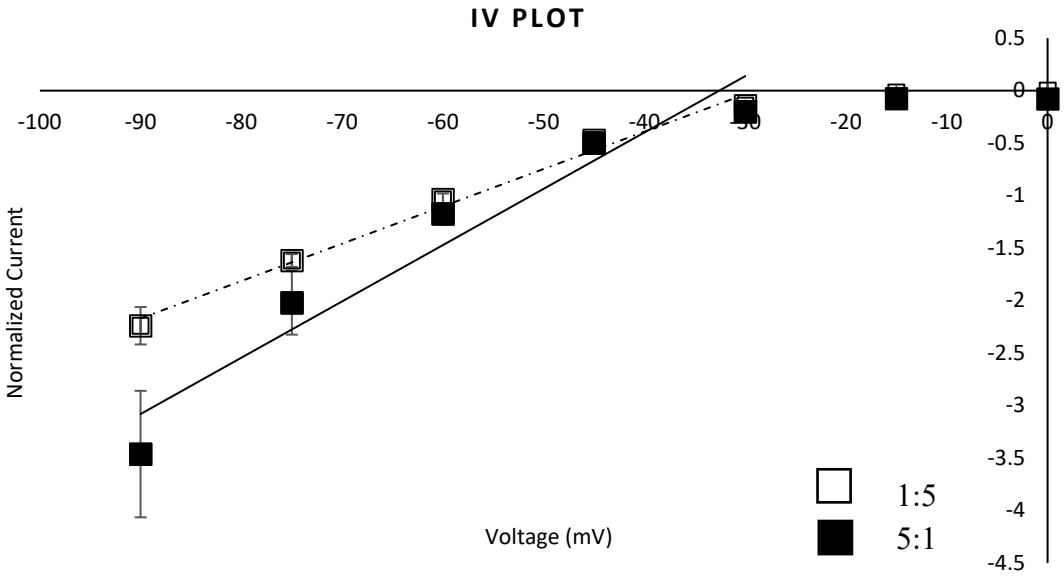

Figure 2.3: IV Plot. 1:5 injected oocytes fit a linear trendline of $y = 0.0356x + 1.033$ ($R^2 = 0.9892$) (n=5) and fit a linear trendline for the 5:1 injected oocytes $y = 0.0537x + 1.7478$ ($R^2 = 0.9362$) (n=8) when fitting points between -90 mV and -30 mV. The reversal potential for both is approximately -30 mV.

A.

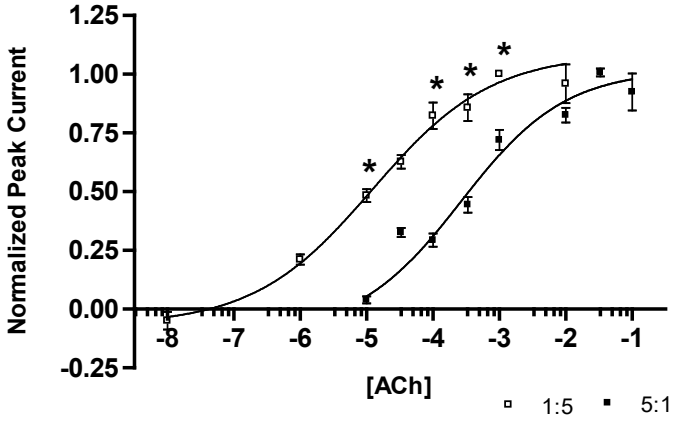

B.

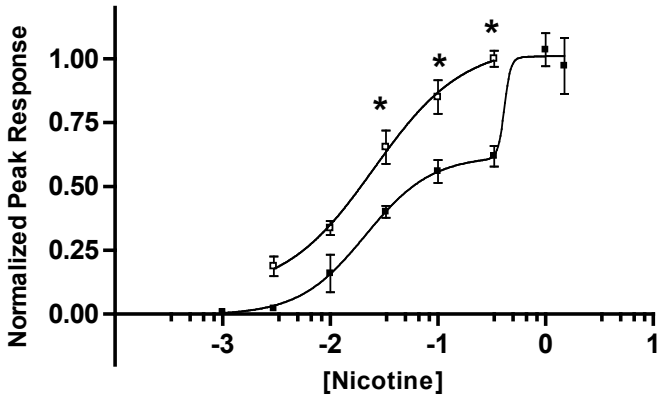

Figure 2.4: Dose-Response Curves. A. ACh Dose-Response. 1:5) EC_{50}=12.2±1.7 μM, n_H=0.49±0.13 (R^2=0.74) (n=14 oocytes, replicates of 4, 1 individual data point identified as an outlier and removed). 1:5) EC_{50}=263.8±1.6 μM, n_H=0.55±0.15 (R^2=0.77) (n=12, replicates of 4, 2 individual data points outliers). The 1:5 injected ratio has a minimum response at ~100 nM and an E_{max} at ~1000 μM ACh. The 5:1 injected ratio has a minimum response at ~10 μM and an E_{max} at ~33 mM ACh (ANOVA, $F_{[15, 258]}$=54.644). A. Nicotine Dose-Response. 1:5) EC_{50}= 25.3 ±1.5 mM, n_H= 1.04±0.46 (R^2=0.6705) (n=6 oocytes, replicates of 3, but not at all concentrations were used for each oocyte, 1 individual data point was identified as an outlier and removed.) (ANOVA, p<0.0001, $F_{[12, 238]}$=30.396 5:1) EC_{50_1}=21.2±1.6 mM, n_{H_1}= 1.41±0.91, EC_{50_2}= 414±7E18 mM, n_{H_2}=14.85±1680 (R^2=0.57) (n=11 oocytes, replicates of 3, but not at all concentrations were used for each oocyte, 3 individual data points were identified as outliers and removed.)

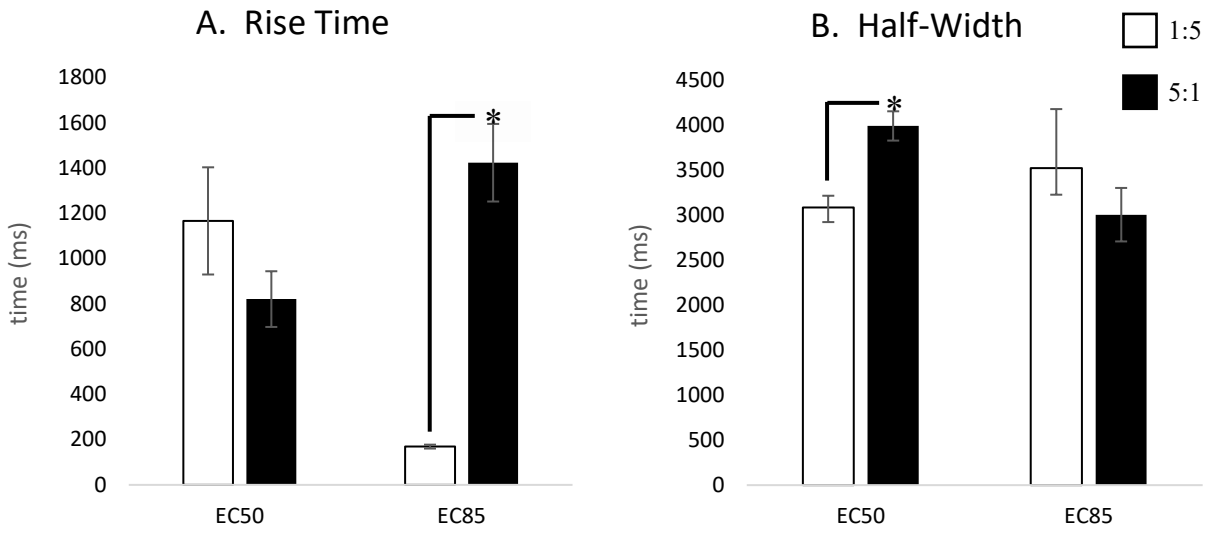

Figure 2.5: Comparison of Rise Time and Half-Width of ACh Dose-Response Curve. Comparisons were made at the EC_{50} (10 µM, 333 µM) and the EC_{85} (333 µM, 10 mM) for the 1:5 and 5:1 mRNA injected ratios respectively. A. Comparison of 10% to 90% rise time. 1:5) 10 µM ($\bar{x}$=mean±SEM) $\bar{x}$=1166±237 ms (n=6, replicates of 3), 333 µM $\bar{x}$=169±9 ms (n =21, replicates of 4, 3 replicate outliers removed). 5:1) 333 µM $\bar{x}$=821±123 ms (n=13, replicates of 4), 10 mM $\bar{x}$=1424±171 ms (n=25, replicates of 4, 3 replicate outliers removed). B. Comparison of half-width. 1:5) 10 µM $\bar{x}$ =3084±130 ms (n=5, replicates of 3, 3 replicate outliers removed), 333 µM $\bar{x}$=3522±654 ms (n=11, replicates of 4). 5:1) 333 µM $\bar{x}$=3988±163 ms (n=13, replicates of 4, 2 replicate outliers removed), 10 mM $\bar{x}$=3003±297 ms (n=21, replicates of 4).

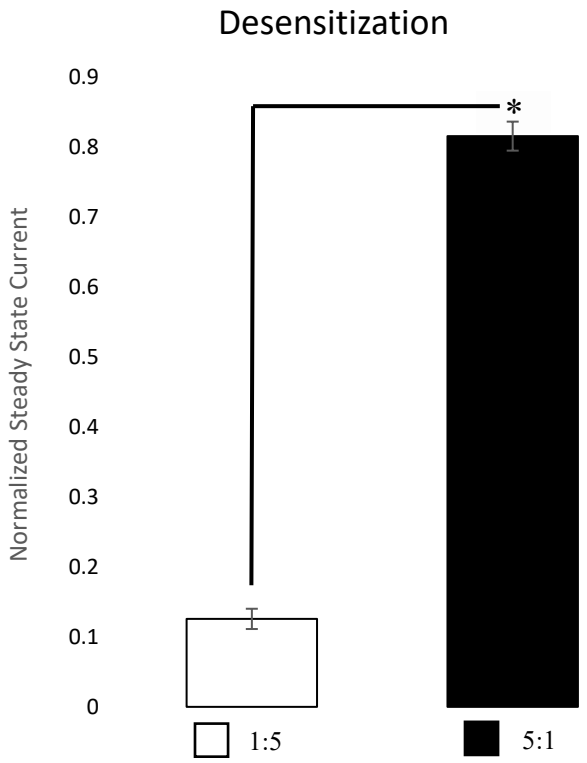

Figure 2.6: Desensitization. Comparisons were made after 30 seconds of continuous ACh application at the EC_{85}. The 1:5 injected oocytes (n=7, replicates of 3, 1 replicate outlier removed) were much more desensitized with very little of the original peak remaining while the 5:1 injected oocytes (n=3, replicates of 3, 1 replicate outlier removed) was only desensitized minimally with much of the original peak remaining at 30 s. A t-test was used to test for significance.

References

Aracava Y, Pereira EF, Maelicke A, Albuquerque EX (2005). Memantine blocks alpha7* nicotnic acetylcholine receptors more potently than N-methyl-D-aspartate receptors in rat hippocampal neurons. J. Pharmacol. Exp. Ther. 312:1195–1205.

Bezaire MJ, Raikov I, Burk K, Vyas D, Soltesz I (2016) Interneuronal mechanisms of hippocampal theta oscillations in a full-scale model of the rodent CA1 circuit. Elife. pii: e18566.

Bussion B, Bertrand D (2001). Chronic Exposure to Nicotine Upregulates the Human α4β2 Nicotinic Acetylcholine Receptor Function. J of Neuro. 21:1819-1829.

Campos-Caro A, Smillie F, Dominguez del Toro E, Rovira J, Vincente-Agullo F, Chapuli J, et al. (1997) Neuronal nicotinic acetylcholine receptors on bovine chromaffin cells: cloning, expression, and genomic organization of receptor subunits. J. Neurochem. 68:488–497.

Carbone AL, Moroni M, Groot-Kormelink PJ, Bermudez I (2009). Pentameric concatenated (α4)2(β2)3 and (α4)3(β2)2 nicotinic acetylcholine receptors: subunit arrangement determines functional expression. B J Pharmacology 156:970-981.

Chavez-Noriega LE, Crona JH, Washburn MS, Urrutia A, Elliott KJ, Johnson EC (1997). Pharmacological Characterization of Recombinant Human Neuronal Nicotinic Acetylcholine Receptors hα2β2, hα2β4, hα3β2, hα3β4, hα4β2, hα4β4 and hα7 Expressed in Xenopus Oocytes.

Journal of Pharmacology and Experimental Therapeutics. 280:346-356

Chavez-Noriega LE, Gillespie A, Stauderman KA, Crona JH, O'Neil Claeps, B, *et al.* (2000). Characterization of the recombinant human neuronal nicotinic acetylcholine receptors α3β2 and α4β2 stably expressed in HEK293 cells. Neuropharmacology 39(13): 2543-2560.

Cobb SR, Buhl EH, Halasy K, Paulsen O, Somogyi P (2005). Synchronization of neuronal activity in hippocampus by individual GABAergic interneurons. Nature 378:75–78.

Covernton PJO, Connolly JG (2000). Multiple components in the agonist concentration-response relationships of neuronal nicotinic acetylcholine receptors. Jour of Neuro Methods. 96:63-70.

Dannenberg H, Pabst M, Braganza O, Schoch S, Niediek J, Bayraktar M, et al. (2015). Synergy of direct and indirect cholinergic septo-hippocampal pathways coordinates firing in hippocampal networks. J Neurosci. 35:8394-410.

Dash B, Lukas RJ, Li MD (2014). A signal peptide missense mutation associated with nicotine dependence alters α2*-nicotinic acetylcholine receptor function. Neuropharmacology. 79:715-25.

Exley R, Moroni M, Sasdelli F, Houlihan L, Lukas R, Sher E, et al. (2006). Chaperone protein 14-3-3 and protein kinase A increase the relative abundance of low agonist sensitivity human α4β2 nicotinic acetylcholine receptors in Xenopus oocytes. J of Neurochem. 98:876-885.

Grando S, Horton R, Pereira E, Diethelm-Okita B, George P, Albuquerque E, et al. (1995). A nicotinic acetylcholine receptor regulating cell adhesion and motility is expressed in human keratinocytes. J. Invest. Dermatol. 105:774–781.

Grando S, Horton R, Mauro T, Kist D, Lee T, Dahl M (1996). Activation of keratinocyte nicotinic cholinergic receptors stimulates calcium influx and enhances cell differentiation. J. Invest. Dermatol. 107:412–418.

Grybko M, Sharma G, Vijayaraghavan S (2010). Functional distribution of nicotinic receptors in CA3 region in the hippocampus. J Mol Neurosci 40:114-20.

Hill JA Jr, Zoli M, Bourgeois JP, Changeux JP (1993). Immunocytochemical localization of a neuronal nicotinic receptor: the beta 2-subunit. J Neurosci 13:1551-68.

Houlihan LM, Slater Y, Guerra DL, Peng JH, Kuo YP, Lukas RJ, et al. (2001). Activity of cytisine and its brominated isosteres on recombinant human α7, α4β2, and α4β4 nicotinic acetylcholine receptors. J of Neurochem. 78:1029-1043

Jackson DC, Burgon RM, Sudweeks SN (2017). Expression of nAChR mRNA in Rat Hippocampal Interneurons. (In-preparation)

Ji D, Dani JA (2000). Inhibition and disinhibition of pyramidal neurons by activation of nicotinic receptors on hippocampal interneurons. J Neurophysiol 83:2682–2690.

Jones S, Yakel JL (1997). Functional nicotinic ACh receptors on interneurones in the rat hippocampus. J Physiol 504:603–610.

Kamens HM, McKinnon CS, Li N, Helms ML, Belknap JK, Phillips TJ (2009). The alpha 3 subunit gene of the nicotinic acetylcholine receptor is a candidate gene for ethanol stimulation. Genes Brain Behav. 6:600-9.

Khiroug SS, Khiroug L, Yakel JL (2004). Rat Nicotinic Acetylcholine Receptor α2β2 channels: Comparison of functional properties with α4β2 channels in *Xenopus* oocytes. Neuroscience. 124:817-822.

Leiser S.C., Bowlby M.R., Comery T.A., Dunlop J (2009). A cog in cognition: How the alpha 7 nicotinic acetylcholine receptor is geared towards improving cognitive deficits. Pharmacol. Ther. 122:302–311.

Lindstrom J. (1996) in Ion Channels, ed Narahashi T. (Plenum Publishing Corp. New York), 4:377–450.

Liu ZW, Yang S, Zhang YX, Liu CH (2003). Presynaptic alpha-7 nicotinic acetylcholine receptors modulate excitatory synaptic transmission in hippocampal neurons. Sheng Li Xue Bao. 55:731-5.

Martin LF, Kem WR, Freedman R (2004) Alpha-7 nicotinic receptor agonists: Potential new candidates for the treatment of schizophrenia. Psychopharmacology. 174:54–64.

Mihovilovic M., Roses A. (1993) Expression of alpha-3, alpha-5, and beta-4 neuronal acetylcholine receptor subunit transcripts in normal and myasthenia gravis thymus. Identification of thymocytes expressing the alpha-3 transcripts. J. Immunol. 151:6517–6524.

Moroni M, Zwart R, Sher E, Cassels BK, Bermudez (2006). α4β2 Nicotinic Receptors with High and Low Acetylcholine Sensitivity: Pharmacology, Stoichiometry, and Sensitivity to Long-Term Exposure to Nicotine. Molecular Pharmacology. 70:755-768.

Nelson ME, Kuryatov A, Choi CH, Zhou Y, Lindstrom J (2003). Alternate Stoichiometries of α4β2 Nicotinic Acetylcholine Receptors. Molecular Pharmacology. 63:332-341.

Papke RL, Boulter J, Patrick J, Heinemann S (1989) Single-channel currents of rat neuronal nicotinic acetylcholine receptors expressed in *Xenopus* oocytes. Neuron 3:589–596.

Rode F, Munro G, Holst D, Nielsen EØ, Troelsen KB, Timmermann DB et al. (2012). Positive allosteric modulation of α4β2 nAChR agonist induced behaviour. Brain Res. 1458:67-75.

Sarter M, Parikh V, Howe WM (2009). nAChR agonist-induced cognition enhancement: Integration of cognitive and neuronal mechanisms. Biochemical pharmacology 78(7): 658-667.

Soderman A, Mikkelsen JD, West M.J, Christensen DZ, Jensen MS (2011). Activation of nicotinic α(7) acetylcholine receptor enhances long term potentation in wild type mice but not in APP (swe)/PS1ΔE9 mice. Neurosci. Lett. 487:325–329.

Sudweeks SN, Yakel JL (2000). Functional and molecular characterization of neuronal nicotinic ACh receptors in rat CA1 hippocampal neurons. J Physiol. 527 Pt 3:515-28.

Szabó GG, Papp O, Máté Z, Szabó G, Hájos N (2014). Anatomically heterogeneous populations of CB1 cannabinoid receptor-expressing interneurons in the CA3 region of the hippocampus show homogeneous input-output characteristics. Hippocampus. 24:1506-23.

Thomsen MS, Hansen HH, Timmerman DB, Kikkelsen JD (2010). Cognitive improvement by activation of alpha7 nicotinic acetylcholine receptors: From animal models to human pathophysiology. Curr. Pharm. Des. 16:323–343.

Timmermann DB, Sandager-Nielsen K, Dyhring T, Smith M, Jacobsen AM, Nielsen EØ, et al. (2012). Augmentation of cognitive function by NS9283, a stoichiometry-dependent

positive allosteric modulator of α2- and α4-containing nicotinic acetylcholine receptors. Br J Pharmacol. 167:164-82.

Ullian E, McIntosh J, Sargent P (1997). Rapid Synaptic Transmission in the Avian Ciliary Ganglion Is Mediated by Two Distinct Classes of Nicotinic Receptors. J. Neurosci. 17:7210–7219.

Ussing CA, Hansen CP, Petersen JG, Jensen AA, Rohde LA, Ahring PK, et al. (2013). Synthesis, pharmacology, and biostructural characterization of novel α4β2 nicotinic acetylcholine receptor agonists. J Med Chem. 56:940-51.

Vernallis A, Conroy W, Berg D (1993). Neurons assemble acetylcholine receptors with as many as three kinds of subunits while maintaining subunit segregation among other receptor subtypes. Neuron. 10:451-464.

Wada E, Wada K, Boulter J, Deneris E, Heinemann S, Patrick J, Swanson LW (1989). Distribution of alpha2, alpha3, alpha4, and beta2 neuronal nicotinic receptor subunit mRNAs in the central nervous system: a hybridization histochemical study in the rat. J. Comp. Neurol. 284:314–355.

Wallace TL, Callahan PM, Tehim A, Bertrand D, Tombaugh G, Wang S, et al. (2011). RG3487, a novel nicotinic alpha7 receptor partial agonist, improves cognition and sensorimotor gating in rodents. J. Pharmacol. Exp. Ther. 336:242–253.

Wang F, Nelson ME, Kuryatov A, Olale F, Cooper J, Keyser K, et al. (1998). Chronic Nicotine Treatment Up-regulates Human α3β2 but Not α3β4 Acetylcholine Receptors Stably Transfected in Human Embryonic Kidney Cells. The Journal of Biological Chemistry. 273:28721-28732.

Wang S, Zhao C, Liu Z, Wang X, Liu N, Du W, Dai Q (2015). Structural and Functional Characterization of a Novel α-Conotoxin Mr1.7 from Conus marmoreus Targeting Neuronal nAChR α3β2, α9α10 and α6/α3β2β3 Subtypes. Mar Drugs. 16:3259-75.

Winzer-Serhan UH, Leslie FM (2005). Expression of α5 nicotinic acetylcholine receptor subunit mRNA during hippocampal and cortical development. J. Comp. Neurol 481: 19–30.

Wu TY, Smith CM, Sine SM, Levandoski MM (2008). Morantel allosterically enhances channel gating of neuronal nicotinic acetylcholine alpha 3 beta 2 receptors. Mol Pharmacol 74:466-75.

Yeh JJ, Yasuda, RP Dávila-García MI, Xiao Y, Ebert S, Gupta T, *et al.* (2001). Neuronal nicotinic acetylcholine receptor α3 subunit protein in rat brain and sympathetic ganglion measured using a subunit-specific antibody: regional and ontogenic expression. Journal of Neurochemistry 77: 336–346.

Zia S, Ndoye A, Nguyen V, Grando S (1997). Nicotine enhances expression of the alpha 3, alpha 4, alpha 5, and alpha 7 nicotinic receptors modulating calcium metabolism and regulating

adhesion and motility of respiratory epithelial cells. Res. Commun. Mol. Pathol. Pharmacol. 97:243–262.

Zwart R, Vijverberg HP (1998). Four pharmacologically distinct subtypes of alpha4beta2 nicotinic acetylcholine receptor expressed in Xenopus laevis oocytes. Mol Pharmacol 54:1124-31.

CHAPTER 3: The Highly Selective Positive Allosteric Modulator 3-furan-2-yl-N-p-tolyl-acrylamide Potentiates α7 and α7β2 Nicotinic Receptors With Different Efficacy

Hugo R. Arias[a,*], Doris Jackson[b], Zhenglan Chen[c], Manish Kumar[c], Eric B. Gonzales[c], Katarzyna M. Targowska-Duda[d], Agnieszka A. Kaczor[e,f], Renqi Huang[c], Glenn H. Dillon[c], and Sterling Sudweeks[b]

[a] Department of Medical Education, California Northstate University College of Medicine, Elk Grove, CA, USA

[b] Department of Physiology and Developmental Biology, College of Life Sciences, Brigham Young University, Provo, UT, USA

[c] Center for Neuroscience Discovery, Institute for Health Aging, University of North Texas Health Science Center at Fort Worth, TX, USA

[d] Department of Biopharmacy, and [e] Department of Synthesis and Chemical Technology of Pharmaceutical Substances with Computer Modeling Lab, Medical University of Lublin, Lublin, Poland

[f] Department of Pharmaceutical Chemistry, School of Pharmacy, University of Eastern Finland, Kuopio, Finland

*Corresponding author. Tel.: (916) 686-8548; fax: (916) 686-7310, E-mail address: hugo.arias@cnsu.edu

Key words: 3-furan-2-yl-N-p-tolyl-acrylamide, PAM-2, positive allosteric modulator, nicotinic acetylcholine receptor (AChR), acetylcholine (ACh), alpha 7, beta 2, homomeric, heteromeric, dose-response, molecular modeling, GABA

No conflicts of interest to be reported.

TABLES, FIGURES AND LEGENDS: 7 Figures, 4 Tables

Acknowledgements

This research was supported by grants from the Polish National Science Center (Sonata funding, UMO-2013/09/D/NZ7/04549) [to K.T-D. (PI) and H.R.A. (Co-PI)], Texas Alzheimer's Research and Care Consortium Investigator Grant Program (354528) (to R-Q.H.), Institute for Aging and Alzheimer's Disease Research (RI6146, to R-Q.H.; and RI6068, to E.B.G.), California Northstate University College of Medicine (to H.R.A.), and internal funding from Brigham Young University (to S.N.S). Calculations were partially performed under a computational grant (G30-18) by the Interdisciplinary Center for Mathematical and Computational Modeling (ICM), Warsaw, Poland, and under resources and licenses from CSC, Finland (to A.K).

Abstract

The activity of 3-furan-2-yl-*N*-p-tolyl-acrylamide (PAM-2) was compared among human (h) α7 and α7β2 nicotinic acetylcholine receptors (AChRs), heteromeric hα1β2γ2 and homomeric hρ1 $GABA_A$ receptor subtypes ($GABA_ARs$), and homomeric hα1 glycine receptors (GlyRs) by electrophysiological methods. The patch-clamp results indicated that although PAM-2 did not affect GlyRs and slightly decreased the activity of hρ1 $GABA_ARs$ (i.e., 300 μM PAM-2 decreased the activity by 30 ± 1%), it moderately enhanced the activity of hα1β2γ2 $GABA_ARs$ (EC_{50} = 56 ± 7 μM; E_{max} = 131 ± 4%) compared to control (100%). These results confirmed the high selectivity of PAM-2 for α7 AChRs. The voltage-clamp results indicated that PAM-2 potentiates hα7 AChRs mainly by increasing current intensity (EC_{50} = 141 ± 1.74 μM; E_{max} = 230%) with higher efficacy than that observed in hα7β2 AChRs (EC_{50} = 186 ± 1.35 μM; E_{max} = 190%). The molecular docking and dynamics results show that PAM-2 interacts differently between the hα7 and hα7β2 models. More specifically, PAM-2 interacts with the archetypic intrasubunit site as well as with the ECD-TMD junction in the hα7 model, whereas it interacts with different ECD-TMD sites in the $h(\alpha7)_2(\beta2)_3$ and $h(\alpha7)_3(\beta2)_2$ stoichiometries. The combination of functional and structural results suggest that the potentiating effect elicited by PAM-2 is determined by its interaction with the intrasubunit site, whereas its activity is mediated by its interaction with junctional sites.

Introduction

Positive allosteric modulators (PAMs) with high selectivity for α7 nicotinic acetylcholine receptors (AChRs) have generated a lot of expectation since these compounds might be used for the treatments of different neurological disorders producing fewer side effects than agonists (reviewed in Arias, 2010; Chatzidaki and Millar, 2015). Among them, PAM-2 (3-furan-2-yl-*N*-p-tolyl-acrylamide) enhances agonist-induced α7 AChR activity in a temperature-sensitive manner and reactivates desensitized α7 AChRs supporting a type II PAM classification, with certain resemblance to type I PAMs when studied at the single-channel level (Arias et al., 2011; Targowska-Duda et al., 2014; Andersen et al., 2016). In conclusion, PAM-2 has pharmacological properties that are in between of type I and type II PAMs, which makes it a distinct α7 PAM.

Previous functional studies demonstrated the PAM-2 has positive allosteric modulatory activity on α7 AChRs, whereas it inhibits human (h)α3β4, hα4β2, hα4β4 AChRs, slightly inhibits N-methyl-D-aspartate (NMDA)-sensitive glutamate receptors (GluRs), slightly potentiates α-amino-3-hydroxy-5-methyl-4-isoxazolepropionic acid (AMPA)-sensitive GluRs, and affects neither kainate-sensitive GluRs, serotonin type 3 receptors, $Na_v1.2$ and $K_v3.1$ voltage-gated ion channels, acetylcholinesterase, nor β-amyloid content, indicating that this ligand presents high receptor selectivity (Arias et al., 2011; 2015a; 2016; Andersen et al., 2016). Nevertheless, the activity of PAM-2 between homomeric α7 and heteromeric α7β2 AChRs has not been studied yet. Interestingly, functional α7β2 AChRs have been characterized in different neuronal types, including hippocampal GABAergic interneurons (Khiroug et al., 2002, Liu et al., 2012; Wu et al., 2016), and forebrain cholinergic neurons (Liu et al., 2009). Since inhibition of hippocampal α7β2 AChRs by β-amyloid might be significant for the observed memory and learning disabilities found in Alzheimer's disease patients (Liu et al., 2012), the modulatory activity

elicited by PAM-2 might alleviate these cognitive problems. To start delineating this supposition, we initiated this study by comparing the activity of PAM-2 between hα7 and hα7β2 AChRs expressed on *Xenopus laevis* oocytes by whole-cell voltage-clamp recordings.

Glycine receptors (GlyRs) and γ-aminobutyric acid type A ($GABA_ARs$), two major inhibitory receptor members from the Cys-loop ligand-gated ion channel superfamily where AChRs also belong (reviewed in Arias, 2011), are important for learning and memory processes (reviewed in Xu and Gong, 2010). $GABA_ARs$ are potentiated by structurally different compounds, including neurosteroids, benzodiazepines, and barbiturates, and the major adult isoform, α1β2γ2 $GABA_AR$, is expressed in brain areas related to cognitive function such as cerebral cortex and hippocampus (reviewed in Sigel and Steinmann, 2012). In addition, GlyRs are potential targets for analgesic and anti-inflammatory drugs, and α1 containing GlyRs are selectively potentiated by ginkgolic acids which are the active components for the antidepressant activity found in *Ginkgo biloba* lipophilic extracts (Maleeva et al., 2015, and references therein). This evidence supports the notion that these receptor subtypes could be modulated by other PAMs. To determine whether the observed procognitive (Potasiewicz et al., 2015; 2017), promnesic (Targowska-Duda et al., 2016), antidepressant-like (Targowska-Duda et al., 2014; Arias et al., 2015), anti-nociceptive and anti-inflammatory (Bagdas et al., 2015) effects elicited by PAM-2 are related to these receptor subtypes, the activity of this ligand was determined on heteromeric hα1β2γ2 and homomeric hρ1 $GABA_AR$ subtypes as well as on homomeric hα1 GlyRs by whole-cell patch-clamp techniques.

Considering that the PAM-2 structure has an amide link susceptible to the metabolic activity of amidases from the liver and/or brain (Pop, 1997), the activity of the potential metabolites *p*-toluidine and 3-(2-furyl)acrylic acid were also tested on the hα7 AChR. Since N,N′-

dicyclohexylurea was found as a byproduct in the synthesis of PAM-2, the PAM activity of this compound was also tested on the hα7 AChR.

Previous molecular docking and molecular dynamics experiments using the *Torpedo* AChR as the template for the construction of the hα7 AChR, demonstrated that the potential active sites for PAM-2 are localized in the transmembrane domain (TMD) (Arias et al., 2016). More specifically, PAM-2 interacted with the intrasubunit site already characterized for PNU-120596, the archetype of type II PAMs, and also with an intersubunit site located between two α7-TMDs that had not been previously characterized and might be important to define the pharmacological differences observed between PNU-120596 and PAM-2 and other type I PAMs (Andersen et al., 2016). By comparing the structural components of the docking sites between the homomeric hα7 and heteromeric hα7β2 AChRs, we demonstrated that PAM-2 binds to the archetypical intrasubunit site in the hα7 AChR as well as to an intersubunit site in the $h(\alpha7)_2(\beta2)_3$ model. Interestingly, this structural difference correlates with the functional results indicating that PAM-2 potentiates hα7 AChRs mainly by increasing current intensity with higher efficacy than that at hα7β2 AChRs.

Materials and Methods

Materials

Glycine (Gly), γ-aminobutyric acid (GABA), penicillin (5000 U/mL)-streptomycin (5 mg/mL), acetylcholine chloride (ACh), fetal bovine serum (FBS), poly-L-lysine hydrobromide, and Dulbecco's Modified Eagle Medium (DMEM) were purchased from Sigma-Aldrich (St. Louis, MO, USA). PAM-2 was synthesized as described previously (Arias et al., 2011). *Xenopus laevis* oocytes were purchased from Ecocyte Bioscience (Austin, TX, USA). Plasmids containing

the hα7 and hβ2 subunit genes were purchased from Origene Technologies (Rockville, MD, USA). One Shot® *E. coli* chemically competent cells were obtained from Invitrogen (Carlsbad, CA, USA). HiSpeed® plasmid purification kit was obtained from QIAGEN Inc. (Valencia, CA, USA). TE buffer (10 mM Tris, 1 mM EDTA, pH 8.0) was purchased from Bioexpress (Layton, UT, USA). PolyJet™ DNA *In Vitro* transfection reagent was obtained from SignaGen Laboratories (Rockville, MD, USA). *Trans*-IT 293 transfection reagent was purchased from Mirus, Bio LLC (Madison, WI, USA). Salts, solvents, and reagents were purchased from commercial suppliers and used as received.

Voltage-Clamp Recording on Xenopus laevis Oocytes Expressing hα7 or hα7β2 AChRs

The hα7 (Origene# SC124074-20) and hβ2 (Origene# SC309051) mRNAs were prepared using the respective subunit gene in the pCMV6-XL4 plasmid. The plasmids were transformed into One Shot® E. coli chemically competent cells, and then isolated and purified using the HiSpeed® plasmid purification kit. Plasmids containing the hα7 and hβ2 genes were linearized with XBa1 and AvrII, respectively (New England BioLabs Inc., Ipswich, MA, USA). The mRNA was then transcribed, capped on the 5' end, and a PolyA tail was added using the mMessage mMachine® T7 Ultra Kit (Ambion, Carlsbad, CA, USA). mRNAs were isolated by LiCl purification, resuspended in Tris-EDTA Buffer, aliquoted, and stored at -20 °C until used.

Human α7 (0.2 or 1.0 μg/μL) and β2 (1.0 μg/μL) AChR subunit mRNAs were injected into *X. laevis* oocytes using a Nanoject II microinjector (Drummond Scientific Company, Broomall, PA, USA). The injection and recording needles of borosilicate glass were pulled by using Model P-97 puller (Sutter Instrument Company,Novato, CA, USA). For homomeric hα7 AChRs, oocytes were injected with 50.6 nL of 0.2 μg/μL hα7 mRNAs. For heteromeric hα7β2 AChRs, the hα7 and hβ2 mRNAs were injected at either the [1:1] or [1:5] hα7:hβ2 ratio (1.0

μg/μL:1.0 μg/μL, 0.2 μg/μL:1.0 μg/μL). The rationale being that a [1:5] (i.e., 0.2:1 μg/μL) ratio would be more likely to produce a higher yield of heteromeric hα7β2 AChRs and relatively less homomeric hα7 AChRs. However, the resulting recordings using either ratio were not statistically different from each other (One-way ANOVA of rise times, decay times, and peak currents, $p>0.05$), indicating the presence of hα7β2 AChRs in oocytes injected with either hα7:hβ2 ratio.

Following injection, the oocytes were incubated for 7-9 days on a rocker between 17-19 °C and stored in OR-2-Ca^{2+} (Ringer's solution, extracellular solution) (pH 7.5) with penicillin-streptomycin (10,000 units/mL; 10 mg/mL).

For the two-electrode whole-cell voltage clamp recordings, ligands were perfused on oocytes clamped at -60 mV. All ligands were dissolved in OR-2-Ca^{2+}, whereas PAM-2 was dissolved in 1% DMSO. Control experiments showed no significant difference in responses with solutions containing 1% DMSO. Solutions were perfused using an 8-valve, computer controlled, pressurized perfusion system (Automate Scientific, Berkeley, CA, USA). Each oocyte was impaled with microelectrodes filled with 3 M KCl and a resistance between 0.1-2 MΩ. Clampex 9.2 was used to run the electrophysiology protocols through a GeneClamp 500B amplifier and Digidata 1322A digitizer. Data was acquired at 5 kHz and filtered at 2 kHz. The data was analyzed using Clampfit 9.2 (Molecular Devices, Sunnyvale, CA, USA).

Patch-Clamp Recording of HEK293 Cells Expressing $GABA_A$Rs or GlyRs

The HEK293 cell line stably expressing recombinant hα1β2γ2 $GABA_A$R subunits or transiently transfected with hα1 GlyR or hρ1 $GABA_A$R subunits were used to investigate the effect of PAM-2 on these receptors. The PolyJet™ DNA *In Vitro* and *Trans*-IT 293 transfection reagents were used for transient transfection of the respective hα1 and hρ1 subunits. Briefly, 0.5 μg of hα1

subunit cDNA was added to cells growing exponentially on poly-L-lysine coated coverslips placed in a 35-mm culture dish. In the case of hρ1, 2 μg of hρ1 subunit cDNA and 2 μg of enhanced green fluorescent protein cDNA was added to cells growing on glass coverslips. Cells that showed expression of the green fluorescent protein were subjected to patch-clamp electrophysiology, as described previously (Snell and Gonzales, 2015). Transfected cells were used for electrophysiological analysis 24-48 h after the transfection.

Whole-cell patch clamp recordings were performed at room temperature (RT) (22-25 °C) at a holding potential of -60 (hα1β2γ2 and hα1) or -70 mV (hρ1). Patch pipettes of borosilicate glass (M1B150F, World Precision Instruments, Inc., Sarasota, FL, USA) were pulled using a P-87 Flaming/Brown or a Sutter P-97 horizontal puller (Sutter Instrument Co., Novato, CA) to a tip resistance of 6-9 MΩ. The pipette solution for the hα1β2γ2 $GABA_A$Rs and hα1 GlyRs contained (in mM): 140 CsCl, 10 EGTA, 10 HEPES, 4 Mg-ATP; pH 7.2. A coverslip containing transfected cells was placed in a small chamber (~1.5 mL) on the stage of an inverted light microscope (Olympus IMT-2) and superfused continuously (5-8 mL/min) with the following external solution containing (in mM): 125 NaCl, 5.5 KCl, 0.8 $MgCl_2$, 3.0 $CaCl_2$, 10 HEPES, 10 glucose, pH 7.3. The external solution for the hρ1 $GABA_A$R contained (in mM): 137 NaCl, 5.4 KCl, 1.8 $CaCl_2$, 1 $MgCl_2$, and 5 HEPES; pH 7.4, whereas the internal recording solution contained: 120 CsCl, 20 tetraehtylammonium chloride, 1 $CaCl_2$, 2 $MgCl_2$, 11 EGTA, and 10 HEPES; pH 7.2 (Snell and Gonzales, 2015). In this case, a Perfusion Fast-Step 77B (Warner Instrument LLC., Hamden, CT, USA) equipped with an array of square capillary tubes was used.

GABA or Gly was prepared in extracellular solution and applied (10-s) to cells containing the hα1β2γ2 $GABA_A$Rs or hα1 GlyRs via gravity flow using a Y-shaped tube positioned near the target cell. With this system, the 10-90% rise time of the junction potential at

the open tip was 60-120 ms (Huang and Dillon, 1999). In the case of the hρ1 $GABA_AR$, the GABA control and PAM-2 containing test solutions were applied for 5 s. A washout period of 90 s followed each recording to ensure a return to baseline current readings was achieved before proceeding to the next recording. Receptor currents were obtained using a patch clamp amplifier (Axopatch 200A, Axon Instruments, Foster City, CA, USA) equipped with a CV201A headstage, whereas a pClamp10.0 (Molecular Devices, Sunnyvale, CA, USA) on an inverted fluorescence microscope equipped with a FITC fluorescence cube was also used to record hρ1 $GABA_AR$ currents.

The hα1β2γ2 $GABA_AR$ and hα1 GlyR currents were low-pass filtered at 5 kHz, monitored on an oscilloscope and a chart recorder (Gould TA240), and stored on a computer (pClamp 6.05, Axon Instruments) for subsequent analysis. Receptors were typically activated with agonist concentrations corresponding roughly to the EC_{30} (10 μM; hα1β2γ2) (Huang et al., 2001) or EC_{50} (9.4 μM; hρ1) value for GABA and the EC_{30} value for Gly (15 μM; hα1) (Chen et al., 2004), respectively. These concentrations were chosen because produce minimal receptor desensitization, which may confound interpretation of results. To monitor the possibility that access resistance changed over time or during different experimental conditions, the current response to a -5 mV voltage pulse was measured at the initiation of each recording and stored on our digital oscilloscope. This stored trace was continually referenced throughout the recording. If a change in access resistance was observed throughout the recording period, the patch was aborted and the data were not included in the analysis.

The concentration-response relationship for PAM-2 on hα1β2γ2 $GABA_ARs$ was analyzed using the following logistic equation (Potasiewicz et al., 2015): $I_{PAM\text{-}2}/I = 1/[1 + (\text{apparent } EC_{50}/[\text{PAM-2}])^{n_H}]$, where I is the current amplitude determined in the absence of PAM-2 (control

assigned as 100%), I_{PAM-2} is the potentiation induced by different concentrations of PAM-2 [PAM-2], apparent EC_{50} is the PAM-2 concentration to produce half-maximal potentiation, and n_H is the Hill coefficient.

Statistical Analysis

The obtained data, expressed as the mean ± SEM, were analyzed using the Origin 6.0 Microcal Software. Statistical analyses were performed using one-way analysis of variance (ANOVA) and t-test (paired or unpaired). Differences will be accepted as significant with $p \leq 0.05$.

Homology Modeling, Molecular Docking, and Molecular Dynamics

The amino acid sequences and numbering of the hα7, hα4, and hβ2 subunits were obtained from the UniProt implemented in ExPASy Molecular Biology Server (http://www.us.expasy.org) (Gasteiger et al., 2003). The hα7 sequence was aligned with the hα4 and hβ2 sequences using Clustal Omega (http://www.ebi.ac.uk/Tools/msa/clustalo/). Structural models of the hα7 as well as of the $h(\alpha7)_2(\beta2)_3$ and $h(\alpha7)_3(\beta2)_2$ stoichiometries were built applying homology modeling methods using the crystal structure of the hα4β2 nAChR obtained at 3.94 Å atomic resolution [PDB ID: 5KXI; www.rcsb.org/pdb/home/home.do (Morales-Perez et al., 2016)] as template. Modeller 9.14 was used to obtain 100 homology models for each template, and subsequently, their Discrete Optimized Protein Energy profiles (Eswar et al., 2006) were assessed. The best model of each template was assessed by its quality by Ramachandran plots, generated by using the Schrödinger suite software (Schrödinger Release 2015-3: Maestro, version 10.3). The β2 subunit in both $h(\alpha7)_2(\beta2)_3$ and $h(\alpha7)_3(\beta2)_2$ stoichiometries was taken from the hα4β2 nAChR crystal structure, and each model optimized using Desmond (Schrödinger suite software).

For the molecular docking procedure, PAM-2 was first built using the semiempirical AM1 method included in Spartan 10 V.1.1.0 (Wavefunction, Inc. Irvine, CA, USA) as previously described (Arias et al., 2016). AutoDock Vina (Trot and Olson, 2010) was used for docking simulations of the flexible ligand into the extracellular (ECD) or transmembrane (TMD) (including ECD-TMD junction) of the whole, rigid, nAChR model under study. The energetically lower poses were selected from each cluster of superposed poses as described previously (Arias et al., 2013; 2016).

To investigate the stability of the best scored complexes, 15-ns molecular dynamics (MD) simulations were subsequently performed for PAM-2 docked to each binding site in the respective AChR model, using Desmond v.3.0.3.1 (Bowers et al., 2006) and OPLS-2005 force field. Each receptor-PAM-2 complex was inserted into 1-palmitoyl-2-oleoyl phosphatidylcholine membranes, solvated with water, and the protein charges neutralized with 0.15 M NaCl as described elsewhere (Arias et al., 2015; 2016). Each complex was first minimized and then subjected to 1-ns MD in NVT (constant number of particles, volume, and temperature) ensemble, followed by 15-ns MD in NPT (constant number of particles, pressure, and temperature) ensemble with fixing constrains on protein backbone as previously described (Arias et al., 2015; 2016). Finally, each complex was simulated in NPT ensemble for 15-ns without any fixing constraints. The total potential energy of each docked model was calculated using the OPLS-2005 force field according to Bowers et al. (2006).

Results

Different PAM-2 Activity Between hα7 and hα7β2 AChRs

Injection of hα7 mRNAs with or without hβ2 mRNAs into *Xenopus laevis* oocytes resulted in functional hα7 and hα7β2 AChRs. For heteromeric hα7β2 AChRs, the hα7 and hβ2

mRNAs were injected at either the [1:1] or [1:5] hα7:hβ2 ratio. The rationale being that a [1:5] (i.e., 0.2:1 μg/μL) ratio would be more likely to produce a higher yield of heteromeric hα7β2 AChRs and relatively fewer homomeric hα7 AChRs. However, the resulting recordings using different ratios were not statistically different from each other (One-way ANOVA of rise times, decay times, and peak currents to PAM-2, $p>0.05$), indicating the presence of hα7β2 AChRs in oocytes injected with either hα7:hβ2 ratio.

Regarding the first series of experiments, the electrophysiological recordings illustrate that the pre-application of PAM-2 caused kinetic changes on both ACh-activated hα7 (Figure 1.A) and hα7β2 (Figure 1.B) AChRs. PAM-2 increased the peak amplitude on both receptor subtypes. To differentiate the effect of PAM-2 between the hα7 and hα7β2 AChRs, two protocols were developed. The concentration-response curves for PAM-2 (Figure 1.C) in the presence of a fixed concentration of ACh was determined on each AChR subtype. Additionally, the concentration-response curves for ACh were determined in the absence and presence of a fixed concentration of PAM-2 (Figures 3.A-B). PAM-2 increased the peak amplitude of both hα7 and hα7β2 (Table 1). At the maximal PAM-2 effect, there is not a significant difference in the fold increase of the peak amplitudes between hα7 and hα7β2. However, because of the differences in their PAM-2 EC_{50} values we observe that there is a statistical difference in relative peak amplitude at 10 μM PAM-2 ($p<0.01$, t-test).

The concentration-response curves for PAM-2, with a fixed ACh concentration, showed significant increases at all PAM-2 concentrations in rise time, half-width, and decay tau when compared to controls that were not exposed to PAM-2 (Figs 2.A-C). These effects were similar at all PAM-2 concentrations (i.e. ANOVA testing showed no significant difference between PAM-2 concentrations). Therefore, we pooled the data from multiple PAM-2 concentrations for

the following t-tests (significance level of 0.05, two-tailed). The rise time values for PAM-2 hα7 and PAM-2 hα7β2, although both significantly different from their respective baselines, were not significantly different from each other (t-test against baselines $p<0.01$, $p<0.01$, respectively, Figure 2.B). Likewise, half-width values from PAM-2 hα7 and PAM-2 hα7β2 were significantly different from their respective baselines (hα7 $p<0.0001$, hα7β2 $p<0.00000001$), but not from each other.

The decay phase of the ACh induced currents was fit using a single exponential equation, yielding tau values. Unlike the rise time and half-widths, the PAM-2 effect on the tau values is statistically different for hα7 than for hα7β2 ($p=0.00816$, Figure 2.C). The hα7 does not show a significant increase in the tau decay, but the trend shows a possible increase. Whereas, the hα7β2 subtypes show a significant increase in the tau decay following PAM-2 exposure when compared to their respective baselines ($p=0.104$, $p<0.001$). Additionally, the hα7β2 has a significantly longer tau value following PAM-2 application compared to the hα7. This allows the two subtypes to be distinguished using PAM-2.

The ACh concentration-response curves for hα7 and hα7β2 are not statistically different from each other. Additionally, in the presence of PAM-2, the concentration-response curves remain similar to each other (Figures 3.A-B; Table 2). PAM-2 significantly increased the rise time values at the lower ACh concentrations for both hα7 and hα7β2 (Figures 3.C-D). Additionally, 20 μM PAM-2 significantly increased the total area at ACh concentrations between 100 μM and 10 mM for both subtypes. In fact, at the maximum ACh concentration (10 mM) PAM-2 (20 μM) differentiates between hα7 and hα7β2 AChRs because of the larger increase in total area of the hα7 subtype (ANOVA, $p<0.001$, Figure 3.F). The hα7 26– fold as compared to

the hα7β2 which AChRs by 26- and 6-fold, respectively (Figure 3.F, Table 1). This is a 4.5-fold difference between the total current in the hα7 and hα7β2 treated with 20 μM PAM-2.

Although there is an increase in rise time for both subtypes when compared to the controls, there is only a slight difference in the effect of PAM-2 either subtype (Figures 3.C-E). The trend shows that hα7β2 AChRs may have longer rise times after PAM-2 applications. This could indicate changes in the channel opening, ACh affinity, or desensitization properties. See Table 2 for the summary of the fits and kinetic changes of Figures 3A-F.

Figure 4 shows the time dependence of the PAM-2's effect on the peak amplitude and current area for both hα7 and hα7β2 AChRs. Both parameters were significantly different than that for the control after only 10 seconds of 20 μM PAM-2 application on both subtypes. Interestingly, the effects became more pronounced over time with continued application of PAM-2. We also observed that the PAM-2 effect was reversible over time. To more easily differentiate the AChR subtypes and to ensure that the maximum effect on peak amplitude was reached, the application of PAM-2 was continued for 4.5 min. The maximal effect of PAM-2 on peak amplitude was reached at 1.5 min, whereas its effect on the current area continued to increase during the entire application. Therefore, we selected 3 min as our point of comparison for the experiments used in Figures 1-3.

Effect of PAM-2 on $GABA_AR$ and GlyR Function

To examine whether PAM-2 affects hα1β2γ2 and hρ1 $GABA_ARs$ or hα1 GlyR activity, different PAM-2 concentrations (i.e., 10-300 μM) were co-applied with 10 μM (Figure 4.A) or 9.4 μM GABA (Figure 4.B) or 15 μM Gly (Figure 5). The results indicated that PAM-2 potentiated GABA-activated hα1β2γ2 $GABA_AR$ currents (Figure 4.A) as well as inhibited hρ1 $GABA_AR$ activity (Figure 4.B) in a concentration-dependent manner. The maximum effects were

observed with 300 μM PAM-2, where hα1β2γ2 currents were increased to 131 ± 4% ($p<0.05$), whereas the hρ1 currents were decreased to 70 ± 1% ($p<0.001$) compared to control (100%) (Table 1). The potentiating EC_{50} value for PAM-2 on hα1β2γ2 $GABA_A$Rs was 56 ± 7 μM (Table 1). The calculated n_H value (1.50 ± 0.20; Table 1) suggests a cooperative mechanism, which is in agreement with the fundamental mechanism of PAMs. In the hα1β2γ2 subtype, the onset of the PAM-2 effect was rapid and completely reversible within 2-3 min. On the other hand, PAM-2 had no effect on GlyR response ($p>0.05$) (Figure 5; Table 1).

Homology Modeling, Molecular Docking, and Molecular Dynamics of PAM-2 at the hα7, $h(\alpha7)_2(\beta2)_3$, and $h(\alpha7)_3(\beta2)_2$ Models

PAM-2 was docked into the ECD or TMD (including ECD-TMD junction) of the whole receptor model. Since PAM-2 activity does not involve the orthosteric sites (Arias et al., 2011), this interaction was not included in Figure 6. Although the ECD is not involved in the PAM-2 activity (Andersen et al., 2016), the observed allosteric site in the $h(\alpha7)_2(\beta2)_3$ model is shown in Figure 6A. The MD results indicated that the interactions summarized in Table 3 are stable during the 50-ns simulations. This is based on the consideration that a ligand in its respective pocket is stable when the RMSD variance value is ≤0.5 Å (Arias et al., 2016). The RMSD mean values for the 50-ns simulation and the RMSD variance values calculated during the last 10-ns are included in Table 4.

In the hα7 model, PAM-2 interacted with both the archetypical intrasubunit and ECD-TMD junction 1 sites (Figure 6). The results using this new hα7 model showed that PAM-2 interacts with the intrasubunit site as previously described in the hα7 model built using the *Torpedo* AChR as template (Arias et al., 2016). More specifically, PAM-2 interacted with residues from M1 (i.e., Leu216, Cys219, Val220, and Ser223, and M4 (i.e., Thr461, Ile464, and Leu465). In

junction 1, PAM-2 interacted with residues from the Cys-loop (i.e., Trp134, Phe135, Pro136, and Phe137), pre-M1 segment (i.e., Thr208, Tyr210, and Gly212), M1 (Leu216), M2-M3 loop (i.e., Leu270 and Ile271), and M4 (i.e., Leu465, Ala468, and Pro469) (Figure 6A).

In the $h(\alpha7)_2(\beta2)_3$ model, PAM-2 interacted with the ECD-TMD junction at three sites called junction 2, and 3 (orientation 1 and 2), which are different from that characterized on the hα7 nAChR (Figure 6A; Table 3). In junction 2, PAM-2 intercalated between both α7 and β2 subunits, interacting with the β1-β2 loop (i.e., α7-Lys46, β2-Glu47, and β2-Arg48), pre-M1 (i.e., β2-Phe211, β2-Tyr212, β2-Asn215, and β2-Leu216), and M2 (i.e., α7-Leu255, α7-Ala258, α7-Glu259, α7-Ala263, β2-Leu257, β2-Lys260, and β2-Ile261) (Figures 6.A-B; Table 3). An H-bond is formed between the PAM-2 nitrogen of the amide moiety and the carbonyl oxygene from the α7-Ala258 backbone. In junction 3 orientation 1, located within the β2 subunit, PAM-2 interacted with residues from the M2-M3 loop (i.e., Lys274 and Tyr275), M3 (i.e., Phe278, β2-Thr279, and Leu282), and M4 (i.e., Cys361, Phe363, Gly364, Gly367, and Met368) (Figures 6.A-C). An H-bond is formed between the carbonyl oxygen of PAM-2 and the α7-Lys274 nitrogen moiety. In junction 3 orientation 2, PAM-2 also interacted with β2 residues from the Cys-loop (i.e., His136, Phe137, Pro138, and Phe139, M1 (i.e., Ile217, Cys220, and Val221), M2-M3 loop (i.e., Leu271, Val272, Tyr275, and Leu276), and M4 (i.e., Met368, Phe369, and Pro372) (Figures 6.A-D; Table 3). Although two residues (i.e., β2-Tyr275 and β2-Met368) are common for two orientations of PAM-2 at ECD-TMD junctioon 3 site at $h(\alpha7)_2(\beta2)_3$ model, there are three possible β2 subunits so these two bindings sites might not be overlapped.

In the $h(\alpha7)_3(\beta2)_2$ model, PAM-2 interacted with ECD-TMD junction 1, 2, and 4, and luminal sites. The junction 1 and 2 sites are observed in the hα7 and $h(\alpha7)_2(\beta2)_3$ model, respectively. In junction 4, PAM-2 docked between two α7 subunits, interacting with residues

from the β1-β2 loop (i.e., Lys46 and Gln48) (this site has the same residue, α7-Lys46, as observed in junction 2 from the h$(\alpha7)_2(\beta2)_3$ model, so change the number but junction 2 is between a7 and b2, while this junction 4 is between two a7 subunits. These are homologous sites that need to be clearly stated, if you use different numbers, you are saying that are two totally different sites), Cys-loop (i.e., Tyr129), and M2 (i.e., Glu259, Pro262, Ala263, and Thr264) from one α7 subunit, and with residues from the ECD (i.e., Asp42, Val43), β1-β2 loop (i.e., Asp44 and Glu45), Cys-loop (i.e., Asn171, Gly172, Glu173, and Trp174), pre-M1 (i.e., Tyr211) from an adjacent α7 subunit. Finally, PAM-2 interacted with the ion channel lumen, more specifically with residues from positions 6', 2', and -2', as well as with additional residues from positions 5', 1', -3', and -4'. Since the binding to this luminal site presented higher energy compared to other non-luminal sites, and considering that PAM-2 does not block hα7 nAChRs at potentiating concentrations (Arias et al., 2011; 2016), this interaction was not further considered.

Discussion

In electrophysiological recordings, the hα7 and hα7β2 are almost indistinguishable. However, with enough replicates we can resolve that the rise time for the hα7 is slightly faster than the hα7β2. This is likely because there are 5 possible ACh binding sites on the hα7 (Corringer, 2000, Changeux, 1998). In addition, the hα7 AChR only requires that one binding site needs to be occupied for full receptor activation and subsequent channel opening (Andersen et al., 2013). Therefore, the likelihood of channel opening is higher for the hα7. However, saturating concentrations of agonists may induce rapid desensitization (Papke et al., 2000). Whereas, the hα7β2 likely only has 2 or 3 ACh binding sites, depending on the subunit stoichiometry, (likely h$\alpha7_2\beta2_3$ or h$\alpha7_3\beta2_2$) and multiple molecules of ACh are required for

receptor activation. Since a α7:β2 1:5 ratio was injected, both hα7_2β2_3 and hα7_3β2_2 might be expressed, producing events that are the result of both receptor stoichiometries. In sum, it is likely that ACh more easily activates and desensitizes the hα7 than the hα7β2; yet, the differences are so minute that it can be difficult to distinguish *in vivo*. Additionally, there are no current pharmacological ways to distinguish the two subtypes *in vivo* during an electrophysiological recording. Therefore, we thought it imperative to see if PAM-2 has a distinguishable effect on the hα7 and hα7β2.

We found that the area under the curve, or total current, distinguishes the hα7 and hα7β2 in the presence of PAM-2. Since, there is a dramatic increase in area this may be evidenced of a change in desensitization. This change in total area may be more evident in the hα7 because it is natively in a more desensitized state. As a metaphor, the hα7 has a greater working distance, and that the change in desensitization is more pronounced since it starts at a higher desensitized state. The change in desensitization for each subtype is supported by the increase in rise time and the increase in peak amplitude for each.

PAM-2 may slow the process of receptors moving from their open to their desensitized states. The voltage clamp results also indicated that the activity of PAM-2 differs between hα7 and hα7β2 AChRs. Namely, PAM-2 increased the tau for the single exponential fit of decay more for the hα7β2 than for the hα7. Both subtypes show an increase in the tau as compared to the baselines, but the changes in the hα7β2 were more significant. Considering, there is not a significant difference in the PAM-2 effect on hα7 and hα7β2 half-width and rise times, but only on the decay phase, it may highlight distinct binding properties of PAM-2 on either subtype.

Interestingly we observed a shift in the ACh EC_{50} value to the right in the hα7β2 ACh concentration-response curve in the presence of PAM-2. A shift to the left is expected for

PAMs, however, in the presence of a PAM the higher the agonist concentration, the higher the ion channel blockade. For this reason, we used 50 μM ACh (represents ~25% of the total peak current for the hα7β2 and the hα7) for our PAM-2 concentration-response curve (Figure 1.C) In the ACh concentration-response curve, even though the ACh EC_{50} in the presence of PAM-2 was shifted to the left, the fold response is still greater compared to the control (Figure 3.B).

Regarding the PAM-2 concentration-response curve (Figure 1.C) we see sharp increases in the $n_{H,}$ as well as maximum fold increases of 2.5 for the hα7 and 2.1 for the hα7β2. For both subtypes, there is a concentration at which you reach the maximum fold increase and increasing the PAM-2 concentration does not result in a more enhanced response. At 10 μM PAM-2, we see a distinguishing difference between the effect of PAM-2 on the hα7 and hα7β2. In sum, even though there are many indistinguishable properties between the hα7 and hα7β2, PAM-2 serves to distinguish the hα7 and hα7β2 from one another.

The patch clamp results indicated that PAM-2 induces only a modest potentiation of GABA-activated hα1β2γ2 $GABA_AR$ currents and slight inhibition of hρ1 $GABA_AR$ currents, but does not influence homomeric hα1 GlyR activity. Since the observed effects on $GABA_ARs$ are produced at non-clinically relevant concentrations, it is unlikely that $GABA_ARs$ and GlyRs, members of the same Cys-loop receptor superfamily as for α7 AChRs, might mediate the beneficial effects elicited by PAM-2, including procognitive (Potasiewicz et al., 2015; 2016), promnesic (Targowska-Duda et al., 2016), antidepressant-like (Targowska-Duda et al., 2014; Arias et al., 2015), anti-nociceptive and anti-inflammatory (Bagdas et al., 2015) activities.

Considering that the PAM-2 structure has an amide link susceptible to the metabolic activity of amidases from the liver and/or brain (Pop, 1997), the activity of the potential metabolites *p*-toluidine and 3-(2-furyl)acrylic acid were tested on the hα7 AChR. The functional results

indicated that neither *p*-toluidine nor 3-(2-furyl)acrylic acid have activity (Table 1), discarding the possibility of PAM-2 active metabolites produced by amidases from the liver and/or brain. However, we cannot rule out the existence of other metabolic pathways producing additional metabolites (e.g., methoxy metabolites) with potential activity. Since N,N′-dicyclohexylurea was found as a byproduct in the synthesis of PAM-2, the PAM activity of this compound was also tested on the hα7 AChR. The results showed no activity for N,N′-dicyclohexylurea, indicating that this precursor is not responsible for the observed PAM-2 activity.

This new study using the crystal structure of the hα4β2 nAChR as the homology template confirms previous results obtained with the hα7 model built using the *Torpedo* AChR as the homology template (Arias et al., 2016). More precisely, these news results indicate that PAM-2 binds to the intrasubunit site characterized for PNU-120596, the archetypical type II PAM (Young et al., 2008; daCosta et al., 2011; Arias et al., 2016). Recent findings using the α7TSLMF mutant (i.e., Ser223Thr, Ala226Ser, Met254Leu, Ile281Met, and Val288Phe) also showed that PAM-2 and PNU-120596 failed to potentiate the quintuple mutant, supporting the notion that these two PAMs share the similar structural determinants within the intrasubunit site (Andersen et al., 2016). This new study also confirms previous results (Arias et al., 2016), indicating that PAM-2 interacts with the ECD-TMD junction at sites that are also observed at both hα7 and $h(\alpha7)_3(\beta2)_2$ nAChRs (i.e., junction 1), and at both $h(\alpha7)_2(\beta2)_3$ and $h(\alpha7)_3(\beta2)_2$ stoichiometries (i.e., junction 2-5), respectively. Interestingly, junction 1 is formed by residues from α7 subunit, junction 3 from the β2 subunit, while junction 2 and 4 is formed by residues located at the interface between α7 and β2 subunits or between two adjacent α7 subunits, respectively.

The existence of the ECD-TMD junction sites, located apart from the archetypical intrasubunit site, might be important to understand the mechanisms underlying the dissimilar activity of PAM-2 between the α7 and α7β2 nAChRs (this work) as well as the different features found between type I and type II PAMs (Andersen et al., 2016; Arias et al., 2016).

Table 3.1: Pharmacologic Activity of PAM-2 on hα7 and hα7β2 AChRs, hα1β2γ2 and hρ1 $GABA_A$Rs, and hα1 GlyRs.

Receptor Type	Method	Ligand (concentration range)	Pharmacologic activity	E_{max} (% control)	EC_{50} (μM)	n_H
hα7 AChR	Two-electrode voltage-clamp on *Xenopus* oocytes injected with hα7 subunit mRNA	PAM-2 (1-80 μM) (>100 μM)	Potentiation Inhibition	246 ± 25 N/A	8.8 ± 1.15 N/A	12.23 ± 13.26 N/A
hα7β2 AChR	Two-electrode voltage-clamp on *Xenopus* oocytes injected with hα7 and hβ2 subunit mRNAs (1:5 ratio)	PAM-2 (1-80 μM) (>100 μM)	Potentiation Inhibition	207 ± 26 N/A	19.5 ± 1.14 N/A	11.74 ± 28.14 N/A
hα1β2γ2 $GABA_AR$	Whole-cell patch clamp on HEK293 cells permanently expressing hα1β2γ2 $GABA_A$Rs	PAM-2 (10-300 μM)	Slight Potentiation	131 ± 4	56 ± 7	1.50±0.20
hρ1 $GABA_AR$	Whole-cell patch-clamp on HEK293 cells transiently expressing hρ1 $GABA_A$Rs	PAM-2 (10-300 μM)	Slight Inhibition	70 ± 1 [a]	~540 [b]	—
hα1 GlyR	Whole-cell patch clamp on HEK293 cells transiently expressing hα1GlyRs	PAM-2 (30-300 μM)	No effect	—	—	—
hα7 AChR	Two-electrode voltage-clamp on *Xenopus* oocytes injected with hα7 subunit mRNA	N,N′-dicyclohexylurea (30-300 μM)	No effect	—	—	—
hα7 AChR	Two-electrode voltage-clamp on *Xenopus* oocytes injected with hα7 subunit mRNA	*p*-Toluidine (10 μM)	No effect	—	—	—
hα7 AChR	Two-electrode voltage-clamp on *Xenopus* oocytes injected with hα7 subunit mRNA	3-(2-Furyl)acrylic acid (10 μM)	No effect	—	—	—

[a] This value corresponds to PAM-2-induced inhibition relative to control (100%).
[b] This IC_{50} value is just an estimation using three different concentrations.

Table 3.2: Kinetics Parameters for ACh in the Absence (Control) and Presence of PAM-2 at the hα7 and hα7β2 AChRs.

Kinetics parameter		hα7		hα7β2	
		Control	+ PAM-2	Control	+ PAM-2
Peak amplitude	ACh EC_{50} (μM)	194±1.17	141±1.74	144±1.12	186±1.35
	n_H	2.33±0.58	1.06±0.51	2.37±0.50	0.99±0.25
	Maximal increase (x-fold)	—	2.3	—	1.9
	R^2	0.734	0.424	0.646	0.552
	ANOVA	—	p<0.0001	—	p<0.0001
Rise time	Maximal increase (x-fold)	—	2.1	—	3.6
	R^2	0.760	0.132	0.445	0.520
	ANOVA	—	p<0.0001	—	p<0.0001
Current area	Maximal increase (x-fold)	—	26.3	—	5.9
	R^2	0.537	0.258	0.684	0.439
	ANOVA	—	p<0.0001	—	p<0.0001

The kinetics parameters are obtained from Figures 2A-F, respectively.

Table 3.3: Molecular Interactions of PAM-2 with Allosteric Sites at the hα7 and hα7β2 Models.

nAChR subtype	Binding site location	Residues involved in ligand binding							
		ECD	Cys loop	Pre-M1	M1	M2 (position)	M2-M3 loop	M3	M4
hα7	ECD-TMD junction 1		W134 F135 P136 F137	T208 Y211 G212	L216		L270 I271		L465 A468 P469
	Intrasubunit				L216 C219 V220 S223			F275	T461 I464 L465
$h(\alpha7)_2(\beta2)_3$	ECD	α7-P17 α7-L18 α7-G83 α7-K87 α7-D89 α7-W86 α7-H105 α7-Y151 β2-P83 β2-H86 β2-F106 β2-N109							
	ECD-TMD junction 2	β1-β2 loop: α7-K46 β2-E47 β2-R48		β2-F211 β2-Y212 β2-N215 β2-L216		α7-L255 α7-A258 α7-E259 α7-A263 β2-L257 β2-K260 β2-I261			
	ECD-TMD junction 3 Orientation 1						β2-K274 β2-Y275	β2-F278 β2-T279 β2-L282	β2-C361 β2-F363 β2-G364 β2-G367 β2-M368
	ECD-TMD junction 3 Orientation 2		β2-H136 β2-F137 β2-P138 β2-F139		β2-I217 β2-C220 β2-V221		β2-L271 β2-V272		β2-M368 β2-F369 β2-P372

Table 3.3: Continued: Molecular Interactions of PAM-2 with Allosteric Sites at the hα7 and hα7β2 Models.

							β2-Y275 β2-L276		
$h(\alpha7)_3(\beta2)_2$	ECD-TMD junction 1		α7-W134 α7-F135 α7-P136 α7-F137	α7-T208 α7-G212	α7-L216 α7-V220		α7-L270 α7-I271 α7-Y274 α7-F275		α7-T349 α7-I352 α7-L353
	ECD-TMD junction 2	β1-β2 loop: α7-E45 α7-K46 β2-R48		α7-Y210 α7-Y211 α7-N214	α7-L215	β2-L256 β2-V257 α7-E259 β2-S259 α7-I260 β2-K260 β2-P264			
	ECD-TMD junction 4	α7-D42 α7-V43 α7-D44 α7-E45 α7-K46 α7-Q48	α7-Y129 α7-N171 α7-G172 α7-E173 α7-W174	α7-Y211		α7-E259 (1') α7-P262 (1') α7-A263 (1') α7-T264 (1')			
	Luminal					α7-G237 (-3') β2-C237 (-4') α7-E238 (-2') β2-G238 (-3') β2-E239 (-2') β2-M241 (1') α7-S241 (2') β2-T242 (2') α7-T245 (6') β2-I245 (5')			

Table 3.4: RMSD Mean and RMSD Variance Values for PAM-2 Interacting with Different Nicotinic Receptor Subtypes, Including hα7, $h(\alpha7)_2(\beta2)_3$, and $h(\alpha7)_3(\beta2)_2$ nAChRs.

Binding site	nAChR subtype		
	hα7	$h(\alpha7)_2(\beta2)_3$	$h(\alpha7)_3(\beta2)_2$
ECD	-	2.051 ± 0.014 (0.002)	-
ECD-TMD junction 1	0.6825 ± 0.008 (0.087)	-	1.599 ± 0.006 (0.017)
ECD-TMD junction 2	-	0.9509 ± 0.010 (0.026)	0.9043 ± 0.008 (0.059)
ECD-TMD junction 3 Orientation 1	1.441 ± 0.008 (0.074)	1.892 ± 0.009 (0.059)	-
ECD-TMD junction 3 Orientation 2	-	1.014 ± 0.012 (0.004)	-
ECD-TMD junction 4	-	-	1.785 ± 0.007 (0.002)
Luminal	-	-	1.446 ± 0.014 (0.007)

The RMSD mean values correspond to the 50-ns simulation, and the RMSD variance values were calculated during the last 10-ns.

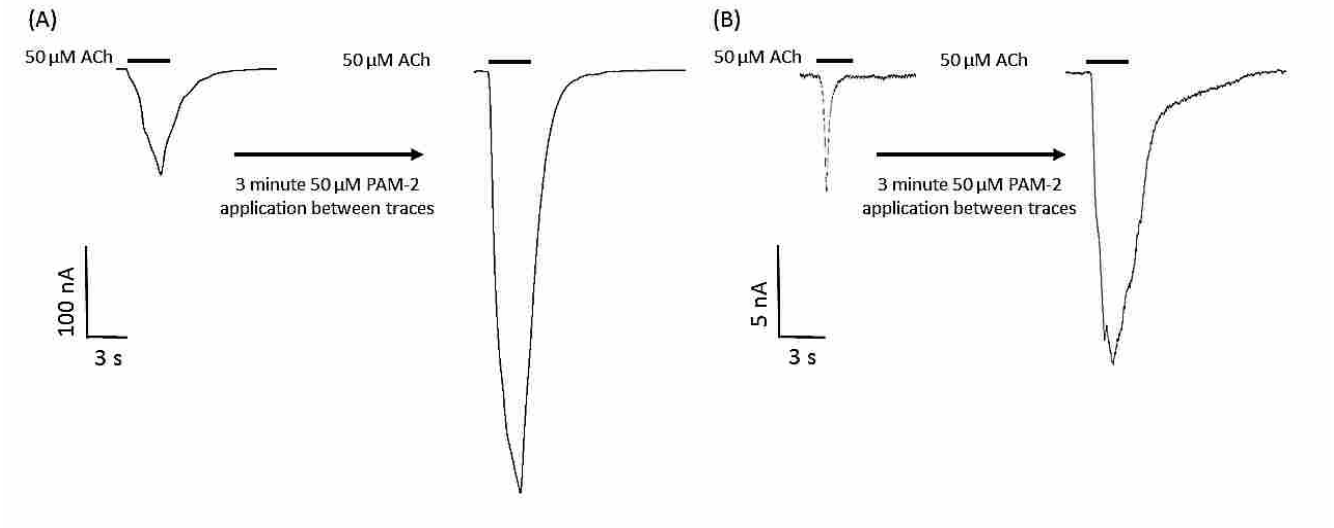

(C)

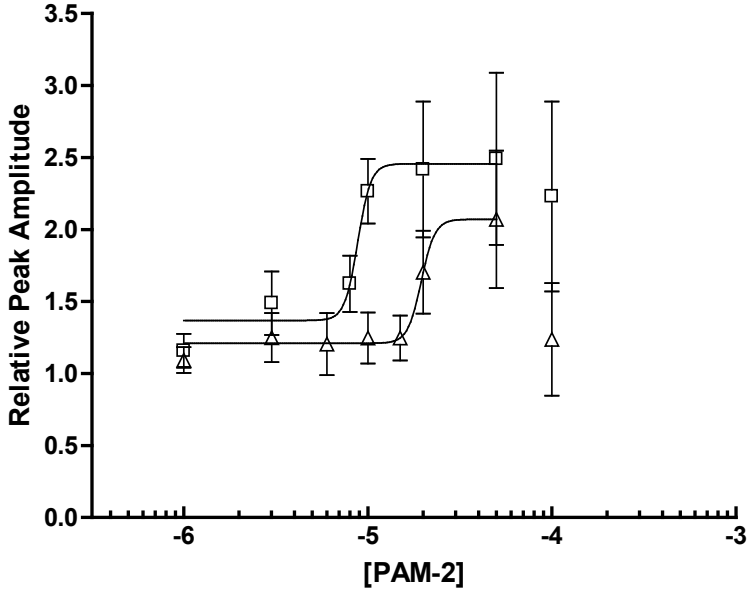

Figure 3.1: Effect of PAM-2 on (A) Homomeric hα7 and (B) Heteromeric hα7β2 AChRs. Acetylcholine (50 µM) was applied for 3 seconds activating each AChR subtype. Although PAM-2 (50 µM) did not appear to affect AChR activity independently, a 3 minute pre-treatment of PAM-2 altered the kinetic properties of both AChRs. We observed an increase in the peak amplitude and total area. The hα7 and hα7β2 were both altered but, the kinetic changes of the hα7 were more pronounced. (C) Effect of PAM-2 on the ACh-induced peak amplitude at the hα7 (■) and hα7β2 (□) AChRs. Increasing concentrations of PAM-2 (1-100 µM) were applied to either the hα7 (n=11) AChR, while ACh was held constant at 50 µM. A 90 second PAM-2 wash was done between each ACh application. The potentiating EC_{50}, E_{max}, and n_H values for PAM-2 at each AChR subtype are summarized in Table 1.

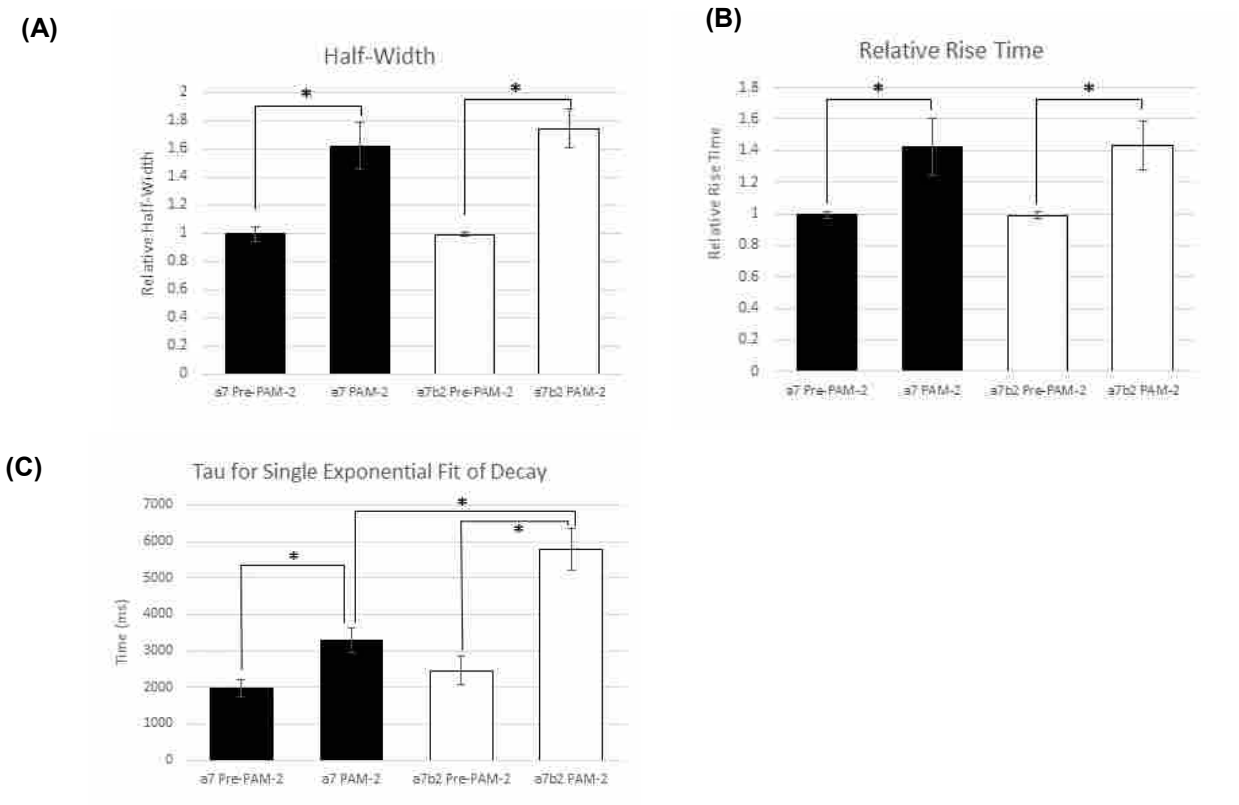

Figure 3.2: Change in Properties of Desensitization After a 3 minute PAM-2 Application. (A) Pooled data of the half-width measurement (width of the peak in ms at 50% of the amplitude) after PAM-2 application when compared to the baseline measurements before the PAM-2 application are statistically different for each subtype (α7 Pre-PAM-2 v. α7 PAM-2, p-value<0.0001, α7β2 Pre-PAM-2 v. α7β2 PAM-2, p-value<0.00000001, t-tests). However, the PAM-2 effect on the half-width for α7 and α7β2 are not statistically different, as well as their comparison on their pre-PAM-2 baselines. (B) Pooled data of the rise-time (time required to increase from 10% to 90% of the peak amplitude) after PAM-2 application when compared to the baseline measurements before the PAM-2 application are statistically different for each subtype (α7 Pre-PAM-2 v. α7 PAM-2, p-value=0.0042, α7β2 Pre-PAM-2 v. α7β2 PAM-2, p-value<0.0014, t-tests). However, the PAM-2 effect on the rise-times for α7 and α7β2 are not statistically different, as well as their comparison on their pre-PAM-2 baselines. (C) Pooled data of the tau for single exponential fit of decay after PAM-2 application when compared to the baseline measurements before the PAM-2 application are statistically different for on the α7β2 AChR (α7 Pre-PAM-2 v. α7 PAM-2, p-value=0.104) (α7β2 Pre-PAM-2 v. α7β2 PAM-2, p-value<0.001, t-tests). In addition, the PAM-2 effect on the tau for single exponential fit of decay for α7 and α7β2 were statistically different (p-value=0.00816), even though the comparisons of their pre-PAM-2 baselines were not. ANOVAs revealed no significant differences in the desensitization properties with various concentrations of PAM-2 (1 μM-100 μM), therefore, all data was pooled.

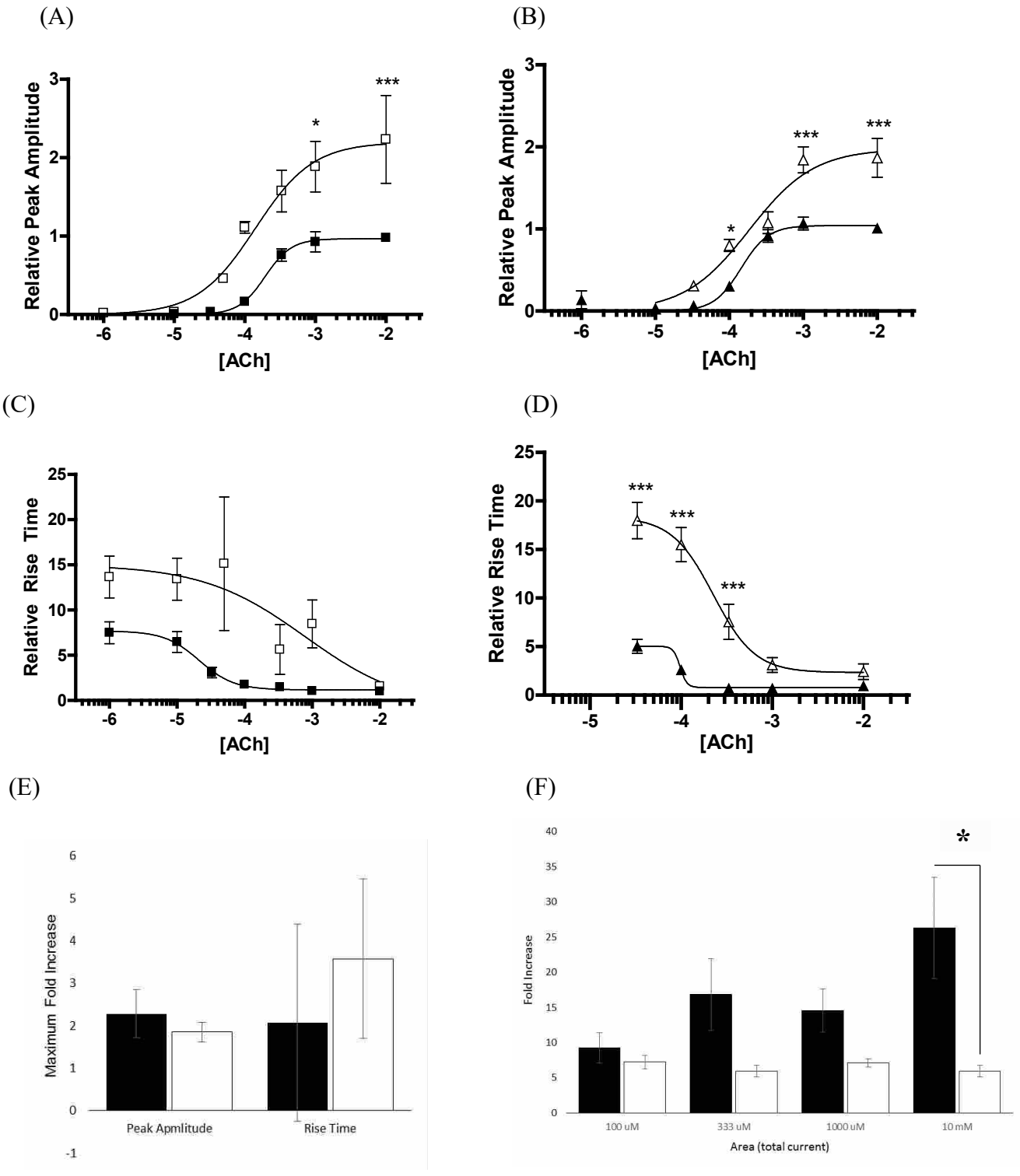

Figure 3.3: Effect of 20 μM PAM-2 on Various Kinetic Parameters Obtained from ACh-induced hα7 and hα7β2 AChR Responses.

Figure 3.3 Continued: The activity of ACh on the respective hα7 (■) (n = 7) and hα7β2 (▲) (n = 14) AChR was compared to that obtained in the presence of 20 μM PAM-2 applied for 3 minutes [hα7 (□), n = 4; hα7β2 (△), n = 9]. The comparison of the relative peak amplitude for the (A) hα7 (■) and (B) hα7β2 (▲) AChRs in the absence versus the presence of PAM-2 [(□), $F_{[13, 118]}$=11.126, p<0.0001; (△), $F_{[12, 234]}$=35.956, p<0.0001] indicated a statistically significant effect by PAM-2. The comparison of the time required for a pulse to rise from 10% to 90% of the peak amplitude (i.e., relative rise time) for the (C) hα7 (■) and (D) hα7β2 (▲) AChRs in the absence versus the presence of PAM-2 [(□), $F_{[12, 111]}$=4.697, p=0.0011; (△), $F_{[9, 227]}$=44.602, p<0.0001] indicated a statistically significant effect by PAM-2. The error bars are the S.E.M. values. The apparent absence of error bars on certain points is due to the scale required for comparison. (*p<0.05, **p<0.01, ***p<0.001). The quantitative parameters for ACh in the absence and presence of PAM-2 at each AChR subtype are summarized in Table 2. (E) Comparison of the difference between the largest PAM-2 effects and the largest control values on both hα7 (black bars) and hα7β2 (white bars) AChRs. Although the peak amplitude and current area are compared at 10 mM ACh, the rise time comparison is made at the minimum ACh concentration because the effect inversely related. (F) The results summarize that PAM-2 has a much greater potentiating effect on homomeric hα7 AChRs compared to that for heteromeric hα7β2 AChRs. The quantitative parameters for ACh in the absence and presence of PAM-2 at each AChR subtype are summarized in Table 2. (F) Fold increase in total current (area) increases with increasing ACh concentrations during 20 μM PAM-2 applications for the hα7 AChRs. However, even though the hα7β2 AChRs show a ~5 fold increase in total area during 20 μM PAM-2 applications, the increase is not observed with increasing ACh concentrations.

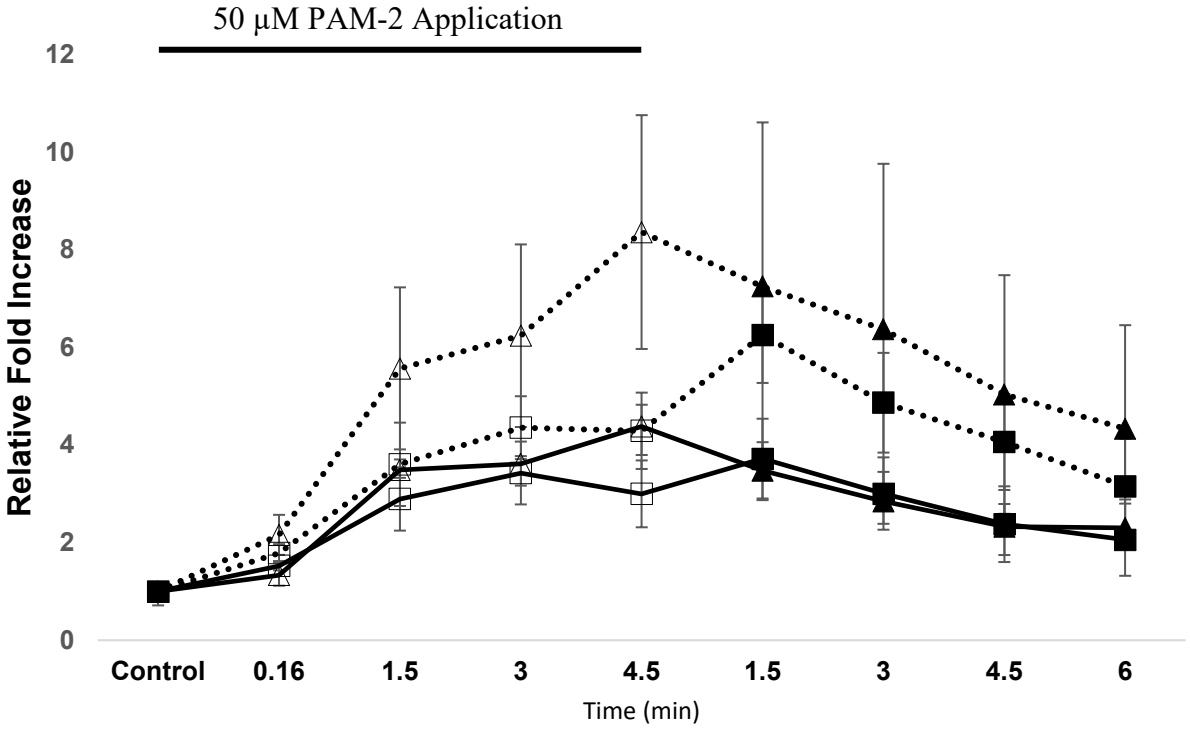

Figure 3.4: Time Dependence of the Change in Peak Amplitude and Current Area of the Respective hα7 (■,□) and hα7β2 (▲,△) AChR Perfused with 50 μM PAM-2.
A significant effect on peak amplitude (▬) and area (….) was observed after 10 seconds of perfusion on both hα7 (peak, $p<0.0001$; area, $p<0.0001$; $n = 6$) and hα7β2 (peak, $p<0.05$; area, $p<0.001$; $n = 3$) AChRs. T-tests were performed at 10 seconds in comparison to the control.

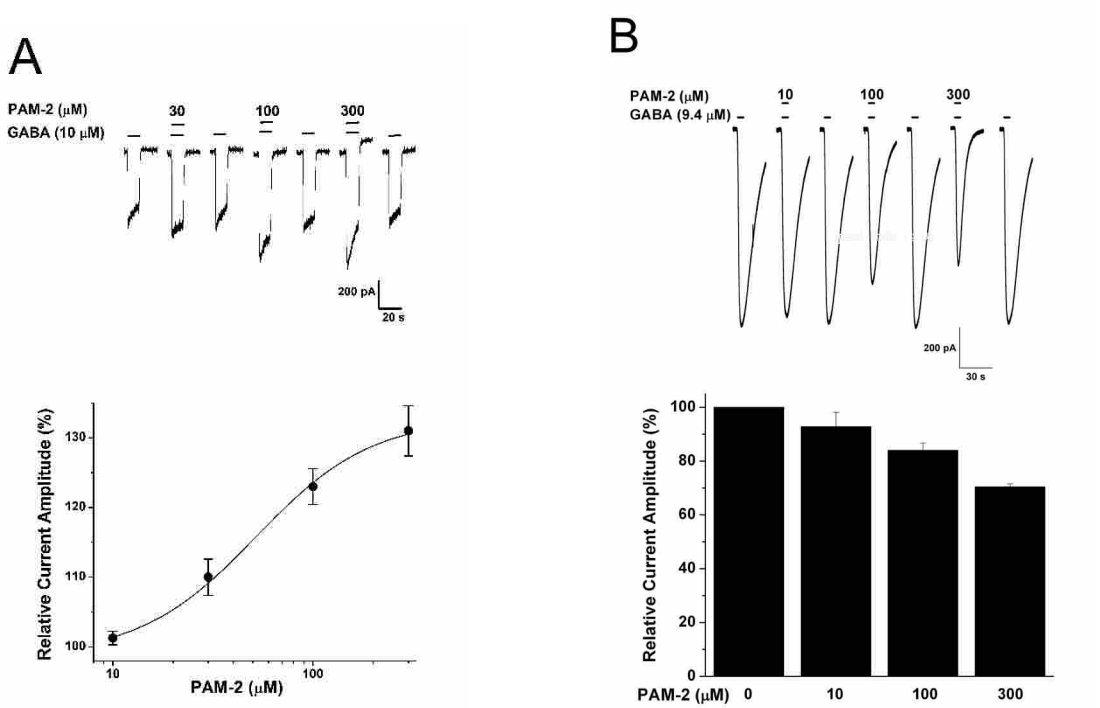

Figure 3.5: Effect of PAM-2 on Heteromeric hα1β2γ2 (A) and Homomeric hρ1 (B) $GABA_A$Rs. (A) Top, representative traces showing GABA-activated hα1β2γ2 $GABA_A$R currents, in the absence and presence of PAM-2, by using whole-cell patch-clamp. Different concentrations of PAM-2 (i.e., 10-300 μM) were co-applied with 10 μM GABA for 10 s. Bottom, the results indicated that PAM-2 potentiated hα1β2γ2 currents in a concentration-dependent manner (n = 3-8). The potentiating EC_{50}, n_H, and E_{max} values were summarized in Table 1. (B) Top, representative traces showing GABA-activated hρ1 $GABA_A$R currents, in the absence and presence of PAM-2, by using whole-cell patch-clamp. Different concentrations of PAM-2 (i.e., 10, 100 or 300 μM) were co-applied with 9.4 μM GABA for 5 s. Bottom, the results indicated that PAM-2 slightly inhibited hρ1 currents in a concentration-dependent manner (n = 3-8; paired t-test; $p<0.01$ and $p<0.001$ for 100 and 300 μM, respectively). All current amplitudes are normalized to the response in the absence of PAM-2 (assigned as 100%). Each data point represents Mean ± SEM. The estimated IC_{50} and E_{max} (%) values are summarized in Table 1.

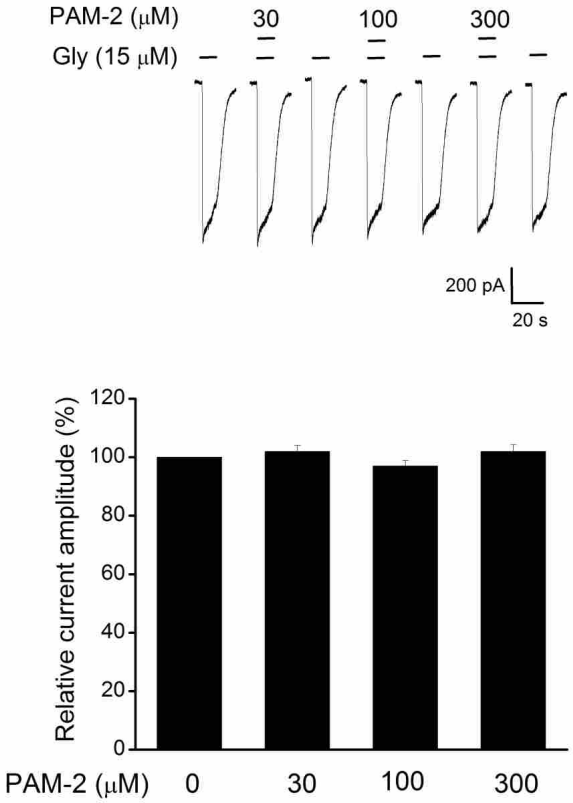

Figure 3.6: Effect of PAM-2 on Recombinant hα1 GlyRs. Top, representative traces showing Gly-activated hGlyR currents, in the absence and presence of PAM-2, by using whole-cell patch-clamp. Different concentrations of PAM-2 (i.e., 30, 100 or 300 μM) were co-applied with 15 μM Gly for 10 s. Bottom, the results indicated that PAM-2 did not affect GlyR function (n = 6-7; paired t-test; $p>0.05$). All current amplitudes were normalized to the response in the absence of PAM-2 (assigned as 100%). Each data point represents Mean ± SEM.

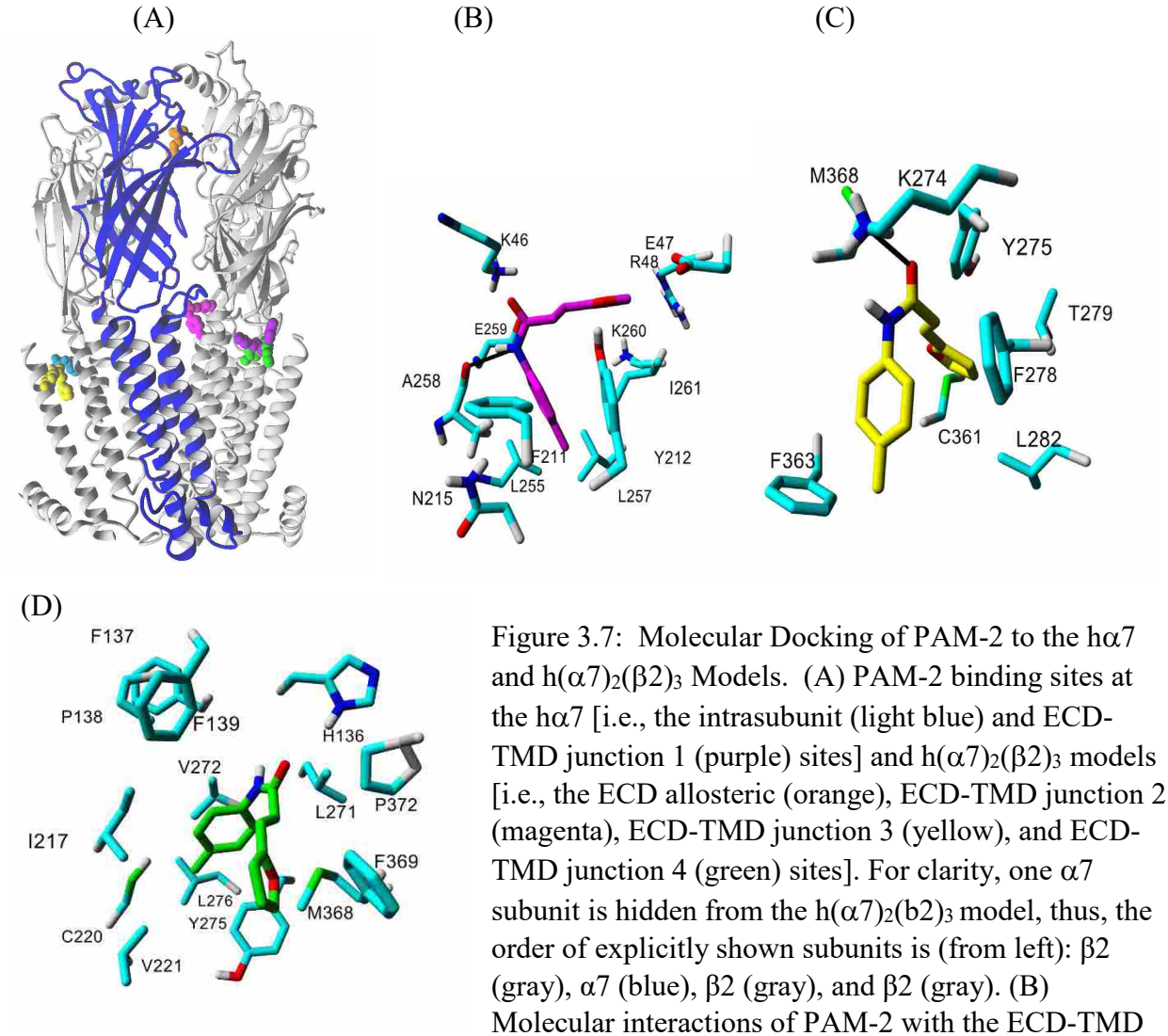

Figure 3.7: Molecular Docking of PAM-2 to the hα7 and h$(\alpha7)_2(\beta2)_3$ Models. (A) PAM-2 binding sites at the hα7 [i.e., the intrasubunit (light blue) and ECD-TMD junction 1 (purple) sites] and h$(\alpha7)_2(\beta2)_3$ models [i.e., the ECD allosteric (orange), ECD-TMD junction 2 (magenta), ECD-TMD junction 3 (yellow), and ECD-TMD junction 4 (green) sites]. For clarity, one α7 subunit is hidden from the h$(\alpha7)_2(b2)_3$ model, thus, the order of explicitly shown subunits is (from left): β2 (gray), α7 (blue), β2 (gray), and β2 (gray). (B) Molecular interactions of PAM-2 with the ECD-TMD junction 2 site (magenta) at the h$(\alpha7)_2(\beta2)_3$. This site, located in the α7/β2 interface, is formed by residues from the β1-β2 loop (i.e., α7-Lys46, β2-Glu47, and β2-Arg48), pre-M1 (i.e., β2-Phe211, β2-Tyr212, β2-Asn215, and β2-Leu216), and M2 (i.e., α7-Leu255, α7-Ala258, α7-Glu259, α7-Ala263, β2-Leu257, β2-Lys260, and β2-Ile261). The black arrow shows the H-bond formed between the PAM-2 nitrogen and the carbonyl oxygene from the α7-Ala258 backbone. (C) Molecular interactions of PAM-2 with the ECD-TMD junction 3 site at orientation 1(yellow) at the h$(\alpha7)_2(\beta2)_3$. This site, located within the β2 subunit, is formed by residues from the M2-M3 loop (i.e., Lys274 and Tyr275), M3 (i.e., Phe278, Thr279, and Leu282), and M4 (i.e., Cys361, Phe363, Gly364, Gly367, and Met368). An H-bond is formed between the carbonyl oxygen of PAM-2 and the α7-Lys274 nitrogen moiety. (D) Molecular interactions of PAM-2 with the ECD-TMD junction 3 site at orientation 2 (green) at the h$(\alpha7)_2(\beta2)_3$. This site is formed only by β2 residues from the Cys-loop (i.e., His136, Phe137, and Pro138, and Phe139), M1 (i.e., Ile217, Cys220, and Val221), M2-M3 loop (i.e., Leu271, Val272, Tyr275, and Leu276), and M4 (i.e., Met368, Phe369, and Pro372). PAM-2 is rendered in ball (A) or stick (B-D) mode, whereas residues as stick mode (element color code). All non-polar hydrogen atoms are hidden.

References

Andersen, N., Corradi, J., Steven M. Sine, and Cecilia Bouzat (2013) Stoichiometry for activation of neuronal α7 nicotinic receptors. Proc. Natl. Acad. Sci. USA 110, 20819-20824.

Andersen, N.D., Nielsen, B.E., Corradi, J., Tolosa, M.F., Feuerbach, D., Arias, H.R., Bouzat, C. (2016) Exploring the positive allosteric modulation of human α7 nicotinic receptors from a single-channel perspective. Neuropharmacology 107, 189-200.

Arias, H.R., 2010. Positive and negative modulation of nicotinic receptors. Adv. Protein Chem. Struct. Biol. 80, 153-203.

Arias, H.R., 2011. Allosteric modulation of nicotinic acetylcholine receptors, in: Pharmacology of Nicotinic Acetylcholine Receptors from the Basic and Therapeutic Perspectives (Arias, H.R., Ed.). Research Signpost, Kerala, India, Chapter 7, pp. 151-173.

Arias, H.R., Gu, R.X., Feuerbach, D., Guo, B.B., Ye, Y., Wei, D.Q., 2011. Novel positive allosteric modulators of the human α7 nicotinic acetylcholine receptor. Biochemistry 50, 5263-5278.

Arias, H.R., Targowska-Duda, K.M., Feuerbach, D., Jozwiak, K., 2015b. The antidepressant-like activity of nicotine, but not of 3-furan-2-yl-N-p-tolyl-acrylamide, is regulated by the nicotinic receptor β4 subunit. Neurochem. Int. 87, 110-116.

Bagdas, D., Targowska-Duda, K.M., Lopez, J.J., Perez, E.G., Arias, H.R., Damaj, M.I., 2015. Antinociceptive and anti-inflammatory properties of 3-furan-2-yl-N-p-tolyl-acrylamide (PAM-2), a positive allosteric modulator of α7 nicotinic acetylcholine receptors, in mice. Anesth Analg. 121, 1369-1377.

Bowie, J.U., Luthy, R., Eisenberg, D., 1991. A method to identify protein sequences that fold into a known three-dimensional structure. Science 253, 164-170.

Bowers, K.J., Chow, E., Xu, H., Dror, R.O., Eastwood, M. P., Gregersen, B. A., et al., 2006. Algorithms for Molecular Dynamics Simulations on Commodity Clusters. D. E. Shaw Research, LLC, New York, NY 10036, USA. Proceedings of the ACM/IEEE Conference on Supercomputing (SC06), November 11–17, Tampa, Florida.

Changeux J.P., Edelstein, S.J. 1998. Allosteric receptors after 30 years. Neuron, 21:959-980.

Chatzidaki, A., Millar, N.S., 2015. Allosteric modulation of nicotinic acetylcholine receptors. Biochem Pharmacol 97, 408-417.

Chen, Z., G.H. Dillon, R.Q. Huang, Molecular determinants of proton modulation of glycine receptors. J Biol Chem, 2004. 279: 876-83.

Corringer, P.J., Le Novere, N., Changeux, P.J. (2000). Nicotinic receptors at the amino acid level. Annu. Rev. Pharmacol. Toxicol. 40:431-458.

daCosta, C.J., Free, C.R., Corradi, J., Bouzat, C., Sine, S.M., 2011. Single-channel and structural foundations of neuronal α7 acetylcholine receptor potentiation. J. Neurosci. 31, 13870-9.

Eswar, N., Webb, B., Marti-Renom, M.A., Madhusudhan, M.S., Eramian, D., Shen M.Y., et al., 2006 Comparative protein structure modeling using Modeller., Curr. Protoc. Bioinformatics John Wiley & Sons, Inc., Supplement 15, 5.6.1-5.6.30.

Gasteiger, E., Gattiker, A., Hoogland, C., Ivanyi, I., Appel, R.D., Bairoch, A., 2003. ExPASy: the proteomics server for in-depth protein knowledge and analysis. Nucl. Acids Res. 31, 3784–3788.

Hassaine, G, Deluz, C, Grasso, L, Wyss, R, Tol, MB, Hovius, R., et al., 2014. X-ray structure of the mouse serotonin 5-HT_3 receptor. Nature 512, 276-281.

Huang, R.Q., G.H. Dillon, Effect of extracellular pH on GABA-activated current in rat recombinant receptors and thin hypothalamic slices. J Neurophysiol, 1999. 82: 1233-43.

Huang, R.Q., C.L. Bell-Horner, M.I. Dibas, D.F. Covery, J.A. Drewe, G.H. Dillon. Pentylenetetrazole-induced inhibition of recombinant gamma-aminobutyric acid type A $GABA_A$ receptors: mechanism and site of action. J Pharmacol Exp Ther, 2001. 298: 986-95.

Khiroug S.S., Harkness P.C., Lamb P.W., Sudweeks S.N., Khiroug L., Millar N.S., Yakel J.L. Rat nicotinic ACh receptor alpha7 and beta2 subunits co-assemble to form functional heteromeric nicotinic receptor channels. J Physiol. 2002;540(Pt 2):425-34.

Laskowski, R.A., MacArthur, M.W., Moss, D.S., Thornton, J.M., 2013. PROCHECK - a program to check the stereochemical quality of protein structures, J. App. Cryst. 26, 283-291.

Liu, Q., Huang, Y., Shen, J., Steffensen, S., Wu, J. (2012) Functional α7β2 nicotinic acetylcholine receptors expressed in hippocampal interneurons exhibit high sensitivity to pathological level of amyloid β peptides. BMC Neuroscience 13, 155.

Liu Q, Huang Y, Xue F, Simard A, DeChon J, Li G, Zhang J, Lucero L, Wang M, Sierks M, et al: A novel nicotinic acetylcholine receptor subtype in basal forebrain cholinergic neurons with high sensitivity to amyloid peptides. J Neurosci 2009, 29:918–929.

Maleeva, G., Buldakova, S., Bregestovski, P. (2015) Selective potentiation of alpha 1 glycine receptors by ginkgolic acid. Front. Mol. Neurosci. 8, 64.

Morales-Perez CL, Noviello CM, Hibbs RE X-ray structure of the human α4β2 nicotinic receptor. Nature. 2016 538(7625):411-415.

Papke RL, Meyer E, Nutter T, Uteshev VV. (2000) α7-selective agonists and modes of α7 receptor activation. Eur J Pharmacol 393:179–195.

Pop, E (1997) Optimization of the properties of brain specific chemical delivery systems by structural modifications. Curr. Med. Chem. 4, 279-294.

Potasiewicz, A., Hołuj, M., Kos, T., Popik, P., Arias, H.R., and Nikiforuk, A. (2016) 3-Furan-2-yl-N-p-tolyl-acrylamide, a positive allosteric modulator of the α7 nicotinic receptor, reverses schizophrenia-like cognitive deficits in rats. *Neuropharmacology,* in press.

Potasiewicz, A., Kos, T, Ravazzini, F, Puia, G, Arias HR, Popik P, et al., 2015. Pro-cognitive activity in rats of 3-furan-2-yl-N-p-tolyl-acrylamide, a positive allosteric modulator of the α7 nicotinic acetylcholine receptor. Br. J. Pharmacol. 172, 5123-5135.

Sigel, E., Steinmann, M.E. (2012) Structure, function, and modulation of $GABA_A$ receptors. J. Biol. Chem. 287, 40224-40231.

Snell, H.S, Gonzales, E.B. (2015) Amiloride and GMQ Allosteric Modulation of the GABA-A ρ 1 Receptor: Influences of the Intersubunit Site. J Pharmacol Exp Ther. 353(3): 551–559.

Targowska-Duda, K.M., Feuerbach, D., Biała, G., Jozwiak, K., and Arias, H.R., 2014. Antidepressant activity in mice elicited by 3-furan-2-yl-N-p-tolyl-acrylamide, a positive allosteric modulator of the α7 nicotinic receptor. Neurosci. Lett. 569, 126-130.

Targowska-Duda, K.M., Wnorowski , A., Budzynska, B., Jozwiak, K., Biała, G., Arias H.R., 2016. The positive allosteric modulator of α7 nicotinic acetylcholine receptors, 3-furan-2-yl-N-p-tolyl-acrylamide, enhances memory processes and stimulates ERK1/2 phosphorylation in mice. Behav. Brain Res. 302, 142-151.

Thompson, J.D., Higgins, D.G., Gibson, T.J., 1994. CLUSTAL W: improving the sensitivity of progressive multiple sequence Alignment through sequence weighting, position-specific gap penalties and weight matrix choice. Nucleic Acids Res. 22, 4673–4680.

Trott, O., Olson, A. J. 2010. AutoDock Vina: improving the speed and accuracy of docking with a new scoring function, efficient optimization, and multithreading. J Comput Chem. 31, 455-61.

Wu J., Liu Q., Tang P., Mikkelsen J.D., Shen J., Whiteaker P., Yakel J.L. Heteromeric α7β2 Nicotinic Acetylcholine Receptors in the Brain. Trends Pharmacol Sci. 2016 Jul;37(7):562-74. doi: 10.1016/j.tips.2016.03.005. Epub 2016 May 11.

Xu, T-L, Gong, N. (2010) Glycine and glycine receptor signaling in hippocampal neurons: Diversity, function and regulation. Prog. Neurobiol. 91, 349-361.

Young, G.T., Zwart, R., Walker, A.S., Sher, E., Millar, N.S., 2008. Potentiation of α7 nicotinic acetylcholine receptors via an allosteric transmembrane site. Proc Natl Acad Sci U S A. 105, 14686-91.

REMARKS

Neuronal nicotinic acetylcholine receptors are highly targeted protein targets used in treating many neurological conditions including cognition, depression, schizophrenia and neurodegeneration (Freedman, 2014, Hurst, 2013). This research is the first of its kind identifying and characterizing the subtypes of the α3β2 nAChR. We have hypothesized that considering the high levels of mRNA α3 and β2 subunit coexpression that the α3β2 nAChR may play a more significant role in hippocampus circuitry than previously believed. In addition, considering the ratio of the mRNA subgroups we sought to differentiate α3β2 nAChR subtypes using electrophysiology. Our results suggest there are at least two distinguishable subtypes of the α3β2 nAChR. This novel result provides new drug targets for neurological conditions.

In addition, we found it intriguing and valuable to characterize PAM-2, an α7* selective positive allosteric modulator, that may be promising drug in cognitive therapeutics (Uteshev, 2014). Positive allosteric modulators that target GABA receptors have been effective in the treating anxiety, depression, and other mood disorders (Nickols, 2014). The current research also suggests in addition to positive allosteric modulators being more effective in treating cognitive disorders, they may also lend fewer negative side effects. Our research using PAM-2 sought to different the PAM-2 effect on α7 nAChR homomers and α7β2 nAChR heteromers. We found that although PAM-2 does have significant effects on both subtypes the effect is distinguishable. Therefore, PAM-2 serves as one of the only methods of distinguishing α7 from α7β2 nAChR in vivo.

The results of each chapter are significant to the field of pharmacology and neuroscience. The enhanced understanding of nAChR subtypes and their positive allosteric modulators are a gateway to many additional studies.

References

Freedman R, (2014). α7-nicotinic acetylcholine receptor agonists for cognitive enhancement in schizophrenia. Annu Rev Med. 65:245-61.

Hurst R, Rollema H, Bertrand D (2013). Nicotinic acetylcholine receptors: from basic science to therapeutics. Pharmacol Ther. 137:22-54.

Nickols HH, Conn PJ (2014). Development of allosteric modulators of GPCRs for treatment of CNS disorders. Neurobiol Dis. 61:55-71.

Uteshev W (2014). The therapeutic promise of positive allosteric modulation of nicotinic receptors. Eur J Pharmacology. 727:181-5.

CIRRICULUM VITAE

Doris Clark Jackson
372 East 100 South, Provo, UT 84606
dorisgclark@gmail.com
(919)885-4998

Education

Brigham Young University, Provo, UT — current
Neuroscience, PhD

Brigham Young University, Provo, UT — Apr 2013
Neuroscience, B.S., GPA: 3.83
Minor: Chemistry

Publications

"Expression of nAChR mRNA in Rat Hippocampal Interneurons." — *In Preparation*
Doris C Jackson, Spencer Thompson, Richard M Burgon, and Sterling N Sudweeks.

"The Human alpha 3 beta 2 Neuronal Nicotinic Acetylcholine Receptor Forms Two Distinguishable Subtypes."
Doris C Jackson, Marcel K Hall, Sterling N Sudweeks. — *In Preparation*

"The highly selective positive allosteric modulator 3-furan-2-yl-N-p-tolyl-acrylamide potentiates α7 and α7β2 nicotinic receptors with different efficacy."
Hugo R. Arias, Doris Jackson, Zhenglan Chen, Manish Kumar, Eric B. Gonzales, Katarzyna M. Targowska-Duda, Agnieszka A. Kaczor, Renqi Huang, Glenn H. Dillon, and Sterling Sudweeks. — *In Preparation*

Presentations

Dissertation Defense — May 2017
"Characterization of Neuronal Nicotinic Acetylcholine Receptors and their Positive Allosteric Modulators."

International Conference on Nicotinic Acetylcholine Receptors, Greece — May 2017
"The α3β2 Neuronal Nicotinic Acetylcholine Receptor Forms Two Distinguishable Subtypes." Young Scientist, Oral Presentation.

Mary Lou Fulton Mentored Research Conference, Provo, UT — Apr 2017
"PAM-2: A Promising Drug in Cognitive Therapeutics." Poster Presentation.

BYU Graduate Student Society, 3 Minute Thesis (3MT), Provo, UT — Feb 2017
"Saving the Synapse through Cognitive Therapies." Oral Presentation.

Graduate-Faculty Discussion, Provo, UT — Jan 2017
"Positive allosteric Modulators: The Growing Field in nAChr Pharmacology." Oral Presentation.

Society for Neuroscience, San Diego, CA — Nov 2016
"Characterization of Human α3β2 nAChRs expressed in Xenopus Laevis Oocytes." Poster Presentation.

Alzheimer's Association International Conference, Toronto, Canada — Jul 2016
"Characterization of Human α3β2 nAChRs expressed in Xenopus Laevis Oocytes." Poster Presentation.

LDS Life Sciences Symposium, Lehi, UT — Jul 2016
"Characterization of Human α3β2 nAChRs expressed in Xenopus Laevis Oocytes." Poster Presentation.

Mary Lou Fulton Mentored Research Conference, Provo, UT — Apr 2016
"Novel Pharmacological Target: Characterization of a3b2 nAChRs expressed in Xenopus Laevis Oocytes." See BYU Library Student Archives. 1st place Graduate Student-Neuroscience. Poster Presentation.

Mary Lou Fulton Mentored Research Conference, Provo, UT — Apr 2016
"PAMs: A Growing Field in Pharmacological Drug Development." Poster Presentation.

Graduate-Faculty Discussion, Provo, UT — Apr 2016
"Characterization of Neuronal Nicotinic Acetylcholine Receptors Expressed in Xenopus Laevis Oocytes." Oral Presentation.

Graduate-Faculty Discussion, Provo, UT — Jan 2015
"β-Amyloid: Interaction and Inhibition of Hippocampal Nicotinic Acetylcholine Receptors." Oral Presentation.

Society for Neuroscience, Washington, DC — Nov 2014
"Interactions of neuronal a7 nAChR with β-Amyloid and the kinase inhibitor Genistein in Xenopus Oocytes." Poster Presentation.

Neuroscience Symposium, SFN Chapter, University of Utah — Oct 2014
"Interactions of neuronal a7 nAChR with β-Amyloid and the kinase inhibitor Genistein in Xenopus Oocytes." Poster Presentation.

Undergraduate Lecture, Neurobiology, Brigham Young University — Apr 2013
Taught 90 students 1-hour lecture on neuronal control of movement.

Journal Club, Biophysics Great Lab, Provo, UT — 2009-10, 2013-14
Presented various peer-reviewed articles that were of significance to our lab group. Sterling Sudweeks Lab Meeting.

Alzheimer's Association International Conference, Honolulu, HI — June 2010
"Characterizing the effects of b-amyloid on neuronal nicotinic acetylcholine receptor subtypes found in the rat hippocampus." Poster Presentation.

Other Conferences Attended

Autism Translation Research Conference, BYU — 2017

Human Anatomy and Physiology Society Conference — 2017

Intermountain Chapter: Society of Neuroscience, Salt Lake City, UT — 2013, 2014

Work Experience

Graduate Teacher's Assistant, Physiology of Drug Mechanisms, PDBio 561 — F 2016
Graded Student Presentations
Taught review sessions and held regular office hours

Graduate Instructor, Physiology and Developmental Biology, PDBio 362 — S 2015
Taught 14 hours of lecture and assisted students outside of class
Helped to generate quizzes and maintain online course software

Teacher's Assistant, Neuroanatomy, Neuro 360 — F 2014-W 2016
Taught weekly review sessions
Assisted with in classroom activities and graded weekly quizzes

Beginning Tennis Instructor, BYU, Stac 181 — F 2014, W 2015
Developed and executed a unit plan
Instructed groups and individuals on the rules and techniques

Teacher's Assistant, Behavioral Neuroscience, Neuro 380 W 2014
Met with students individually to prepare for examinations
Taught tests review for the students

Teacher's Assistant, Cellular Biology, PDBio 360 F 2013, S 2014
Prepared the classroom for each class period
Provided tutoring and review sessions on a weekly basis

Research Assistant, Dr. Sudweeks 2010-2017
Mentored and trained new lab members
Designed experiments that lead to publications

Teacher's Assistant, Neurobiology, Neuro 205 Dec 2012-Apr 2013
Wrote quizzes, reviewed exams, and taught review sessions weekly.

Certified Nursing Assistant, Country View Manor, Provo, UT Dec 2009-Jan 2011
Promoted to provide daily restorative care for ~20 residents
Evaluated, designed, and implemented care plans

Honors and Awards

Research Presentation Award, BYU GSS F 2014, W 2017
byugss@byu.edu

Research Assistantship Award F 2015, S 2016, W 2017
Paul Reynolds
paul_reynolds@byu.edu, (801)422-1933

Mary Lou Fulton Mentoring Research Conference, 1st Place Neuroscience 2016
Patricia Wilson
patricia_wilson@byu.edu, (801)422-1355

Half-Tuition Academic Scholarship, Brigham Young University 2009-2011, 2013
Christian Hansen
christian_hansen@byu.edu, (801)422-7075

Golden Key International Honors Society 2009, 2010, 2011, 2013
Invitation for Membership

Undergraduate Research Travel Award 2010
Richard Bobo
richard_bobo@byu.edu, (801)422-7860

Summer Medical and Dental Education Program, Stipend Recipient — Jul 2009
University of Nebraska Medical Center, Omaha, Nebraska

Memberships

Human Anatomy and Physiology Society — 2017

Society for Neuroscience — 2013, 2014, 2016

ISTAART (Alzheimer's Association) — 2016, 2010

Service and Volunteer Experience

Brain Awareness Week — 2010, 2013
Collaborated with local elementary and high schools
Engaged students in activities about the brain
Trenton Simmons, simmons.trenton@gmail.com

Full-time Missionary Service — Mar 2011-Aug 2012
Missionary: The Church of Jesus Christ of Latter-Day Saints
Improved communities through weekly service
Brent Olson, brent@theolsons.net

Science Fair Judge, Provo, UT — 2010
Judged K-12 district level science fair projects

4-H Youth Mentor — 2008-2010
Designed weekly activities concerning social, family, and academics
Autumn Linsley, autumn.linsley@usu.edu

Software

Microsoft Word
Microsoft Excel
Microsoft Powerpoint
EndNote
Clampex 9.0
Clampfit
Snap Gene
Adobe Connect
GraphPad Prism, InStat
Brain Storm

References

Sterling Sudweeks, Associate Professor, Department of Physiology and Developmental Biology, Neuroscience Center, BYU
595 WIDB, Provo, UT 84602
801.422.8752
Sterling_Sudweeks@byu.edu

Mike Brown, Associate Professor, Department of Physiology and Developmental Biology, Neuroscience Center, BYU
2028 LSB, Provo, UT 84602
801.422.5859
michael_brown@byu.edu

R Paul Evans, Assistant Professor, Microbiology & Molecular Biology, BYU
3139 LSB, Provo, UT 84602
801.422.3259
evansp@byu.edu

Johnathan Wisco, Associate Professor, Physiology and Developmental Biology (Human Anatomy), BYU
2028 LSB, Provo, UT 84602
801.422.2402
jjwisco@byu.edu

Glenna Padfield, Student Activities Program Coordinator
203C RB, Provo, UT 84602
801.422.1601
glenna_padfield@byu.edu

Arminda Suli, Assistant Professor, Department of Physiology and Developmental Biology, Neuroscience Center, BYU
3048 LSB, Provo, UT 84602
801.422.2646
asuli@byu.edu